ผลของขนาดผลึกและอุณหภูมิในการเผาที่มีต่อความเสถียรทางความร้อนของผลึกเดี่ยวขนาดนาโนเมตรของออกไซด์ของโลหะทรานซิชัน

นางสาว จิรธนา ผึ่งผดุง

วิทยานิพนธ์นี้เป็นส่วนหนึ่งของการศึกษาตามหลักสูตรปริญญาวิศวกรรมศาสตรมหาบัณฑิต

สาขาวิชาวิศวกรรมเคมี ภาควิชาวิศวกรรมเคมี

คณะวิศวกรรมศาสตร์ จุฬาลงกรณ์มหาวิทยาลัย

ปีการศึกษา 2544

ISBN 974-03-1317-5

EFFECT OF CRYSTALLITE SIZE AND CALCINATION TEMPERATURE ON THE THERMAL STABILITY OF SINGLE NANOCRYSTAL OF TRANSITION METAL OXIDES

Miss Jirathana Phungphadung

A Thesis Submitted in Partial Fulfillment of the Requirements
for the Degree of Master of Engineering in Chemical Engineering
Department of Chemical Engineering
Faculty of Engineering
Chulalongkorn University
Academic Year 2001
ISBN 974-03-1317-5

Thesis Title	Effect of crystallite size and calcination temperature on the thermal stability of single nanocrystal of transition metal oxides
By	Miss Jirathana Phungphadung
Field of study	Chemical Engineering
Thesis Advisor	Professor Piyasan Praserthdam, Dr.Ing.
Thesis Co-advisor	Miss Waraporn Tanakulrungsank, D.Eng.

Accepted by the Faculty of Engineering, Chulalongkorn University in Partial Fulfillment of the Requirements for the Master's Degree

.....……..……...Dean of Faculty of Engineering
(Professor Somsak Panyakeow, D.Eng.)

Thesis Committee

.....Chairman
(Associate Professor Ura Pancharoen, D.Eng.Sc.)

.....Thesis Advisor
(Professor Piyasan Praserthdam, Dr.Ing.)

.....Thesis Co-advisor
(Waraporn Tanakulrungsank, D.Eng.)

.....Member
(Suphot Phatanasri, D.Eng)

.....Member
(Assistant Professor M.L. Supakanok Thongyai, Ph.D.)

จิรธนา ผึ่งผดุง: ผลของขนาดผลึกและอุณหภูมิในการเผาที่มีต่อความเสถียรทางความร้อนของผลึกเดี่ยวขนาดนาโนเมตรของออกไซด์ของโลหะทรานซิชัน (EFFECT OF CRYSTALLITE SIZE AND CALCINATION TEMPERATURE ON THE THERMAL STABILITY OF SINGLE NANOCRYSTAL OF TRANSITION METAL OXIDES) อ. ที่ปรึกษา : ศ. ดร.ปิยะสาร ประเสริฐธรรม, อาจารย์ที่ปรึกษาร่วม: อ. ดร. วราภรณ์ ธนะกุลรังสรรค์, 105 หน้า ISBN 974-03-1317-5

ผลึกเดี่ยวขนาดนาโนเมตรของโครเมียม(III)ออกไซด์ (Cr_2O_3) สังเคราะห์ได้จากปฏิกิริยาไกลโคเทอร์มอลของโครเมียมอะเซติลอะเซโตเนต ในสารละลาย 1,4-บิวเทนไดออล ที่อุณหภูมิ 250 และ 300 องศาเซลเซียส ผลิตภัณฑ์ที่ได้มีลักษณะอสัณฐาน เมื่อเผาที่อุณหภูมิ 350 องศาเซลเซียส จะได้ผลึกโครเมียมออกไซด์ ผลิตภัณฑ์ที่ได้จากการสังเคราะห์ที่อุณหภูมิต่ำกว่าจะได้ผลึกที่มีขนาดเล็กกว่า หลังจากนั้นจึงนำผลิตภัณฑ์ที่ได้ไปทำการเผาที่อุณหภูมิตั้งแต่ 500 จนถึง 900 องศาเซลเซียส งานวิจัยนี้ได้ให้นิยามความเสถียรทางความร้อนในเทอมของ BET/BET_0 โดย BET เป็นค่าพื้นที่ผิวของผลิตภัณฑ์หลังจากผ่านการเผาที่อุณหภูมิต่างๆ และ BET_0 เป็นค่าพื้นที่ผิวของผลิตภัณฑ์ที่ได้จากการสังเคราะห์ โครเมียมออกไซด์ที่มีขนาดผลึกใหญ่กว่าจะมีความเสถียรทางความร้อนที่ดีกว่า นอกจากนี้ได้ทำการสังเคราะห์ไทเทเนียม(IV)ออกไซด์ (TiO_2) แมงกานีส(III)ออกไซด์ (Mn_2O_3) ไอรอน(III)ออกไซด์ (Fe_2O_3) ซิงก์(II)ออกไซด์ (ZnO) และนิเกิล(II)ออกไซด์ (NiO) ที่สภาวะเดียวกัน และเปรียบเทียบความเสถียรทางความร้อนของผลึกโลหะออกไซด์เหล่านี้ พบว่าความเสถียรทางความร้อนของผลึกต่างๆ จะเป็นดังนี้ คือไทเทเนียมออกไซด์ >โครเมียมออกไซด์>แมงกานีส ออกไซด์ >ไอรอนออกไซด์ >ซิงก์ออกไซด์ >นิเกิลออกไซด์ ซึ่งเป็นผลเนื่องมาจากความแตกต่างของพลังงานในการแตกพันธะของโลหะออกไซด์เหล่านี้

ภาควิชา……วิศวกรรมเคมี…….. ลายมือชื่อนิสิต…….

สาขาวิชา……วิศวกรรมเคมี…… ลายมือชื่ออาจารย์ที่ปรึกษา……..…

ปีการศึกษา..……2544……. ลายมือชื่ออาจารย์ที่ปรึกษาร่วม……...

#4370250421 : MAJOR CHEMICAL ENGINEERING
KEY WORD: metal oxide/thermal stability/nanocrystalline/glycothermal

JIRATHANA PHUNGPHADUNG : EFFECT OF CRYSTALLITE SIZE AND CALCINATION TEMPERATURE ON THE THERMAL STABILITY OF SINGLE NANOCRYSTAL OF TRANSITION METAL OXIDES THESIS ADVISOR: PROF. PIYASAN PRASERTHDAM, Dr.Ing. THESIS CO-ADVISOR: WARAPORN TANAKULRUNGSANK, D.Eng. 105 pp. ISBN 974-03-1317-5

Single nanocrystalline chromium(III)oxide, Cr_2O_3, has been synthesized by glycothermal reaction of chromium acetylacetonate in 1,4-butanediol at 250°C and 300°C. The amorphous products changed to chromium oxide crystal after calcined at 350°C. The product obtained from lower reaction temperature has smaller crystallite size. The product was calcined at temperature range of 500 to 900°C. In this work thermal stability was defined as BET/BET_0 where BET is the surface area of the product after calcined at various temperatures and BET_0 is the surface area of the as-synthesized product. Chromium oxide with larger crystallite size exhibited higher thermal stability. Titanium(IV)oxide (TiO_2), manganese(III)oxide (Mn_2O_3), iron(III)oxide (Fe_2O_3), zinc(II)oxide (ZnO) and nickel(II)oxide (NiO) were synthesized by the same preparation method and the thermal stability of transition metal oxides were compared. The thermal stability of the metal oxides revealed in the order of; TiO_2> Cr_2O_3> Mn_2O_3> Fe_2O_3> ZnO> NiO, which resulted from the difference in the bond dissociation energy of these metal oxides

Department…Chemical Engineering…… Student's signature……
Field of Study Chemical Engineering….. Advisor's signature……...
Academic year……2001……...Co-advisor's signature……...

ACKNOWLEDGEMENTS

The author would like to express her greatest gratitude to her advisor, Professor Dr. Piyasan Praserthdam for his invaluable guidance throughout this study. Special thanks to Dr. Waraporn Tanakulrungsang, her co-advisor, for her kind supervision of this research. In addition, I would also be grateful to Associate Professor Ura Pancharoen, as the chairman, Dr. Suphot Phatanasri and Assistant Professor M.L. Supakanok Thongyai, as the member of thesis committee.

Many thanks for his kind suggestions and useful help to Mr. Okorn Mekasuwandumrong and many best friends in Chemical Engineering department who have provided encouragement and cooperation throughout this study.

Finally, she also would like to dedicate this thesis to her parent who have always been the source of her support and encouragement.

CONTENTS

	PAGE
ABSTRACT (IN THAI).....	iv
ABSTRACT (IN ENGLISH).....	v
ACKNOWLEDGEMENTS.....	vi
LIST OF TABLES.....	ix
LIST OF FIGURES.....	xi
CHAPTER	
I INTRODUCTION.....	1
II LITERATURE REVIEWS.....	5
III THEORY.....	10
3.1 Catalytic properties for transition metal oxides.....	10
3.2 Bulk structure of transition metal oxide.....	13
3.3 Preparation of unsupported single component oxides	14
IV EXPERIMENTAL.....	20
4.1 Chemicals.....	20
4.2 Instrument and apparatus.....	21
4.3 Synthesis of metal oxides.....	23
4.4 Characterization.....	23
V RESULTS AND DISCUSSION.....	27
5.1 Formation of transition metal oxides.....	27
5.1.1 Formation of pure chromium oxide.....	27
5.1.2 Formation of pure titanium oxide.....	39
5.1.3 Formation of pure manganese oxide.....	45
5.1.4 Formation of pure iron oxide.....	56
5.1.5 Formation of pure zinc oxide.....	63
5.1.6 Formation of pure nickel oxide.....	71
5.2 Determination of the thermal stability of the products	76
VI CONCLUSIONS AND RECOMMENDATION.....	86
6.1 Conclusions.....	86
6.2 Recommendation for future studies.....	86
REFERENCES.....	87

CONTENTS (CONT.)

	PAGE
APPENDICES	90
Appendix A. CALCULATION OF CRYSTALLITE SIZE……..	91
Appendix B. CALCULATION OF SPECIFIC SURFACE AREA.....…….	94
Appendix C. CALCULATION OF CRYSTALLITE SIZE FROM TEM PHOTOGRAPH.....	97
VITA.....	105

LIST OF TABLES

TABLE **PAGE**

1.1 Examples of chemical processes that make use of transition metal oxides…….. 1

3.1 Properties that are important in the surface chemistry of transition metal oxides……. 10

3.2 Oxidation states and stereochemistry of Chromium…… 11

4.1 Operation condition of gas chromatograph (GOW-MAC)……. 24

5.1 BET surface area and crystallite size of the as-synthesized and calcined products chromium oxide synthesized at different reaction temperature…… 32

5.2 BET surface area and crystallite size of the as-synthesized and calcined products titanium oxide synthesized at different reaction temperature……. 42

5.3 BET surface area and crystallite size of the as-synthesized and calcined products manganese oxide synthesized at different reaction temperature……..……... 49

5.4 BET surface area and crystallite size of the as-synthesized and calcined products iron oxide synthesized at different reaction temperature…… 58

5.5 BET surface area and crystallite size of the as-synthesized and calcined products zinc oxide synthesized at different reaction temperature…… 67

5.6 BET surface area and crystallite size of the as-synthesized and calcined products nickel oxide synthesized at different reaction temperature…… 73

5.7 Thermal stability data for metal oxides synthesized at different temperature…… 79

5.8 Crystallite size data of product before calcination (d_0) and calcined product at 900°C…… 82

5.9 Strength of chemical bonds between metal ion and oxygen ion…… 84

LIST OF TABLES (CONT.)

TABLE **PAGE**

5.10 Heat of formation of transition metal oxides……. 85
C.1 The particle size of chromium oxide synthesized at 250°C observed from TEM photograph……. 98
C.2 The particle size of chromium oxide synthesized at 300°C observed from TEM photograph…….. 99
C.3 The particle size of titanium oxide synthesized at 300°C observed from TEM photograph……. 100
C.4 The particle size of manganese oxide synthesized at 300°C observed from TEM photograph……. 101
C.5 The particle size of iron oxide synthesized at 300°C observed from TEM photograph…… 102
C.6 The particle size of zinc oxide synthesized at 200°C observed from TEM photograph……. 103

LIST OF FIGURES

FIGURE **PAGE**

4.1 Schematic diagram of the autoclave reactor……..…… 22

4.2 Schematic diagram of the reaction apparatus for the synthesis of metal oxides…….. 22

4.3 Schematic diagram of BET apparatus system……... 26

5.1 XRD patterns of as-synthesized product obtained from reaction of Cr acetylacetonate (a) at 250°C and (b) at 300°C…… 28

5.2 XRD patterns of chromium oxide obtained after calcined at 350°C of product (a) synthesized at 250°C and (b) synthesized at 300°C.. 29

5.3 TGA thermogram of product obtained from reaction of Cr acetylacetonate at 300°C……. 29

5.4 XRD patterns of chromium oxide synthesized at 250 °C after calcined at (a) 350°C (b) 500°C (c) 600°C (d) 700°C (e) 800°C and (f) 900°C……... 30

5.5 XRD patterns of chromium oxide synthesized at 300 °C after calcined at (a) 350°C (b) 500°C (c) 600°C (d) 700°C (e) 800°C and (f) 900°C…….…….. 31

5.6 (a) TEM photograph of as-synthesized product obtained from reaction of Cr acetylacetonate at 250°C (b) TEM photograph of chromium oxide synthesized at 250°C after calcined at 350°C. **(**c) TEM photograph of chromium oxide synthesized at 250°C after calcined at 600°C **(**d**)** TEM photograph of chromium oxide synthesized at 250°C after calcined at 800°C (e**)** TEM photograph of chromium oxide synthesized at 250°C after calcined at 900°C.. 33

5.7 (a) TEM photograph of as-synthesized product obtained from reaction of Cr acetylacetonate at 300°C (b) TEM photograph of chromium oxide synthesized at 300 °C after calcined at 350°C. (c) TEM photograph of chromium oxide synthesized at 300°C after calcined at 600°C (d) TEM photograph of chromium oxide

LIST OF FIGURES (CONT.)

FIGURE **PAGE**

synthesized at 300°C after calcined at 800°C (e**)** TEM photograph of chromium oxide synthesized at 300°C after calcined at 900°C.. 36

5.8 XRD patterns of titanium oxide synthesized at 250°C (a) before and after calcined at (b) 500°C (c) 600°C (d) 700°C (e) 800°C and (f) 900°C……. 40

5.9 XRD patterns of titanium oxide synthesized at 300°C (a) before and after calcined at (b) 500°C (c) 600°C (d) 700°C (e) 800°C and (f) 900°C…… 41

5.10(a) TEM photograph of as-synthesized titanium oxide synthesized at 250°C (b)TEM photograph of titanium oxide synthesized at 250°C after calcined at 900°C…….. 43

5.11(a) TEM photograph of as-synthesized titanium oxide synthesized at 300°C (b)TEM photograph of titanium oxide synthesized at 300°C after calcined at 900°C…….. 44

5.12 XRD patterns of as-synthesized product obtained from reaction of Mn acetylacetonate at (a) 250°C and (b) 300°C……... 46

5.13 XRD patterns of manganese oxide obtained after calcined at 500°C of product (a) synthesized at 250°C and (b) synthesized at 300°C…… 47

5.14 TGA thermogram of product obtained from reaction of Mn acetylacetonate at 250°C……... 47

5.15 TGA thermogram of product obtained from reaction of Mn acetylacetonate at 300°C……... 48

5.16 XRD patterns of manganese oxide synthesized at 250°C after calcined at (a) 500°C (b) 600°C (c) 700°C (d) 800°C (e) 900°C and (f) 1000°C…….. 50

5.17 XRD patterns of manganese oxide synthesized at 300°C after calcined at (a) 500°C (b) 600°C (c) 700°C (d) 800°C (e) 900°C

LIST OF FIGURES (CONT.)

FIGURE **PAGE**

and (f) 1000°C…….. 51

5.18 (a) TEM photograph of as-synthesized product synthesized at 250°C(b) TEM photograph of manganese oxide synthesized at 250°C after calcined at 500°C (c) TEM photograph of manganese oxide synthesized at 250°C after calcined at 900°C…….. 52

5.19 (a) TEM photograph of as-synthesized product synthesized at 300°C(b) TEM photograph of manganese oxide synthesized at 300°C after calcined at 500°C (c) TEM photograph of manganese oxide synthesized at 300°C after calcined at 900°C…….. 54

5.20 XRD patterns of iron oxide obtained from synthesized at (a) 250°C and (b) 300°C…… 57

5.21 XRD patterns of iron oxide synthesized at 250°C (a) before and after calcined at (b) 500°C (c) 600°C (d) 700°C (e) 800°C and (f) 900°C…… 59

5.22 XRD patterns of iron oxide synthesized at 300°C (a) before and after calcined at (b) 500°C (c) 600°C (d) 700°C (e) 800°C and (f) 900°C…… 60

5.23 (a) TEM photograph of as-synthesized iron oxide synthesized at 250°C (b) TEM photograph of iron oxide synthesized at 250°C after calcined at 900°C……..…. 61

5.24 (a) TEM photograph of as-synthesized iron oxide synthesized at 300°C (b) TEM photograph of iron oxide synthesized at 300°C after calcined at 900°C……..…. 62

5.25 XRD patterns of zinc oxide synthesized at 200°C (a) before and after calcined at (b) 500°C (c) 600°C (d) 700°C (e) 800°C and (f) 900°C…… 64

5.26 XRD patterns of zinc oxide synthesized at 250°C (a) before and after calcined at (b) 500°C (c) 600°C (d) 700°C (e) 800°C and

LIST OF FIGURES (CONT.)

FIGURE **PAGE**

(f) 900°C…… 65
5.27 XRD patterns of zinc oxide synthesized at 300°C (a) before and after calcined at (b) 500°C (c) 600°C (d) 700°C (e) 800°C and (f) 900°C…… 66
5.28(a) TEM photograph of as-synthesized zinc oxide synthesized at 200°C (b) TEM photograph of zinc oxide synthesized at 200°C after calcined at 900°C……..…. 68
5.29(a) TEM photograph of as-synthesized zinc oxide synthesized at 250°C (b) TEM photograph of zinc oxide synthesized at 250°C after calcined at 900°C……..…. 69
5.30(a) TEM photograph of as-synthesized zinc oxide synthesized at 300°C (b) TEM photograph of zinc oxide synthesized at 300°C after calcined at 900°C……..…. 70
5.31 XRD patterns of as-synthesized product obtained from reaction of Ni acetylacetonate (a) at 250°C and (b) at 300°C…… 72
5.32 TGA thermogram of product obtained from reaction of Ni acetylacetonate at 300°C……... 72
5.33 XRD patterns of nickel oxide synthesized at 300°C (a) before and after calcined at (b) 500°C (c) 600°C (d) 700°C (e) 800°C and (f) 900°C…… 74
5.34 (a) TEM photograph of as-synthesized nickel oxide synthesized at 300°C (b) TEM photograph of nickel oxide synthesized at 300°C after calcined at 900°C……..…. 75
5.35 Mechanism of glycothermal reaction for the titanium oxide formation…… 76
5.36 Mechanism of glycothermal reaction for the metal oxides formation (where M = Cr,Fe and Zn)……. 77
5.37 Propose mechanism of glycothermal reaction for the metal oxides

LIST OF FIGURES (CONT.)

FIGURE **PAGE**

formation (where M = Ni and Mn)……...……. 77

5.38 The relation between log BET/BET_0 and log T (K)/$\sqrt{d_0}$ of metal oxides synthesized at different reaction temperature….. 80

5.39 Relation between d/d_0 versus d_0 of different metal oxides……. 83

A.1 The observation peak of chromium oxide to calculate the crystallite size…….. 92

A.2 The graph indicating the value of the line broadening attribute to the experimental equipment from the α-alumina standard…… 93

C.1 TEM photograph of as-synthesized chromium oxide…… 98

C.2 The particle size distribution of chromium oxide synthesized at 250°C……. 99

C.3 The particle size distribution of chromium oxide synthesized at 300°C……. 100

C.4 The particle size distribution of titanium oxide synthesized at 300°C……. 101

C.5 The particle size distribution of manganese oxide synthesized at 300°C……. 102

C.6 The particle size distribution of iron oxide synthesized at 300°C. 103

C.7 The particle size distribution of zinc oxide synthesized at 200°C. 104

CHAPTER I

INTRODUCTION

Transition metal oxides are technologically important materials that have found many applications. For example, in the chemical industry, these oxides are the functional components in the catalyst used in a large number of processes to convert hydrocarbons to other chemicals. They are also used as electrode materials in electrochemical processes.

Among these applications, the use of transition metal oxides as catalysts is the most technologically advanced and economically important. It is also an area in which much progress has been made in recent years in terms of the understanding of the fundamental processes that occur, primarily because advances in instrumentation and experimental techniques have made it possible to study the chemistry of the interface between the transition metal oxide and the fluid phase in greater detail than ever before. In addition to being used as catalysts, transition metal oxides are also precursors for other important catalysts. Some of the chemical processes that make use of transition metal oxides are list in Table 1.1

Table 1.1 Examples of chemical processes that make use of transition metal oxides.

Process	Example
Oxidative dehydrogenation	Production of formaldehyde from methanol and butadiene from butenes
Selective oxidation	Production of maleic anhydride from benzene or butene
Selective ammoxidation	Production of acrylonitrile from propene
Selective reduction	Reduction of NO, selective hydrogenation of unsaturated ketones
Water-gas shift	Production of hydrogen

In catalysis field, both supported chromium and chromium oxide (Cr_2O_3) have been known for many decades as active in many reaction such as polymerization [1], dehydrogenation and dehydrocyclization [2-7] and selective catalytic reduction of NOx with ammonia [8]. Chromium oxide is a superb support for oxidation catalysts, particularly oxidation catalysts for total conversion of the combustibles to CO_2 and water vapor. Moreover, chromium oxide surface films that form on alloy surfaces are the basis for providing high-temperature corrosion resistance [9]. Chromium oxide powders are widely used in the preparation of plasma-sprayed wear-resistant coatings in e.g.textiles and chemical industries [10].

The synthesis of Cr_2O_3 nanoparticles has been carried out by various techniques, e.g., precipitation [11], mechanochemical reaction and subsequent heat treatment[12], oxidation chromium in oxygen [13], sol-gel method [10,14], cryogel method [15] and sonochemical method [16].

There are many processes to synthesis metal oxide. Oxides can be prepared in the form of single crystals, or polycrystalline or amorphous samples [17]. For studies where surface atomic arrangements need to be known, single crystal samples are used from well-ordered crystallographic surface planes can be prepared. There are many well-established methods to grow single crystals. For most practical purposes where a large specific surface area is essential. Among the approaches being taken to achieve the preceding goal is the development of method for producing very fine-grained materials. So nanostructure materials are very interested because they can have properties quite different from conventional materials.

Materials are called “nanostructured” when their average grain or structural domain sizes are below 100 nm. The physical and chemical properties of these materials have drawn considerable attention from researchers in the field of catalysts, semiconductors and ceramics. Nanostructured catalysts not only have higher surface area, but also are expected to show improved catalytic activity and selectivity. The development of new synthesis methods for high-volume production of nanometer-sized materials is currently of high interest for the production of catalysts as well as for other uses that may benefit from powders having very fine crystallite sizes.

In most of the synthetic processes, the alkoxides are hydrolyzed in an alcoholic solution yielding amorphous (or hydrated) metal oxide with large-surface area, however their surface areas are drastically decreased on calcination at the temperatures where corresponding oxide begin to crystallize. Recently, Inoue et al. have examined the thermal reaction of metal alkoxide in glycols or other organic media and demonstrated that a number of novel or characteristic crystalline products can be obtained directly without bothersome procedures such as purification of the reactants or handling in inert atmosphere.

In this work, single nanocrystalline of chromium oxide and other transition metal oxide were prepared by thermal reaction in organic solvents, which is called the Glycothermal method. The study of the thermal stability of chromium oxide and other transition metal oxides in the first series in periodic table with different as-synthesized crystallite size was shown by the correlation between the as-synthesized crystallite size and the calcination temperature. The objectives of this work is:

1. To study the effect of crystallite size on thermal stability of nanocrystalline chromium oxide and other transition metal oxide in the first series of periodic table.

2. To obtain the novel method in synthesis of nanocrystalline chromium oxide with higher specific surface area.

The present study is arranged as followed

Chapter II presents a literature reviews of the novel synthesis of metal oxides in organic media.

Chapter III presents the theory that related to this work. Physical and chemical properties of chromium oxide, preparation processes, chromium oxide uses and others.

The experimental systems and the catalyst preparation are presents in Chapter IV.

Chapter V is including of the experimental results of the characterization of catalyst samples. The X-Ray Diffraction (XRD) patterns, BET surface area are explained.

The overall conclusion emerged from this research are follow in Chapter VI.

The samples of calculation of BET surface area and crystallite size are given in APPENDICES parts at the end of this thesis.

CHAPTER II

LITERATURE REVIEWS

Recently much attention has been denoted on the catalyst preparation to fine the methods that produced materials having good catalytic properties. Transition metal oxide play major roles in catalysis field.

For chromium oxide, there are many studies involved supported chromium oxide catalysts [1-7]. The supports that are widely use for supported chromium oxide catalyst are Al_2O_3, TiO_2, SiO_2 and ZrO_2. These chromium oxide-based catalysts are active in dehydrogenation reaction of alkane compounds. It has been accepted that the species form of chromium oxide determines the catalytic properties of these systems. Most of studies have been focus on behavior of chromium species on support's surface. Another part of studies is about preparation of chromium oxide powders. M.Chatterjee [10] has synthesis chromium oxide microspheres by the sol-gel method. The solvent extraction technique was followed for the preparation of the sols. The dried microspheres were heat-treated at 200-1300°C with 1 h at different temperature. The gel was found to show initial crystallization of Cr_2O_3 at 400 °C and complete crystallization at about 1300 °C. Spherical powder after calcination at 1300 °C showed a particle size range of 3-10 μm.

A. E. Gash et.al [14] reported the new sol-gel synthetic route of transition metal oxide by using inorganic salt precursor instead of metal alkoxides precursor. They report the use of epoxides as gelation agents for the sol-gel synthesis of chromia aerogel from simple Cr (III) inorganic salts. Preliminary synthetic studies have shown that this method can be used to prepare monolithic aerogels of other transition and main group metal oxides, as long as the formal oxidation state of the precursor metal ion is $\geq 3+$.

With application of aerogel method, Kirchnerova [15] preparation of alumina and chromia cryogel-based catalyst. Word " Cryogel " is come from using freeze-drying process in gel-dried step in aerogel method. This method has several

advantages: wide range of low cost precursors, low cost solvent but the morphology of product obtained from this method are amorphous with low surface area.

Sonochemical method is another method for preparation of chromium oxide powders. Arul Dhas et.al [16] studies the preparation of ultrafine chromium oxide and manganese oxide powder by the application of ultrasound irridation which call sonochemical method. They used $(NH_4)_2Cr_2O_7$ dissolved in distilled water. The resulting saturated solution was exposed to high-intensity ultrasound radiation. The resulting solid product was washed throughly with hot water and ethanol and dried in vacuum. Chromium oxide and manganese oxides obtained from this method are amorphous. When the products were heat-treated, chromium oxide displays its crystallization at about 627 °C. On the other hand manganese oxide had crystallization temperature at about 527 °C. The particle size of amorphous Cr_2O_3 and Mn_2O_3 were observed by Transmission Electron Microscope (TEM) and calculated from surface area and density. The particle size that observed by TEM for amorphous Cr_2O_3 is 200 nm and 50 nm for Mn_2O_3. Particle size calculated from surface area and density of Cr_2O_3 and Mn_2O_3 are 64 and 53 nm respectively.

There is another field that can apply to synthesis of chromium oxide such as mechanochemical process [12]. Tsuzuki synthesis chromium oxide nanoparticles by mechanical milling of $Na_2Cr_2O_7$ forming amorphous Cr_2O_3.

From all studies above, various methods are used to prepare chromium oxide and other metal oxides catalyst, however the particle size of samples prepare by these method are relatively large. Hydrothermal method is one method that have been widely applied for the synthesis of a variety of ceramics materials [18-19]. Inoue et al. has developed novel method for the synthesis of several metal oxides in organic media. These methods have the advantage that the products consist of microcrystalline particles but are sufficiently high thermal stability.

Inoue et al. [20] reported that the thermal reaction of gibbsite in ethylene glycol at 250 °C yielded an ethylene glycol derivative of boehmite, in which organic moieties is incorporated covalently between the layer structure of boehmite. This

reaction has been extended to the reaction of gibbsite in higher homologues of ethylene glycol, and they have found that microcrystalline χ-alumina is formed under quite mild condition. The synthetic process as mentioned above, the use of glycol (organic solvent) instead of water in the system is different method from the conventional methods. This method was called " Glycothermal method ".

Inoue et al. [21] when gibbsite was treated in glycol at 300°C, the glycol derivative on boehmite was get. A commercial gibbsite was suspended in 1,4-butanediol. The suspension was set in 300 ml autoclave and then heated to 300°C at rate 2.5°C/min. XRD patterns showed that product comprised with α-Al_2O_3 and well crystallite boehmite. Tem pictures of product showed each α-Al_2O_3 particle was a single crystal hexagonal plate shape. Suggest that microcrystalline α-Al_2O_3 could prepare from glycothermal reaction of gibbsite.

And Inoue et al. [22] also found that this reaction in inert organic solvents such as toluene, benzene and/or others, thermal decomposition of aluminum alkoxide occurred and yielded a product compose of 4 to 20 nm particles having the χ-alumina mixture. The χ-alumina was stable and maintained a surface area above 100 m^2/g until its transformation at 1150 °C to be α-alumina. With this result, they have applied this method for zirconia synthesis and reported that thermal decomposition of zirconium alkoxides in organic solvents yielded tetragonal zirconia, which had a large surface area and a fairly high thermal stability. However, zirconium n-alkoxides which decomposed into glycols, did not decompose at 300 °C in inert organic solvent [23].

Inoue et al.[23] synthesized thermally zirconia by hydrolysis of zirconium alkoxides. Zirconium n-butoxide suspended in toluene. In the gap 30 ml of toluene was added and then heated to 200-300 °C and held at this temperature for 2 h. When autoclave was cooled, 30 ml of distilled water was added. The autoclave was heated again at 250-300 °C in the same way. and the nanocrystalline (5.8 nm) monoclinic zirconia, which showed high thermal stability, was retained. And the obtained zirconia maintained large surface area of 162 and 72 m^2/g even after calcination at

500 °C and 900 °C. And the pretreatment in toluene above 250 °C was essential avoid the formation of tetragonal formed.

Inoue et al. [24] found that microcrystalline binary oxide were directly formed when a mixture of two alkoxides, acetylacetonate and/or acetates was heated in 1,4-butanediol at elevated temperature under autogeneous pressure of the glycol (glocothermal reaction). An example was synthesis was synthesis of gadolinium gallium garnets (GGG) by reaction of mixed gallium acetylacetonate with gadolinium acetate. This reaction has been extended to the reaction of a stoichiometric mixture of aluminium isopropoxide (AIP) and yittrium acetate, and found that crystalline yittrium aluminium garnet (YAG) is formed under similar condition. No other phases were detected. The uncalcined YAG had a large surface area (107 m^2/g) which decreased to 44 m^2/g and 10 m^2/g after calcination at 1000 °C and 1300 °C. YAG was composed of agglomerates of almost spherical particles having a relatively narrow size distribution with an average particle size of approximately 30 nm. The use of ethylene glycol instead of 1,4-butanediol in the synthetic system afforded amorphous product [25].

Kominami et al. [26] synthesized the microcrystalline titanium (IV) oxide in the anatase form by thermal decomposition of titanium (IV) alkoxide in organic solvent. Titanium-tert-butoxide (TTB) dissolved in organic solvent in test tube. In the gap between the autoclave wall and the test tube, 30 ml of solvent was added. Autoclave was heated to 300 °C. The products had a crystallite size of 9 nm and a surface area higher than 100 m^2/g. Primary and Secondary alkoxides were not decomposed in the similar conditions, indicating that the thermal stability of C-O bonds in alkoxides was a decisive factor of their decomposition. The products shown high surface area even after calcine at 550 °C. This product had high photocatalytic activity in the photocatalytic mineralization of acetic acid in aerated aqueous solutions because of the high crystallinity and high surface area.

Kominami et al. [27] synthesized the nanosized titanium (IV) oxide in the anatase form by hydrolysis of titanium (IV) alkoxide. Titanium n-butoxide dissolved in toluene in test tube. In the gap between the autoclave wall and the test tube, mixture

of toluene and water was added. When the temperature rose, water was dissolved at high temperature (150-300 °C). The elevation of the reaction temperature and an increased of reaction time had effect on the crystallite sized of products. In this method, rutile transformation temperature was higher and the thermal stability was improved. For example product obtained by the reaction at 300 °C for 24 h possessed a surface area of 54 m^2/g even after calcination at 900 °C and began to transform to the rutile phase at around 1000 °C.

Many papers as mentioned above, the synthesis of several metal oxides and binary metal oxides in organic solvents are explained. The product was produced by this novel method have a large surface area and high thermal stability. This novel method may be a new route to prepare micro- and nanocrystalline metal oxides.

CHAPTER III

THEORY

3.1 Catalytic properties for transition metal oxides

Understanding catalysis requires an understanding of surface chemistry, which deals with the bonding and reaction of an adsorbate with the surface and the influence of the surface on the bonding and reaction between adsorbates. It is apparent that an important part of any effort toward obtaining such an understanding is the ability to characterize the physical and chemical properties of a surface. In recent years much progress has been made in the understanding of metallic surface. There are significant differences between the chemistry of transition metal oxides and the corresponding metals. Table 3.1 provides a list of properties that are important in the surface chemistry of transition metal oxides. Many of them either do not apply or apply only to a limited extent to the metals.

Table 3.1 Properties that are important in the surface Chemistry of transition metal oxides.

Presence of cations and anions in stoichiometric ratios and in well defined structural relationships
Possibility of covalent and ionic bonding between cations and anions
Presence of a strong electric field normal to the surface due to the coulombic nature of the ionic lattice
Presence of surface acidity and basicity
Presence of cationic and anionic vacancies
Ability of cations to undergo oxidation and reduction
High mobility of lattice oxygen and the possibility that the lattice oxygen are reactants in a reaction

3.1.1 Chromium oxide

Chromium (atomic number 24) belong to Group VIB of the periodic table whose other members are molybdenum and tungsten. An early application of chromium compounds was as pigments, particularly chrome yellow, $PbCrO_4$. The most important application of chromium, namely its use as an alloying element. In it compounds, chromium may use any of its six *3d* and *4s* electrons and may show any oxidation state from –2 to +6.

The various oxidation states and sterochemistry are summarized in Table 3.2.

Table 3.2 Oxidation states and stereochemistry of Chromium

Oxidation state	Coordination number	Geometry	Example
Cr(-II)	-	-	$Na_2[Cr(CO)5]$
Cr(-I)	6	octahedral	$Na_2[Cr_2(CO)_{10}]$
Cr(0)	6	octahedral	$Cr(CO)_6$
Cr(I)	6	octahedral	$[Cr(C_6H_5)_2]$
Cr(II)	4	tetrahedral	$CrCl_2(CH_3CN)_2$
	6	octahedral	$CrCl_2$
Cr(III)	4	tetrahedral	$CrCl_4$
	6	octahedral	Cr_2O_3
Cr(IV)	4	tetrahedral	Ba_2CrO_4
	6	octahedral	CrO_2
Cr(V)	4	tetrahedral	CrO_4^{3-}
	6	octahedral	$[CrOCl_5]$
	8	dodecahedral	CrO_8^{3-}
Cr(VI)	4	tetrahedral	CrO_3
			CrO_2Cl_2

Those of +2, +3 and +6 are the most important, whereas the –1 and –2 oxidation states are of little significance. Commercial applications center about +6 state, with some interest in the +3 state. Research interest at the present centers around kinetic studies involving the +3 state and structural studies of the π-bonded complexes of the lower oxidation states.

Chromium (III) Oxide, Cr_2O_3, has the rhombohedral structure of α-Al_2O_3 and α-Fe_2O_3.

3.1.2 Titanium oxide (TiO_2)

Titania has attracted attention as interesting supports for metal catalysts such as Pt and Pd, since strong interaction was found between the oxides and the metals. On the other hand, titania were found to exhibit super acidity when combine with a small amount of SO_4^{2-}. Titania is also used as a good catalyst for photocatalytic reaction.

3.1.3 Manganese Oxide (Mn_2O_3)

Manganese oxide are generally active catalysts for oxidation reactions and also active electrode materials for dry cell. Probably due to the high oxidation activity, very few studies have been reported foe acid-base properties and catalysis of Manganese oxide. MnO_2 has been claimed to be efficient for the hydration of nitriles to amides. Manganese oxide is prepared in various ways, e.g. chemical or electrochemical oxidation, hydrolysis and thermal decomposition of manganese salts.

3.1.4 Iron Oxide (Fe_2O_3)

α- and γ-Fe_2O_3, Fe_3O_4 and FeO are ordinary oxides of iron. Iron oxide catalysts are practically used for oxidation or dehydrogenation reactions as single oxides promoted by alkalis or as mixed oxides. Typical examples are dehydrogenation

of ethyl benzene, water gas shift reaction (Fe_2O_3-Cr_2O_3), ammoxidation of propylene (Fe_2O_3-Sb_2O_5) and dehydrogenation of methanol (Fe_2O_3-MoO_3).

3.1.5 Nickel Oxide (NiO)

Nickel oxide has high catalytic activity for hydrogenation and isomerization of olefins. NiO mixed with solid acids such as SiO_2, SiO_2-Al_2O_3 are active for dimerization of olefins. The active site has been suggested to be a combination of a low valent nickel and an acid site.

3.1.6 Zinc Oxide (ZnO)

ZnO is being coordinated with four oxide ions. ZnO produces H_2 and CO_2 from formic acid. This selectivity indicates that ZnO is a solid base. The acidity and basicity increase when ZnO is mixed with other oxides. ZnO-TiO_2 reveals high activity for hydration of ethylene. A mixed oxide catalyst consisting of ZnO and Fe_2O_3 is a good basic catalysts for the methylation by mathanol of phenol to 2,6-xylenol.

3.2 Bulk structure of transition metal oxide

With the exception of some complex oxides of unusual stoichiometries, multicomponent compounds and oxides that are only stable at high temperature and high pressure, the bulk structures of most transition metal oxides are known. An examination of the known structures shows that transition metal oxides exist in many different crystallographic forms. There does not appear to be a simple generalization that relates the structure to the stoichiometry or the position in the periodic table. There is perhaps one generalization which is the fact that the ionic radii of transition metals are smaller than that of O^{2-}. Thus the oxygen ions are usually close-packed with the smaller metal ions situated in the octahedral and tetrahedral holes among the oxygen ions.

Oxides commonly studies as catalytic materials belong to the structural classes of corundum, rocksalt, perovskite, spinel, rutile and layer structure. These are the

structures often reported for the oxides prepared by common methods under mild conditions. In some cases, other structures exist. Furthermore, the structures indicated represent the general type.

3.3 Preparation of unsupported single component oxides

Single component oxides may be prepared by thermal oxidation of the metal. Usually, the metal samples are available in forms that have low surface area such as pellets, course powder or foils. The kinetics of oxidation is slow because lattice diffusion of metal and oxygen ion is necessary. Therefor, high temperatures are used to obtained reasonable rates. The result is that the surface areas of the oxides obtained are low.

For many practical purposes where the available surface area is critical, the oxides are commonly prepared by the decomposition of precursor compounds containing the desired metal ion in air or oxygen. Usually, preference is given to precursor compounds that decompose at low temperatures to minimize sintering of the resulting oxide, which causes low surface area. Carbonates, bicarbonates, hydroxide, nitrates and oxalates are usually preferred over sulfates for this reason. The decomposition may also be carried out in vacuo to lower the decomposition temperatures.

3.3.1 Effect of preparation method

3.3.1.1 Crystallographic Phases

It is rather common that different preparation methods result in oxides of different crystallographic phases. One example that is of significant industrial interest is the preparation of titanium oxide (TiO_2). Titanium oxide exists in three crystallographic forms: rutile, anatase and brookite. The brookite phase is seldom formed.

Common titanium compounds are not soluble in water. Very pure TiO_2 can be prepared by hydrolysis of prepurified $TiCl_4$ or Ti alkoxides. The resulting solid is best

regarded as hydrous titanium oxide. Subsequent calcination in air produces TiO_2. Normally, rutile is the predominant form, but anatase is often present in minor amounts. The anatase form can be produced by hydrolysis of Ti halides at temperature around 600 °C, or via low temperature calcining (~700 °C) of precipitated titanic acid $H_2TiO_3 \cdot nH_2O$.

The phases obtained by hydrothermal treatment of amorphous hydrous ZrO_2 gel depend on the other salts present in the mixture. Only the monoclinic phase is produced using KF or NaOH, while a mixture of both phases is produced using LiCl, KBr or no salt.

3.3.1.2 Morphology of oxide crystallites

The preparation method determines the morphology of the final product as well as its crystallographic phases. In general, the higher temperature of calcination, the coarser and the more crystalline is the final powder. Some examples of preparing different morphologies are described below.

ZnO is the first example. If ZnO is prepared at high temperature by ignition of zinc in an oxidizing atmosphere, a three-dimensional crystalline sample of a low surface area is obtained. Electron microscopy shows that the sample consists of crystallites of about 700 nm long and 300 nm wide, exposing the prismatic face on the long side and the polar faces on the short side. Small crystals grown from vapor transport are needles of hexagonal cross-section, about 0.1 cm long and 0.001 cm in diameter. A powder prepared from $ZnCO_3$ precipited from a nitrate solution with sodium carbonate followed by washing and conversion to oxide by calcining has a high surface area about 36 m^2/g. The resulting oxide contains hexagonal platelets about 15 nm across.

Haematite α-Fe_2O_3 is another example. It is reported that dirtribution of the exposed planes depends on the precipitation method and the temperature of oxygen pretreatment. Precipitation at high pH from aqueous ferric nitrate leads to the formation of geothite (α-FeOOH) with a smaller amount of haematite. Mainly haematite is formed at low pH.

In addition to preparing oxides with exposure of different crystallographic planes in the crystallites of different samples, it is also possible to prepare oxide particles of different macroscopic shapes by careful control of reaction condition.

Chromium oxide has been prepared by several methods. The physical and chemical properties of chromium oxide are quite different by the process of preparation.

3.3.2 Various preparation method

3.3.2.1 Precipitation Method

Precipitation method involves the growth of crystals from a solvent of different composition to the crystals. This is achieved by bringing the solution into supersaturation, either by changing the temperature, the salt concentration, the pH, or by exploiting the slow release of some hydrolysis products in a water solution. The solvent may be one of the constituents of the desired crystals, e.g., crystallization of salt hydrate crystals using water as the solvent. Or the solvent may be entirely separate liquid element or compound in which the crystals of interest are partially soluble, e.g., SiO_2 and various high melting silicates may be precipitated from low melting borate or halide melts.

A variety of particle sizes and shapes can be produced, depending on the reaction conditions. Moreover, the particles can be agglomerates of much finer primary particles.

Chromium oxide catalysts can be prepared by precipitate a hydrous chromium gel by adding aqueous ammonia (NH_4OH) to a solution of chromium nitrate ($Cr(NO_3)_3 \cdot 9H_2O$) at a controlled rate. The morphology of the resulting material was determined by the rate of addition of ammonia solution. For example, slow addition over 10 h of 150 ml of 1 M ammonia solution into 0.71 mol/l chromium nitrate solution resulted in precipitation of a hydrous chromia gel with a dark green color.

The rapid addition in 30 min of the same solutions and quantities as above resulted in precipitation of a hydrous gel with a light grey color. The resulting gels were then dried at 100 °C for 24 h before heating in flowing hydrogen at 380 °C for 3 h.

3.3.2.2 Sol-Gel Method

Sol-gel chemistry is based on inorganic polymerization reaction. When ultrafine colloidal dispersions lose fluid they can turn into a highly viscous mass. Such a mass is called a gel. When chemical methods are used to turn solution of metal compounds into gels, we are dealing with sol-gel process. Highly reactive and pure ceramic powders can be prepared from such gels. Two routes are usually described in the literature depending on whether the precursor is an aqueous solution of an inorganic salt or an alkoxide in an organic solvent.

For this method, preparative process of chromium oxide involves two steps

1) Preparation of a Cr(III) sol via hydrolysis of the corresponding chloride solution with an organic amine solution followed by the solvent extraction of the hydrolytic acid (HCl) generated

2) Formation of gel microspheres by producing an emulsion of sol droplets and their subsequent neutralization with a base.

3.3.2.3 Hydrothermal Method

Hydrothermal methods utilize water under pressure and at temperature above its normal boiling point as a means of speeding up the reactions between solids. The water performs two roles. The water-as solids or vapor-serves as the pressure transmitting medium. In addition, some or all of the reactants are partially soluble in the water under pressure and these enables reactions to take place in, or with the aid of, liquid and/or vapour phases. Under these conditions, reactions may occur that, in the absence of water, would occur only at much higher temperatures. The method is therefore particularly suited for the synthesis of phases that are unstable at higher temperature. It is also a useful technique for growth of single crystals, by arranging

for a suitable temperature gradient to be present in the reaction vessel, dissolution of the starting material may occur at the hot end and reprecipitation at the cooler end.

Since hydrothermal reactions must be carried out in closed vessels. The pressure- temperature relations of water at constant volume are important. The critical temperature of water is 374°C. Below 374°C, two fluid phases, liquid and vapour, can coexist. Above 374°C only one fluid phase, supercritical water ever exists. At pressures below saturated steam curve liquid water is absent and the vapour phase is not saturated with respect to steam.

The design of hydrothermal equipment is basically a tube, usually of steel, closed at one end. The other end has a scre cap with a gasket of soft copper to provide a seal. Alternatively, the bomb may be connected directly to an independent pressure sorce, such as a hydraulic ram: this is kno as the “colld seal” method. The reaction mixture and an appropriatr amount of water are placed inside the bomb which is then sealed and placed inside an oven at the required temperature.

For the growth of single crystals by hydrothermal methods it is often necessary to add mineralizer. A mineralizer is any compound added to the aqueous solution that speeds up its crystallization. It usually operates by increasing the solubility of the solute through the formation of soluble species that would not usually be in the water. For instance, the solubility of quartz in water at 400°C and 2 kbar is to small to permit the recrystallization of quartrz, in a temperature gradient, within a reasonable space of time. On addition of NaOH as a mineralizer, however, large quartz crystals may be readily grown. Using the following condition, crystals of kilogram size have been grown: quartz and 1.0 M NaOH solution are held at 400°C and 1.7 kBar: at this temperature some of the quartz dissolves. A temperature gradient is arranged to exist in the reaction vessel and at 360 °C the solution is supersaturated with respect to quartz which precipitates onto a seed crystal.

3.3.2.4 Glycothermal method

Glycothermal method has been developed for synthesis of metal oxide and binary metal oxide by using glycol solvents such as 1,4-butanediol instead of water in hydrothermal method. The use of glycol instead of water in synthetic procedure, intermediate phase occurred to be different form and have found that stabilities of the intermediate phase by this method was not strong so, this intermediate phase was easily converted to product under quite mild condition.

CHAPTER IV

EXPERIMENT

This chapter is explanation about the experimental system and the experimental procedures that used in this work. The chemicals that used in the metal oxides preparation are presented in section 4.1. The lists of experimental equipment are shown in section 4.2. In section 4.3, the metal oxides preparation is presented. The characterization is presented in section 4.4.

4.1 Chemicals

The lists of chemicals used in these experiments were shown in the following

1. Ultra high purity nitrogen gas (99.99% vol.) with oxygen and moisture content less than 3 ppm was supplied by Thai Industrial Gas Co.Ltd.
2. Chromium acetylacetonate $[CH_3COCH=C(O-)CH_3]_3Cr$ was manufactured by Aldrich ChemicalCompany, USA..
3. Iron acetylacetonate $[CH_3COCH=C(O-)CH_3]_3Fe$ was manufactured by Aldrich ChemicalCompany, USA..
4. Manganese acetylacetonate $[CH_3COCH=C(O-)CH_3]_3Mn$ was manufactured by Aldrich Chemical Company, USA..
5. Nickel acetylacetonate $[CH_3COCH=C(O-)CH_3]_2Ni$ was manufactured by Aldrich ChemicalCompany, USA..
6. Titanium tert-butoxide ($Ti[O(CH_2)_3CH_3]_4$) was manufactured by Aldrich Chemical Company, USA..
7. Zinc acetylacetonate $[CH_3COCH=C(O-)CH_3]_2Zn$ was manufactured by Merck Co., Ltd., Germany.
8. 1,4-Butanediol ($HO(CH_2)_4OH$) was manufactured by Aldrich ChemicalCompany, USA..

4.2 Instruments and apparatus

4.2.1 Autoclave reactor: The autoclave is made of stainless steel with 1000 cm^3 volume and 10 cm inside diameter. There are the iron jacket which used to reduce the volume of autoclave to be 300 ml and the beaker were used to contain the reactant. This consists of a pressure gauge within the range of 0 to 140 bar and a relief valve, which used to control pressure in the autoclave. This autoclave can be operated at high temperature and pressure. The reaction was carried out under autogenous pressure, which gradually increased as the temperature was raised.

4.2.2 Automatic Temperature controller: This consists of a magnetic switch connected to a variable voltage transfer and a RKC temperature controller connected to a thermocouple with 0.5 mm diameter attached to the reactant mixtures in autoclave.

4.2.3 Electrical furnace (Heater): This supplied the required heat for the reaction to the autoclave.

4.2.4 Gas controlling system: Nitrogen are equipped with a pressure regulator (0-150 bar) and needle valves were used to release gas from autoclave.

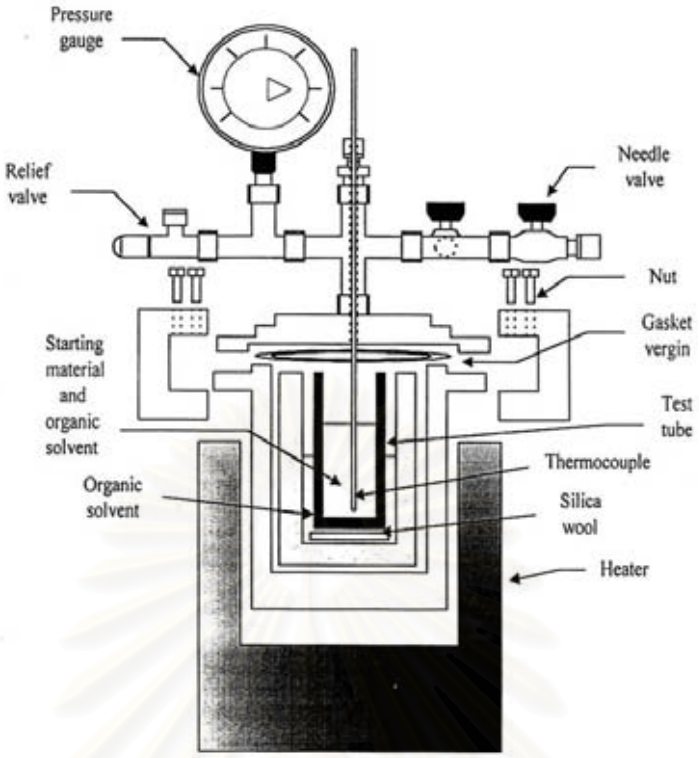

Figure 4.1 Schematic diagram of the autoclave reactor.

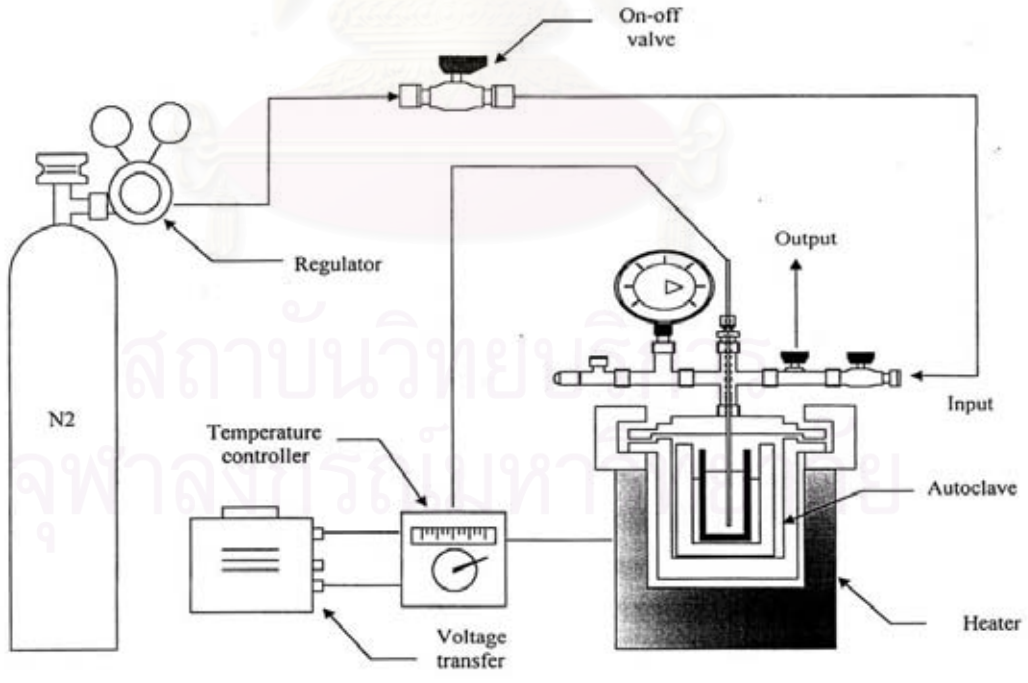

Figure 4.2 Schematic diagram of the reaction apparatus for the synthesis of metal oxides.

4.3 Synthesis of metal oxides

Metals acetylacetonate (Cr, Zn, Ni, Mn, Fe and Ti) 15g was dissolved in 100 cm^3 of organic solvents in a test tube, which was then set in an autoclave. In the gap between the test tube and autoclave wall was added with 30 cm^3 of organic solvent. The autoclave was purged with nitrogen. Then heated to the desired temperature (200 - 300 ° C) at a rate of 2.5°C min^{-1} and at that temperature for 2 h. Autogeneous pressure during the reaction gradually increased as temperature was raised. After the autoclave was cooled, the resulting powders were washed repeatedly with methanol by centrifugation and dried in air. The calcination of the thus obtained product carried out in air in a box furnace. The product was heated at a rate of 10°C min^{-1} to desired temperature (500, 600, 700, 800 and 900 °C) and held at that temperature for 1 h.

4.4 Characterization

4.4.1 X-Ray diffraction Patterns (XRD)

X-Ray Diffraction (XRD) patterns of the catalyst samples were determined by using Ni-filtered CU Kα radiation in the 2θ range of 10 to 80°C (SIEMENS XRD D5000, Petrochemical Engineering Research Laboratory, Chulalongkorn University). Crystallite size was calculated from the half-height width of the 101 diffraction peak using the Scherrer equation. The value of the shape factor, K, was taken to be 0.9 and α-Al_2O_3 was used to be internal standard. The sample of calculation was shown in APPENDIX.

4.4.2 Morphology

Morphology of the samples was observed by a JEOL TEM-200CX transmission electron microscope (TEM), which operated at 100 kV at the Scientific and Technological Research Equipment Center (STREC), Chulalongkorn University.

4.4.3 Thermogravimetric analysis (TGA)

The crystallization pattern of the samples during heating up was analyzed by Shimadzu TGA model 50. The sample was loaded in a platinum pan located in a furnace. The purging gas was N_2 with flow rate 30 ml./min. The furnace temperature was programmed to raise from room temperature to 600 °C at a constant rate of 10 °C/min. The data were displayed and record using a microcomputer.

4.4.4 BET Surface Area Measurement

The specific surface area (S_{BET}) of the samples were calculated using the Brunauer-Emmett-Teller (BET) single point method on the basis of nitrogen uptake measured at liquid-nitrogen boiling point temperature equipped with a gas chromatograph.

4.4.4.1 BET Apparatus

The apparatus of BET surface area measurement consisted of two feed lines for helium and nitrogen. The flow rate of the gas was controlled by means of fine-metering valve on the gas chromatograph. The cell which used to contain samples were made from pyrex glass. The operation condition of gas chromatograph (GOW-MAC) is shown in Table 4.1

Table 4.1 Operation condition of gas chromatograph (GOW-MAC)

Model	GOW-MAC
Detector	TCD
Helium flow rate	30 ml min^{-1}
Detector temperature	80°C
Detector current	80mA

4.4.4.2 Measurement

The mixture gases of helium and nitrogen flowed through the system at the nitrogen relative pressure of 0.3. The samples was placed in the cell, ca. 0.2 to 0.5 g, which was then heated up to 150°C and held at this temperature for 2 h. The samples was cooled to room temperature and was measured the specific surface area. There are three steps to measure the specific surface area.

Step (1) Adsorption step: The samples that set in the cell was dipped into the liquid nitrogen. Nitrogen gas that flowed through the system was adsorbed on the surface of the catalyst sample until equilibrium was reached.

Step (2) Desorption step: the cell with nitrogen gas adsorbed sample was dipped into the water at room temperature. The adsorbed nitrogen gas was desorbed from the surface of the sample. This step was completed when the indicator line was in the same position of the base line.

Step (3) Calibration step: 1 ml of nitrogen gas at atmospheric pressure was injected through the calibration port of the gas chromatograph and the area was measured. The area was the calibration peak. The calculation method is explained in APPENDIX C.

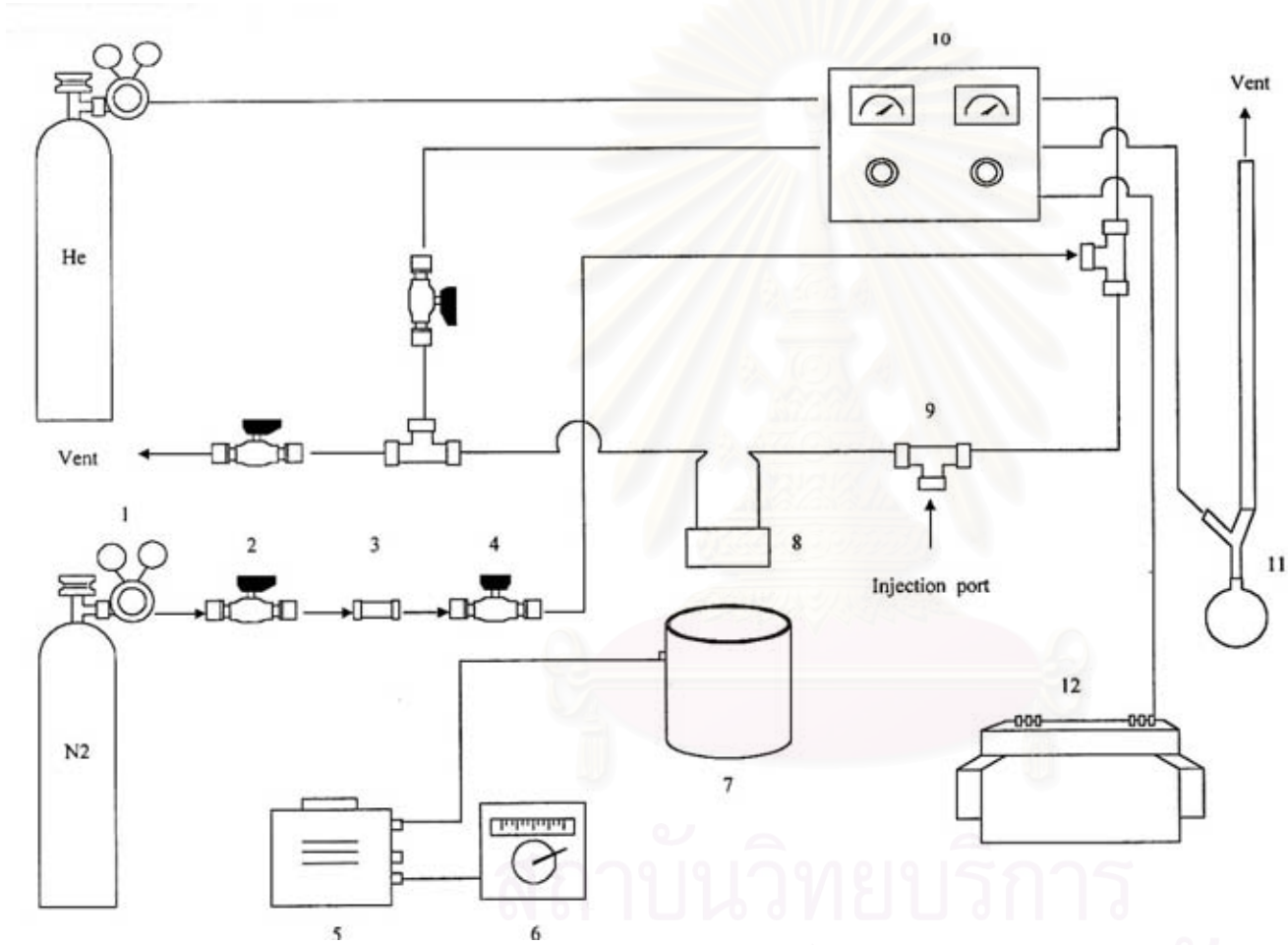

1. Pressure regulator
2. On-off valve
3. Gas filter
4. Needle valve
5. Voltage transformer
6. Temperature controller
7. Heater
8. Sample cell
9. Three-way
10. Gas chromatograph with TCD
11. Bubble flow meter
12. Indicator

Figure 4.3 Schematic diagram of BET apparatus system.

CHAPTER V

RESULTS AND DISCUSSION

This chapter can be divided into two sections. The first section concerns with the formation and characterization results of each transition metal oxides. The second section is the discussion of thermal stability of metal oxides.

5.1 Formation of transition metal oxides

The first series transition metals are including of Scandium (Sc), Titanium (Ti), Vanadium (V), Chromium (Cr), Manganese (Mn), Iron (Fe), Cobalt (Co), Nickel (Ni), Copper (Cu) and Zinc (Zn). Scandium compounds (Alkoxides and acetylacetonate) which can be used, as precursor in glycothermal reaction cannot find in commmercial sales. Vanadium oxide (V_2O_5) has melting point temperature at 690°C [28] which lower than the maximum calcination temperature used in this study. Copper oxide and Cobalt oxide have too large particle size. So in this work will study only six transition metal oxides as described below.

5.1.1 Formation of pure chromium oxide (Cr_2O_3).

Chromium oxide has been synthesized in 1,4-butanediol at different reaction temperatures (250°C and 300°C). The XRD patterns of products obtained from synthesized at 250°C and 300°C were shown in Figure 5.1. The XRD patterns of the products obtained by both reactions show amorphous structure. A TEM photograph of amorphous product is shown in Figure 5.6(a) and Figure 5.7(a) of product synthesized at 250°C and 300°C, respectively. The products that synthesized at 300°C was analyzed by thermogravimetric analysis (TGA) method, using heating rate of 10°C/min from room temperature to 800°C. From TGA curves in Figure 5.3, it is found that the differentiate weight loss during heating step are distinctly observed at 300°C. So the products obtained by both reaction were calcined at 350°C. When it was characterized by XRD, the XRD patterns in Figure 5.2 shown the crystallization

of chromium oxide are occurs. The crystallite size, which calculated by the XRD broadening at 2θ ~55°[16] was 16.2 nm for product synthesized at 250°C and 25.0 for product synthesized at 300°C. The particle size observed by the transmission electron micrographs (TEM) of the product is in good agreement with the crystallite size, indicating that each primary particle observed by TEM is a single crystal. Chromium oxide synthesized by this method has smaller crystallite size than chromium oxide synthesized by sol-gel method [10] and sonochemical method [16].

Both chromium oxide obtained from calcination at 350°C was calcined again at temperature of 500 to 900°C. The XRD patterns of all products after calcined which shown in Figures 5.4 and 5.5 were almost identical to product after calcined at 350°C except that the peaks were more sharp. Figures 5.6 and 5.7 show TEM photographs of chromium oxide before and after calcination at various temperatures. The BET surface area and crystallite size of the products synthesized at each reaction temperature was summarized in Table 5.1.

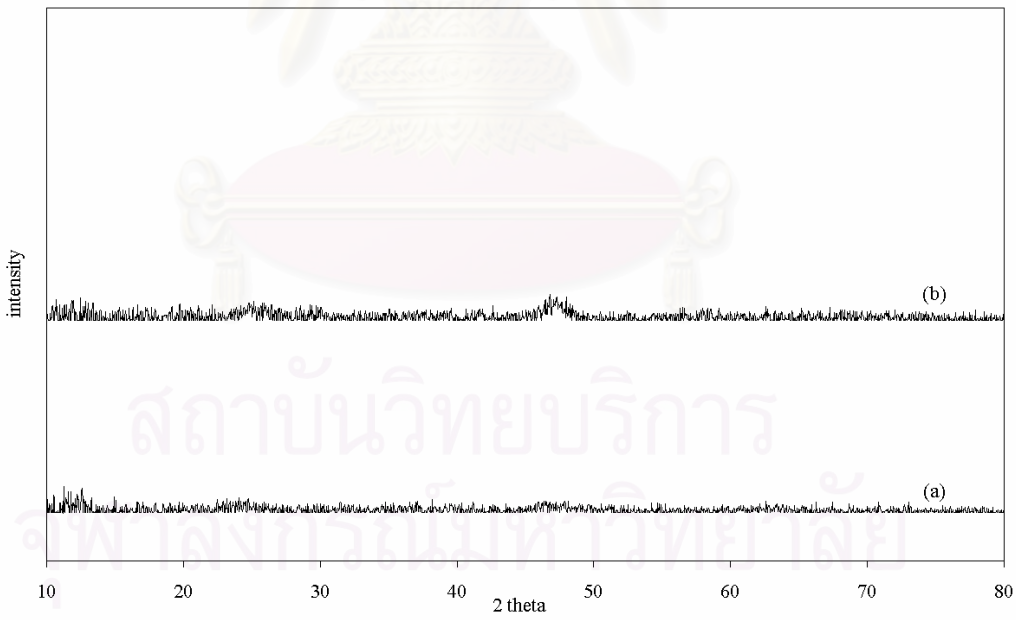

Figure 5.1 XRD patterns of as-synthesized product obtained from reaction of Cr acetylacetonate (a) at 250°C and (b) at 300°C.

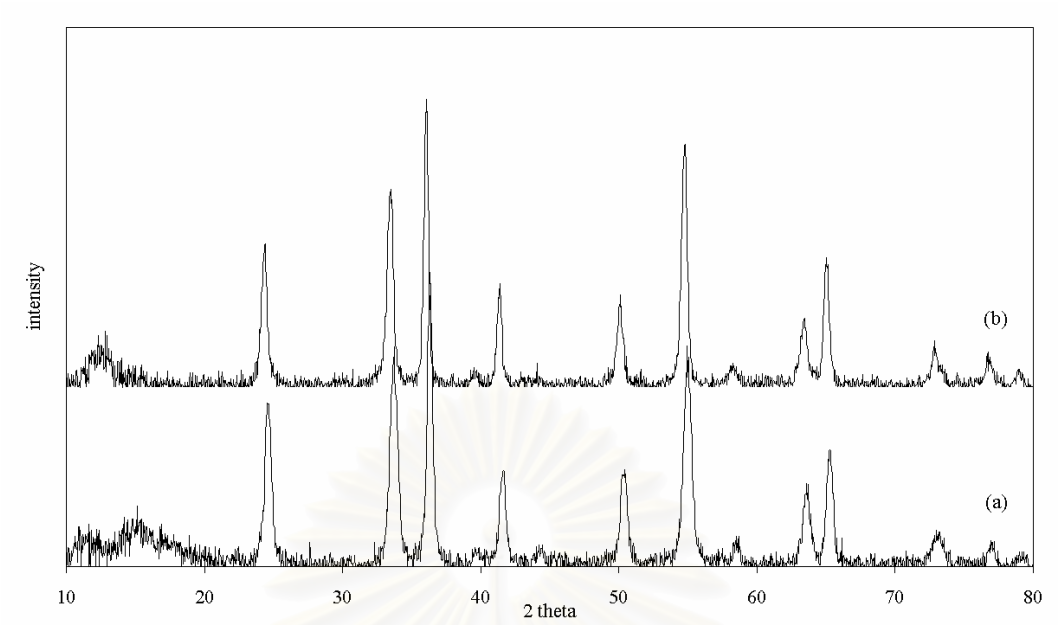

Figure 5.2 XRD patterns of chromium oxide obtained after calcined at 350°C of product (a) synthesized at 250°C and (b) synthesized at 300°C.

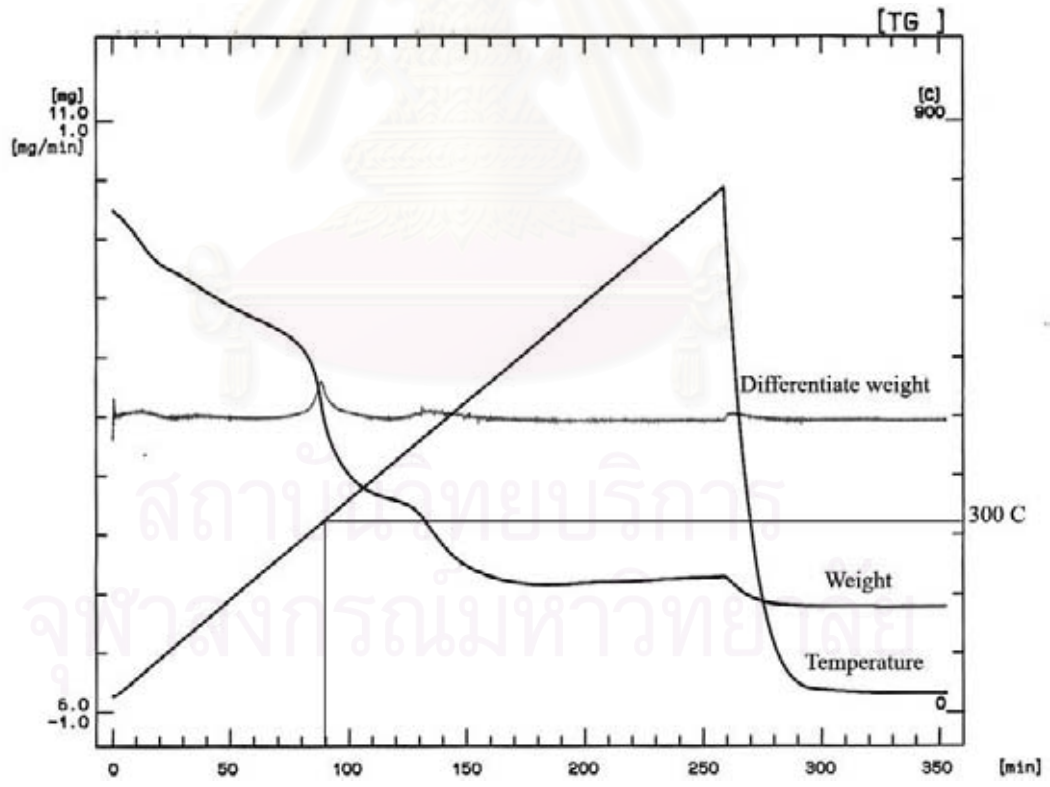

Figure 5.3 TGA thermogram of product obtained from reaction of Cr acetylacetonate at 300°C.

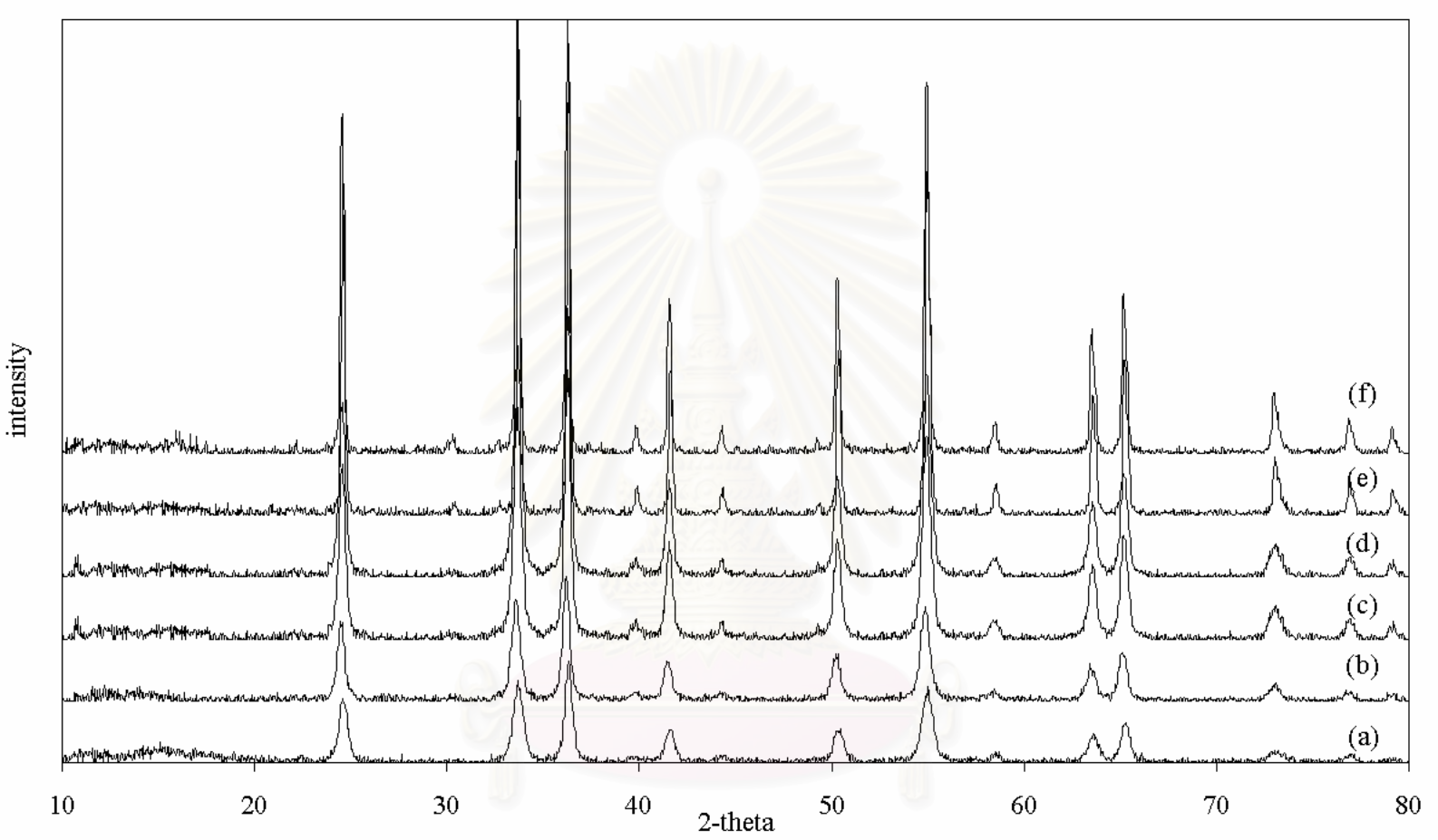

Figure 5.4 XRD patterns of chromium oxide synthesized at 250°C after calcined at (a) 350°C (b) 500°C (c) 600°C (d) 700°C (e) 800°C and (f) 900°C.

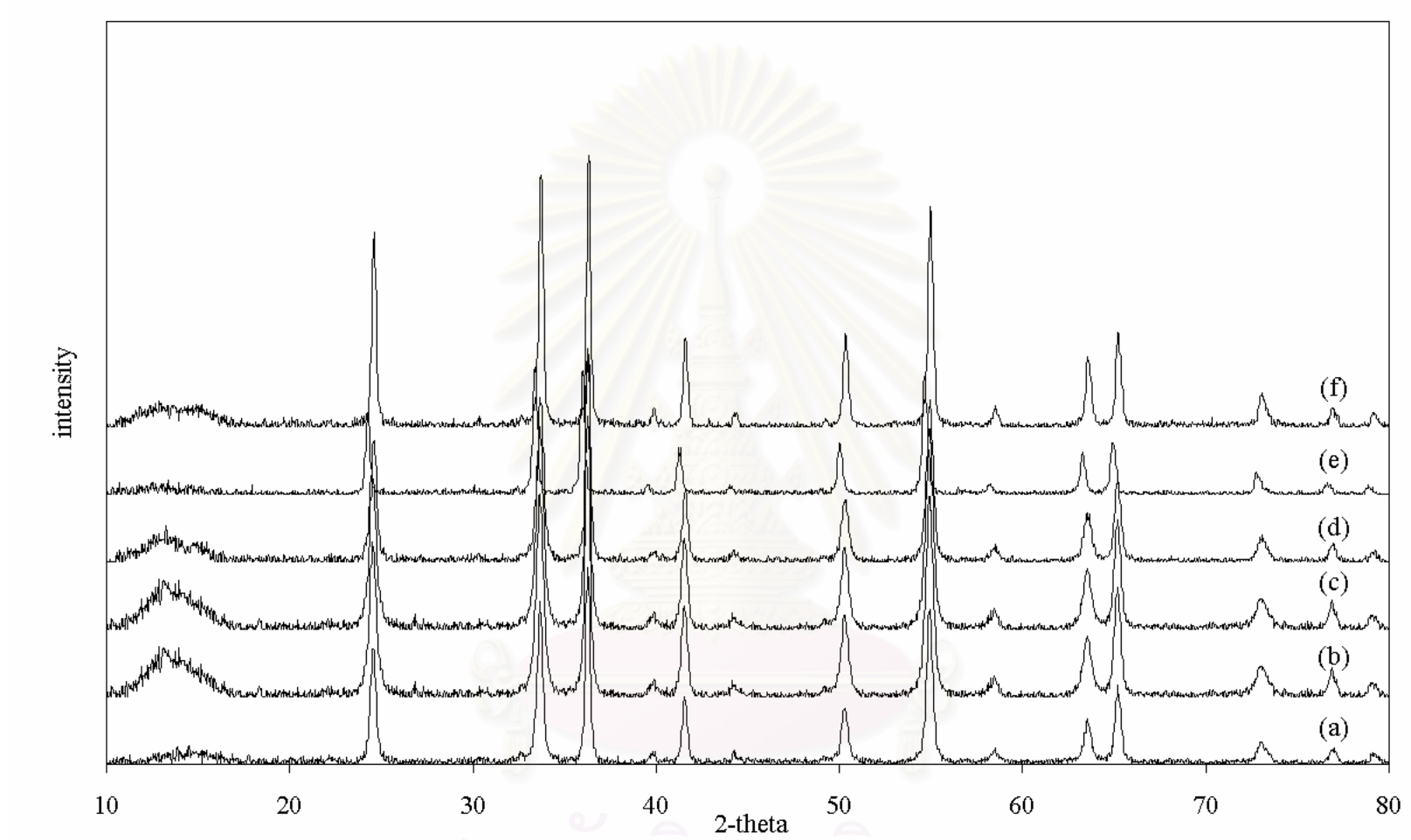

Figure 5.5 XRD patterns of chromium oxide synthesized at 300°C after calcined at (a) 350°C (b) 500°C (c) 600°C (d) 700°C (e) 800°C and (f) 900°C.

Table 5.1 BET surface area and crystallite size of the as-synthesized and calcined products chromium oxide synthesized at different reaction temperature.

Reaction temperature, °C	Calcination temperature, °C	Surface area (m^2/g)		d^c (nm)
		S_1[a]	S_2[b]	
250	350	57.3	71.8	16.2(17.1)[d]
	500	42.7	60.2	19.1
	600	37.5	37.9	32.4
	700	28.9	23.9	48.2
	800	10.6	18.8	61.3
	900	5.1	13.1	70.7
300	350	42.9	46.1	25.0(24.8)[d]
	500	40.5	39.0	29.8
	600	37.3	34.7	33.3
	700	28.7	29.5	39.2
	800	19.2	22.5	51.2
	900	8.3	15.9	57.4

[a] Surface area measured by BET method(Appendix B)

[b] Surface area calculated from crystallite size(Appendix B)

[c] Crystallite size from the line broadening using Scherrer equation.

[d] Particle size observed from TEM photograph.

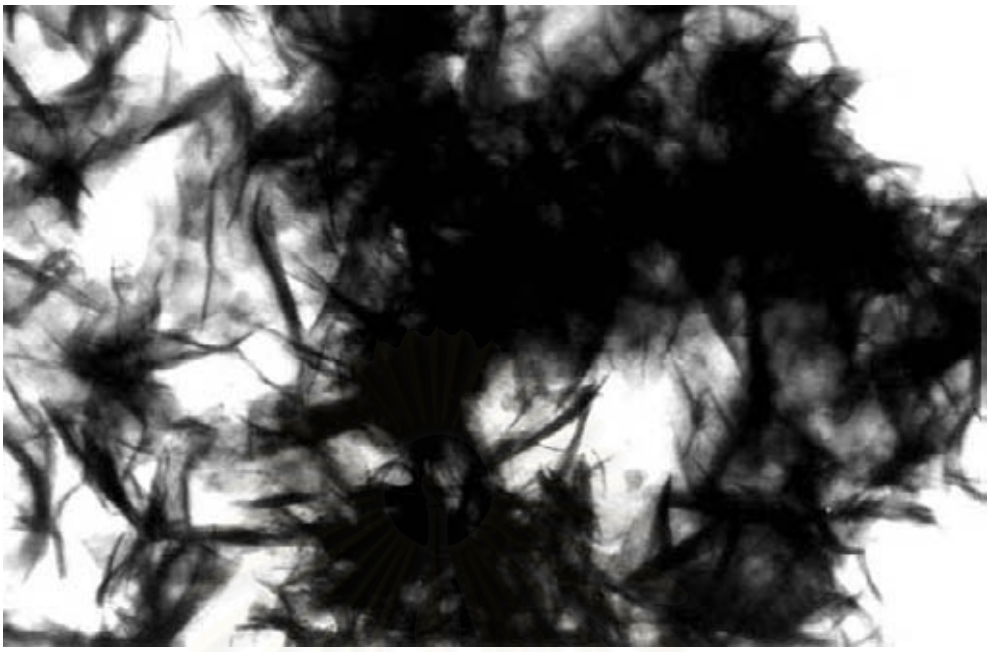

Figure 5.6 (a) TEM photograph of as-synthesized product obtained from reaction of Cr acetylacetonate at 250°C (x150,000).

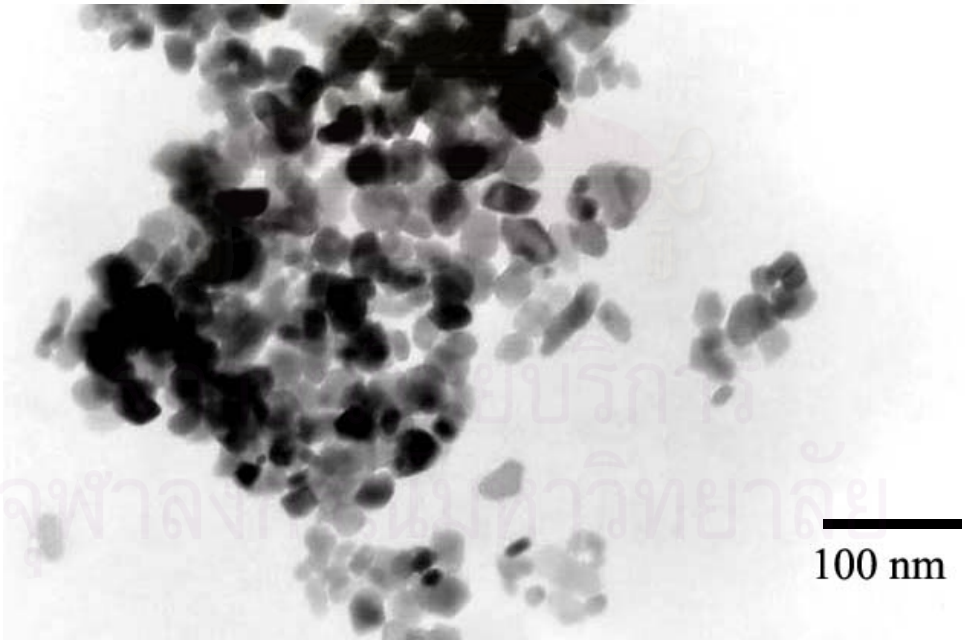

Figure 5.6(b) TEM photograph of chromium oxide synthesized at 250°C after calcined at 350°C (x150,000).

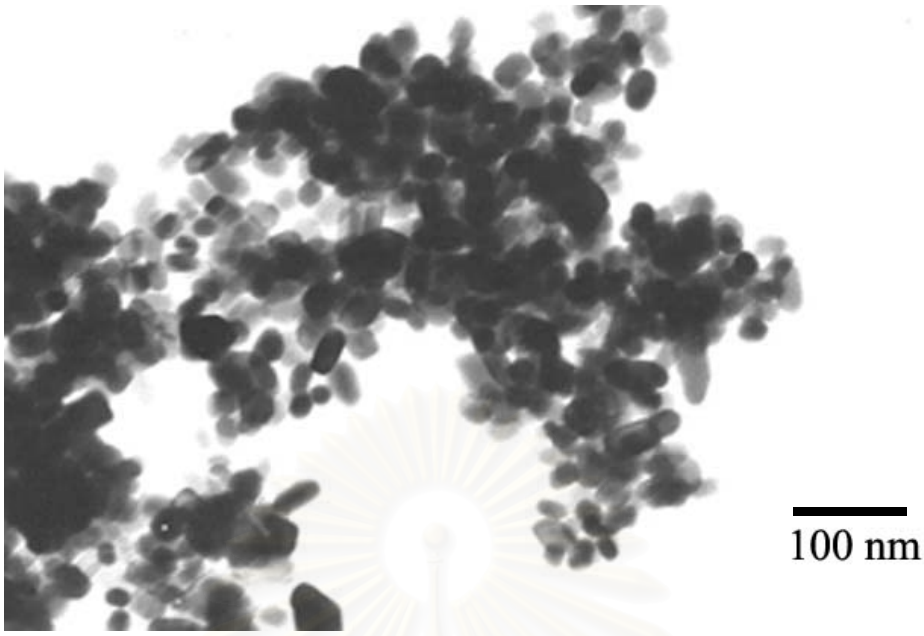

Figure 5.6(c) TEM photograph of chromium oxide synthesized at 250°C after calcined at 600°C (x100,000).

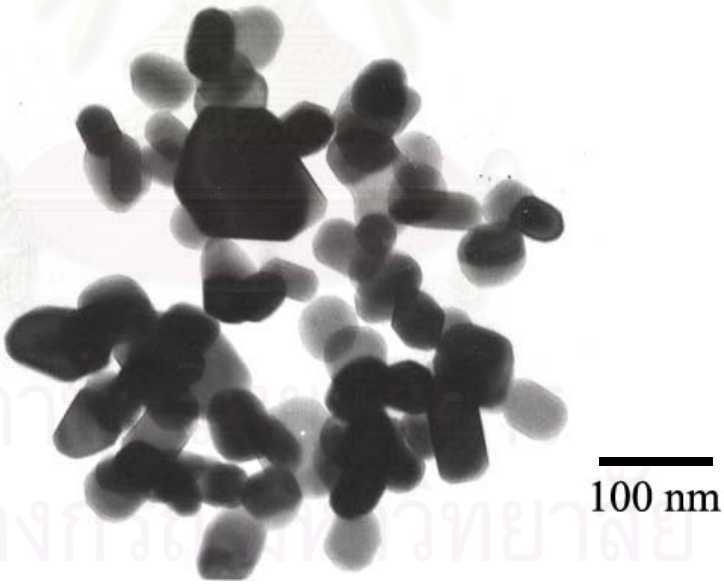

Figure 5.6(d) TEM photograph of chromium oxide synthesized at 250°C after calcined at 800°C (x100,000).

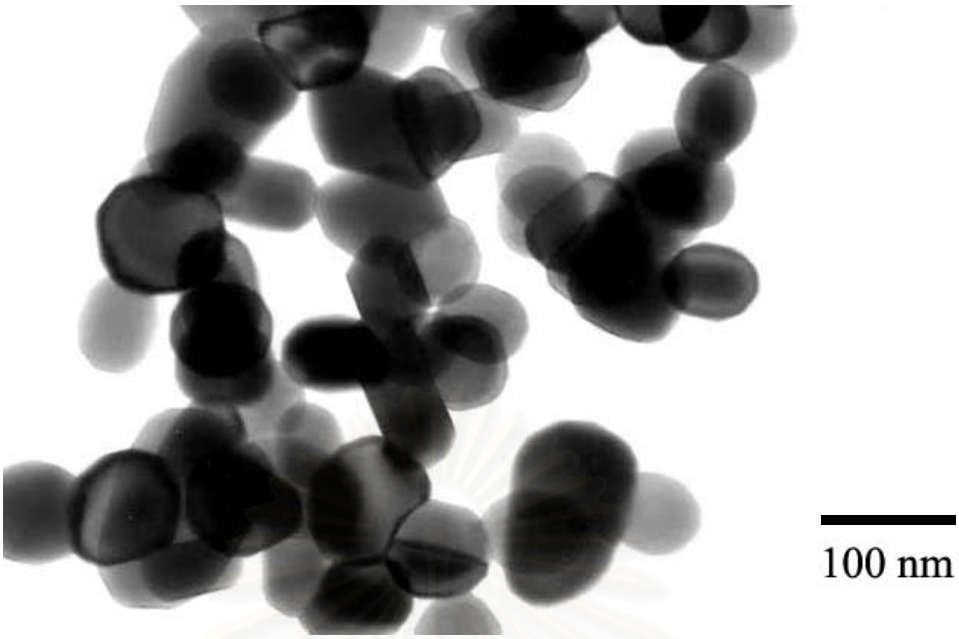

Figure 5.6(e) TEM photograph of chromium oxide synthesized at 250°C after calcined at 900°C (x100,000).

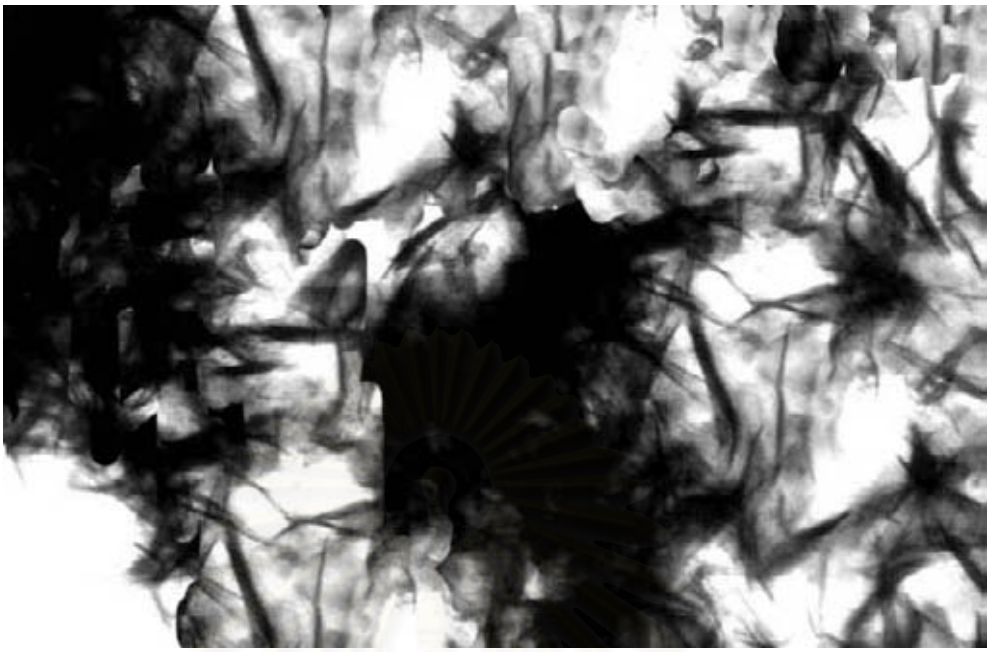

Figure 5.7 (a) TEM photograph of as-synthesized product obtained from reaction of Cr acetylacetonate at 300°C (x150,000).

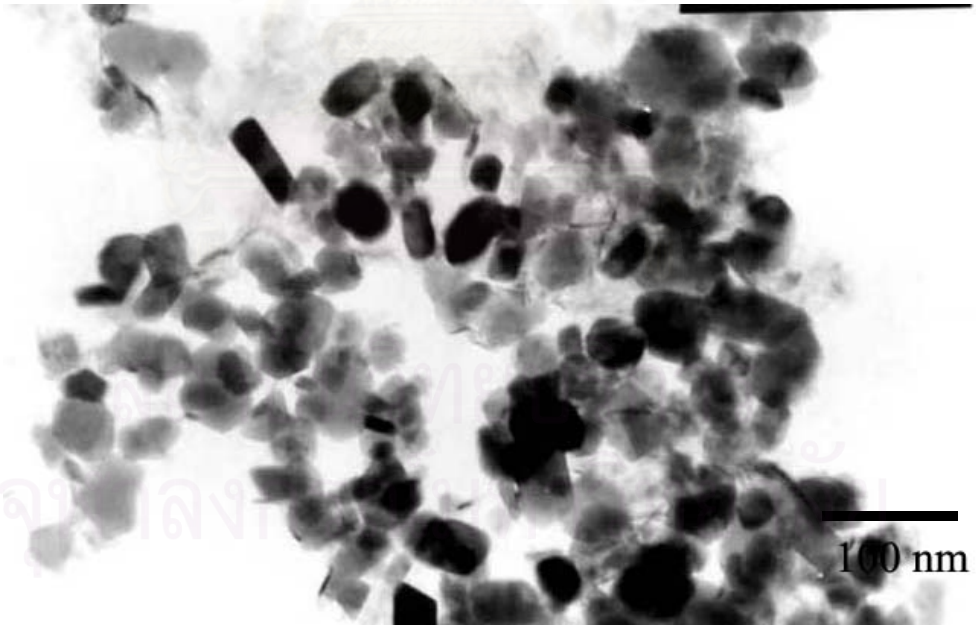

Figure 5.7(b) TEM photograph of chromium oxide synthesized at 300°C after calcined at 350°C (x150,000).

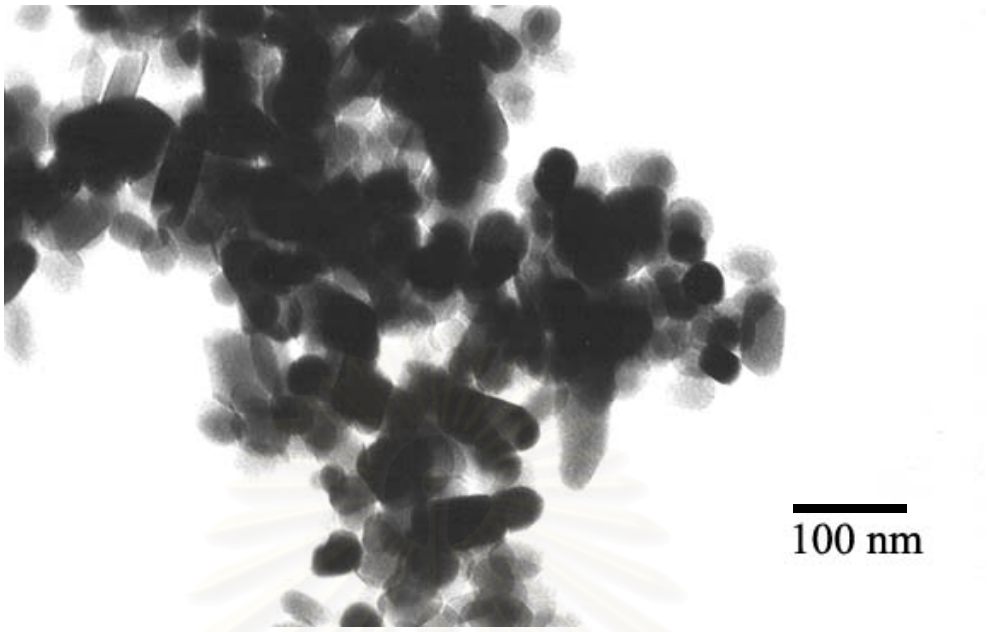

Figure 5.7(c) TEM photograph of chromium oxide synthesized at 300°C after calcined at 600°C (x100,000).

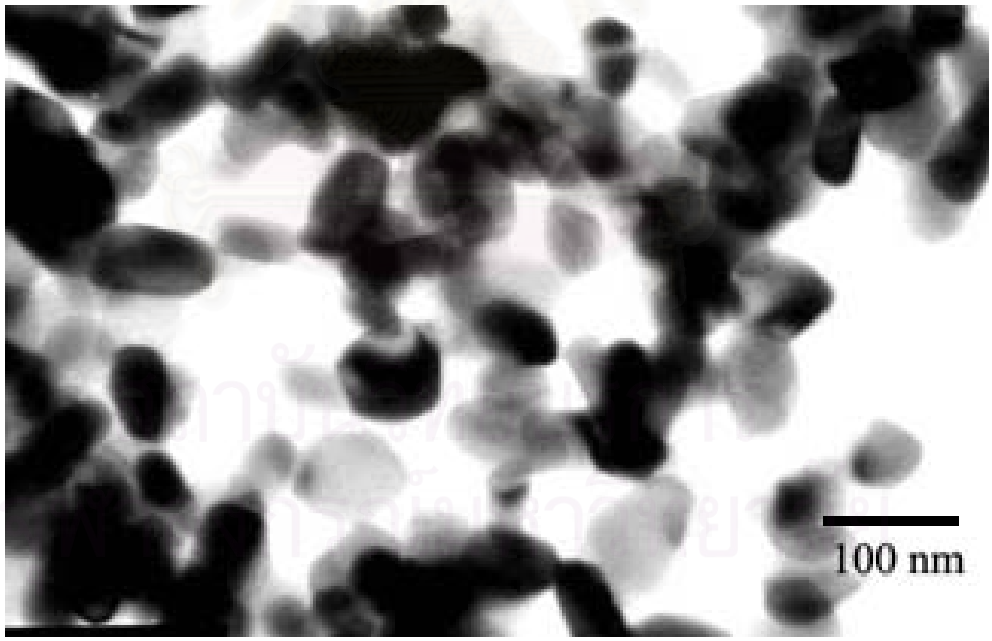

Figure 5.7(d) TEM photograph of chromium oxide synthesized at 300°C after calcined at 800°C (x100,000).

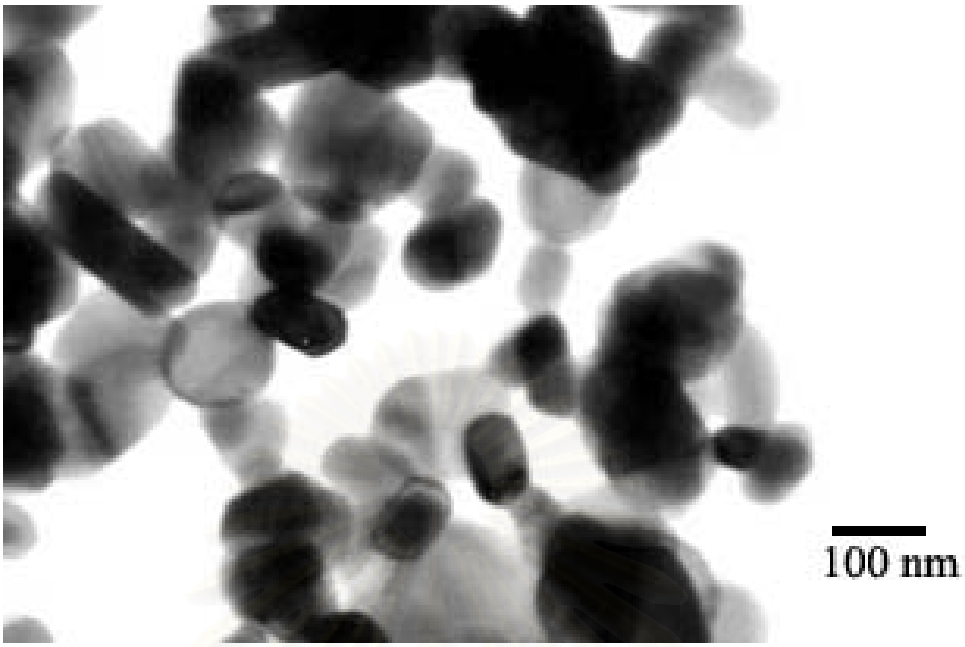

Figure 5.7(e) TEM photograph of chromium oxide synthesized at 300°C after calcined at 900°C (x100,000).

5.1. 2 Formation of pure titanium oxide (TiO_2).

Reaction of titanium tert-butoxide in 1,4-butanediol at 250°C and 300°C under autogeneous pressure yielded nanocrystalline anatase titanium oxide. The XRD patterns of the as-synthesized product obtained from glycothermal reaction is given in Figures 5.8 and 5.9, which show that anatase phase was formed without contamination with other phases of titanium oxide such as rutile and brookite. The crystallite size, which calculated by the XRD broadening, was 7.3 and 14.2 nm, respectively. It was shown that the crystallite size depends on the reaction temperature. The average particle size determined from the transmission electron micrograph (TEM) of the product (Figures 5.10 and 5.11) were in good agreement with the crystallite size. This suggests that each particle observed by TEM is a single crystal of anatase.

The as-synthesized titanium oxide were calcined at temperature 500 to 900°C. The BET surface area and crystallite size of products after calcination are summary in Table 5.2. The specific surface area of products is measured by two methods. The first method is the single point BET method and the other is calculated from crystallite size. Comparison of these two values of the as-synthesized product, it is shown that the particle morphology is closely to spherical shape. From Figure 5.8 and 5.9, there is a different between XRD patterns of product after calcined. For anatase titanium oxide obtained from reaction temperature 300°C, these products still preserved the anatase structure even after calcined at 900°C. But at the same calcination temperature titanium oxide prepared at 250°C was transformed to rutile phase. It shown that product with larger crystallite size has higher thermal stability.

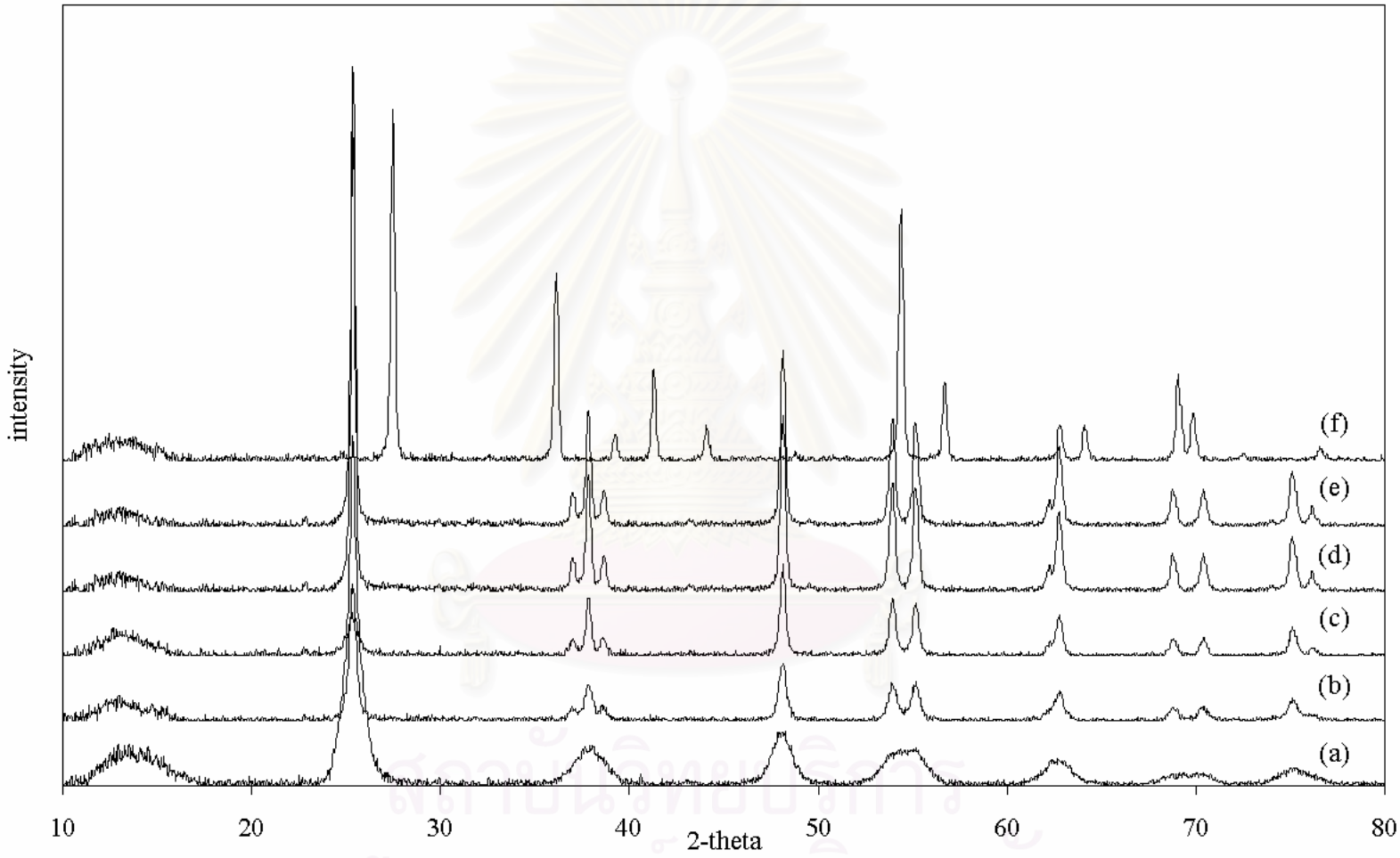

Figure 5.8 XRD patterns of titanium oxide synthesized at 250 °C (a) before and after calcined at (b) 500°C (c) 600°C (d) 700°C (e) 800°C and (f) 900°C.

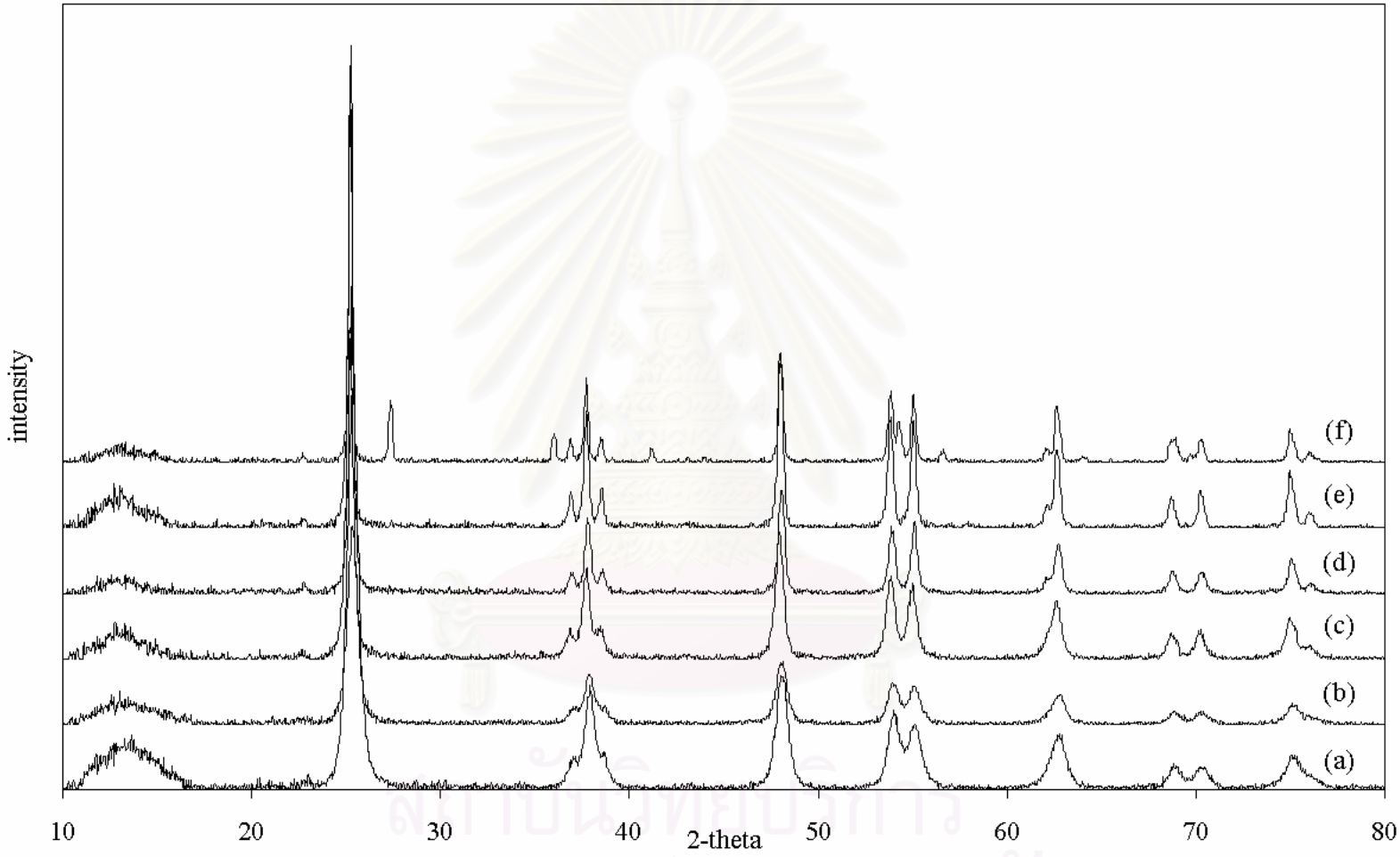

Figure 5.9 XRD patterns of titanium oxide synthesized at 300 °C (a) before and after calcined at (b) 500°C (c) 600°C (d) 700°C (e) 800°C and (f) 900°C.

Table 5.2 BET surface area and crystallite size of the as-synthesized and calcined products titanium oxide synthesized at different reaction temperature.

Reaction temperature, °C	Calcination temperature, °C	Surface area (m^2/g)		d^c (nm)
		S_1[a]	S_2[b]	
250	As-synthesized	140.1	196.9	7.3(8.1)[d]
	500	73.4	65.2	21.9
	600	16.3	40.9	34.9
	700	9.3	27.9	51.3
	800	5.6	19.2	74.5
	900	3.9	16.7	85.9
300	As-synthesized	74.3	100.1	14.2(15.2)[d]
	500	67.5	95.3	15.1
	600	61.5	63.4	22.6
	700	45.6	43.9	32.5
	800	38.3	27.6	51.7
	900	24.1	12.8	111.5

[a] Surface area measured by BET method(Appendix B)

[b] Surface area calculated from crystallite size(Appendix B)

[c] Crystallite size from the line broadening using Scherrer equation.

[d] Particle size observed from TEM photograph.

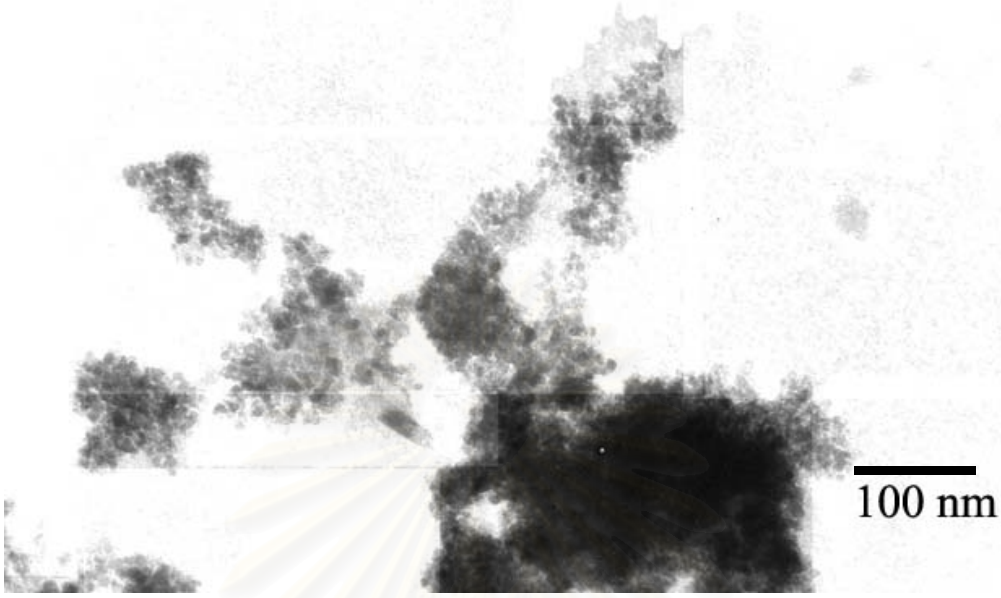

Figure 5.10 (a) TEM photograph of as-synthesized titanium oxide synthesized at 250°C (x150,000).

Figure 5.10(b) TEM photograph of titanium oxide synthesized at 250°C after calcined at 900°C (x100,000).

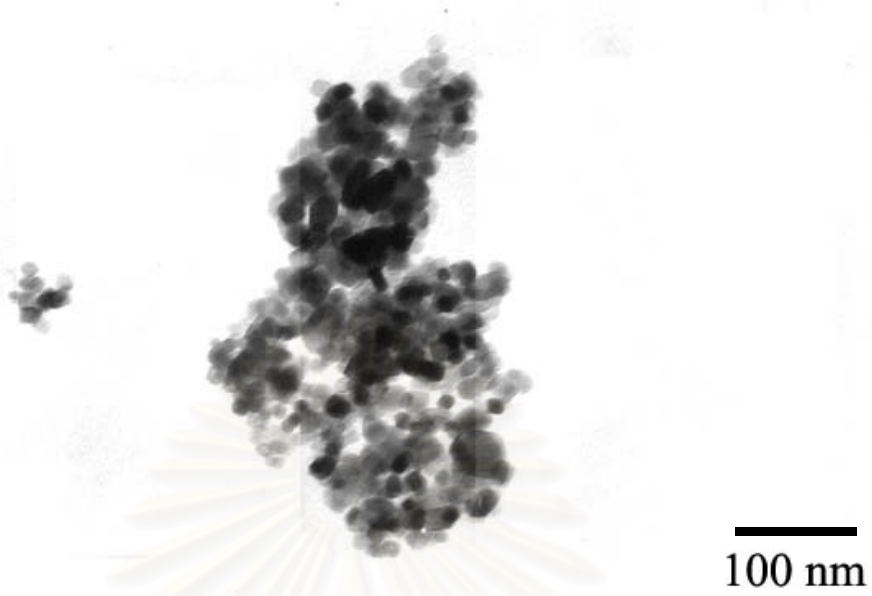

Figure 5.11 (a) TEM photograph of as-synthesized titanium oxide synthesized at 300°C (x150,000).

Figure 5.11 (b) TEM photograph of titanium oxide synthesized at 300°C after calcined at 900°C (x100,000).

5.1.3 Formation of pure manganese oxide (Mn_2O_3).

The glycothermal reaction of manganese acetylacetonate at 250^0C and 300^0C yield products with different structure. The products obtained from synthesized at 300°C are Mn_3O_8 as shown in Figure 5.12(b). The reaction at 250°C yields an unidentified phase product. The XRD patterns of the as-synthesized unidentified phase product are shown in Figure 5.12(a). By the thermogravimetric analysis method, the decomposition of product was studied. The temperature was raised from room temperature, with the heating rate of 10ºC/min, up to 700ºC. From TGA graph as shown in Figure 5.14, the differentiate weight loss are occurred at about 500°C, while the TGA thermogram of product obtained from synthesized at 300°C as shown in Figure 5.15, the differentiate weight has occur more than one step. This differentiate weight may cause from the loss of oxygen of Mn_3O_8 to form Mn_2O_3. From both TGA result indicated that the formation of manganese oxide (Mn_2O_3) from glycothermal reaction is different from the formation of chromium oxide. The mechanism of the formation of manganese oxide may be composed of at least two steps, the formation of unidentified phase, change to Mn_3O_8 and then formation of Mn_2O_3 has occur.

By the TGA result, both product were calcined at 500°C. The XRD patterns of the calcined product in Figure 5.13 show that the manganese oxide phase (Mn_2O_3) was formed after calcined without any contaminate phase. The products were attributed to be the as-synthesized manganese oxide.

The products were calcined at the temperature of 600°C to 1000°C. The crystallite size and BET surface area was investigated. The crystallite sizes that calculated from Scherrer equation of manganese oxide are 35.9 and 47.6 nm from the product synthesized at 250°C and 300°C, respectively. These results are in good agreement with the particle size observed by TEM. It is suggested that the products are single crystal manganese oxide. When compare the particle size of manganese oxide obtained by this method with product synthesized by other method. This method gives product with smaller crystallite size. From the sonochemical method [16] obtained manganese oxide with the particle size of 60 nm. The XRD patterns of

all products after calcined were shown in Figures 5.16 and 5.17. The XRD patterns were almost identical to the as-synthesized products except that the XRD peaks were sharper. BET surface area of product synthesized at 250°C is 14.13 m^2/g and 12.4 m^2/g for product synthesized at 300°C. The surface area measured by BET method is less than surface area calculated by using crystallite size, it is indicated that the morphology of product is not spherical shape. The crystallite size and BET surface area of as-synthesized and products after calcination at various temperatures are listed in Table 5.3.

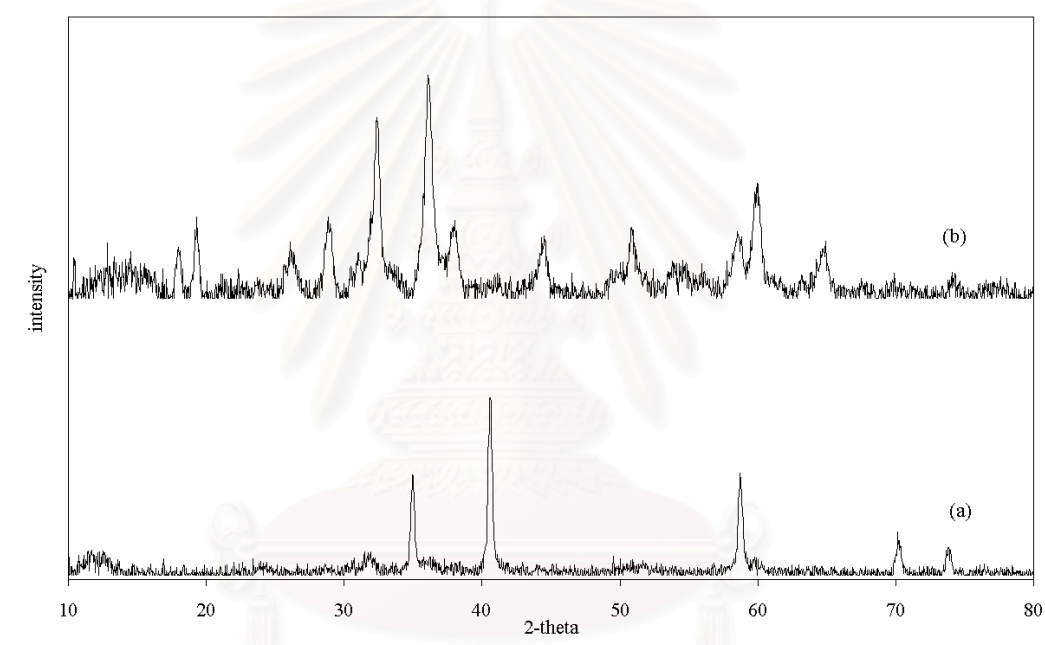

Figure 5.12 XRD patterns of as-synthesized product obtained from reaction of Mn acetylacetonate (a) at 250°C and (b) at 300°C.

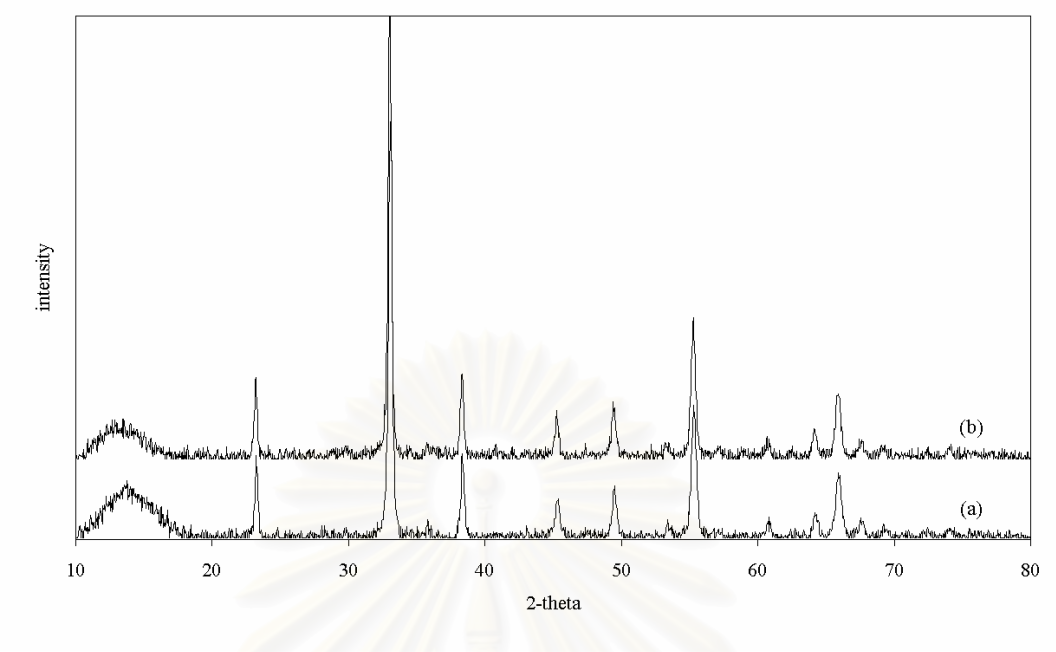

Figure 5.13 XRD patterns of manganese oxide obtained after calcined at 500 °C of product (a) synthesized at 250 °C and (b) synthesized at 300 °C.

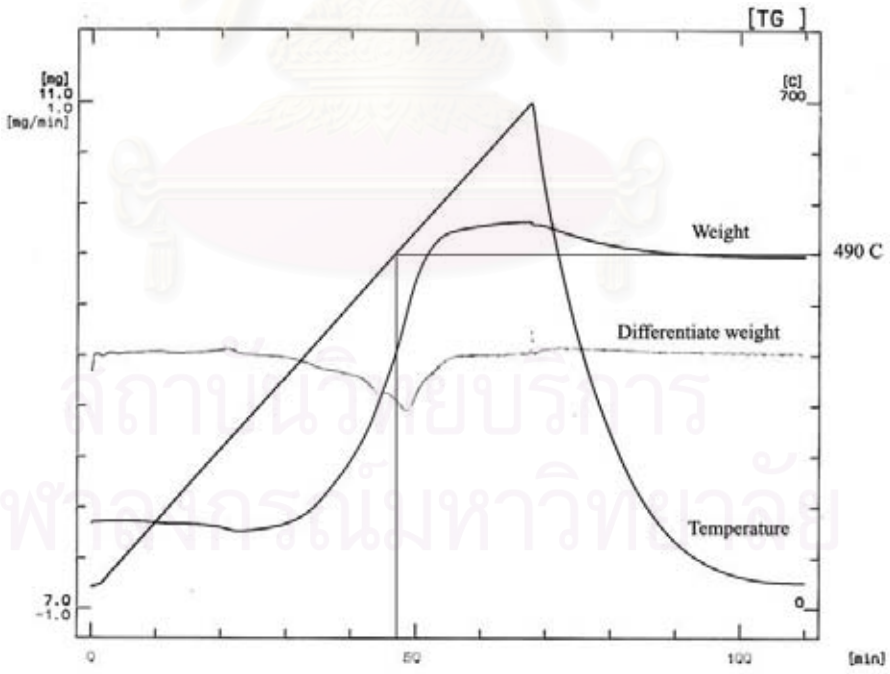

Figure 5.14 TGA thermogram of product obtained from reaction of Mn acetylacetonate at 250° C.

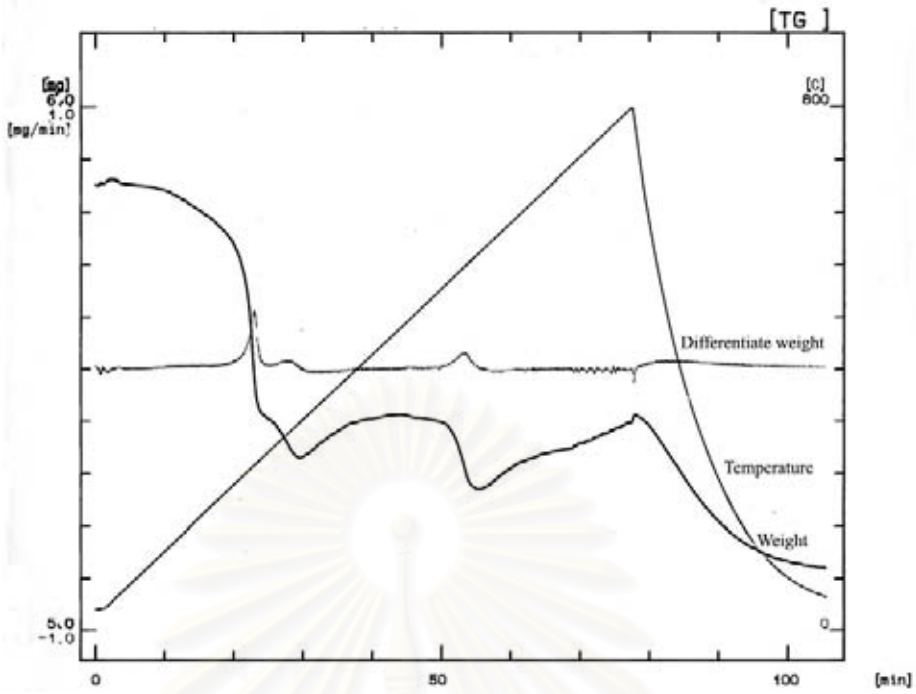

Figure 5.15 TGA thermogram of product obtained from reaction of Mn acetylacetonate at 300° C.

Table 5.3 BET surface area and crystallite size of the as-synthesized and calcined products manganese oxide synthesized at different reaction temperature.

Reaction temperature, °C	Calcination temperature, °C	Surface area (m^2/g)		d^c (nm)
		S_1[a]	S_2[b]	
250	500	14.2	37.1	35.9(37.8)[d]
	600	8.1	31.6	42.1
	700	5.7	17.7	65.3
	800	4.4	14.2	73.8
	900	3.1	14.5	91.4
	1000	1.9	10.0	133.1
300	500	12.4	28.0	47.6(46.1)[d]
	600	9.2	23.6	56.3
	700	7.3	21.3	62.4
	800	5.9	16.9	78.8
	900	4.6	16.0	85.3
	1000	2.2	-	*

[a] Surface area measured by BET method(Appendix B)

[b] Surface area calculated from crystallite size(Appendix B)

[c] Crystallite size from the line broadening using Scherrer equation.

[d] Particle size observed from TEM photograph.

*Can not determined by Scherrer equation

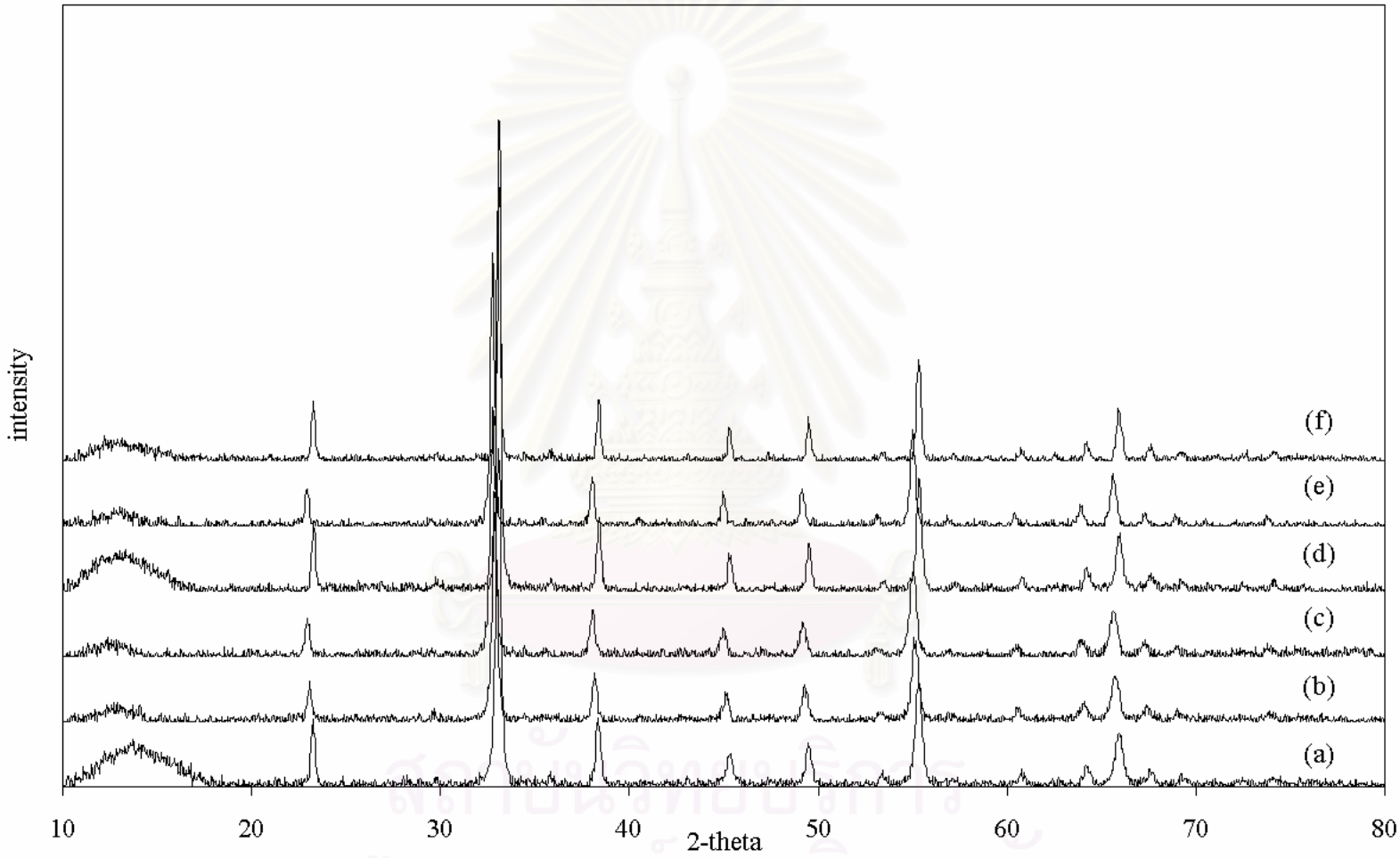

Figure 5.16 XRD patterns of manganese oxide synthesized at 250 °C after calcined at (a) 500°C (b) 600°C (c) 700°C (d) 800°C (e) 900°C and (f) 1000°C.

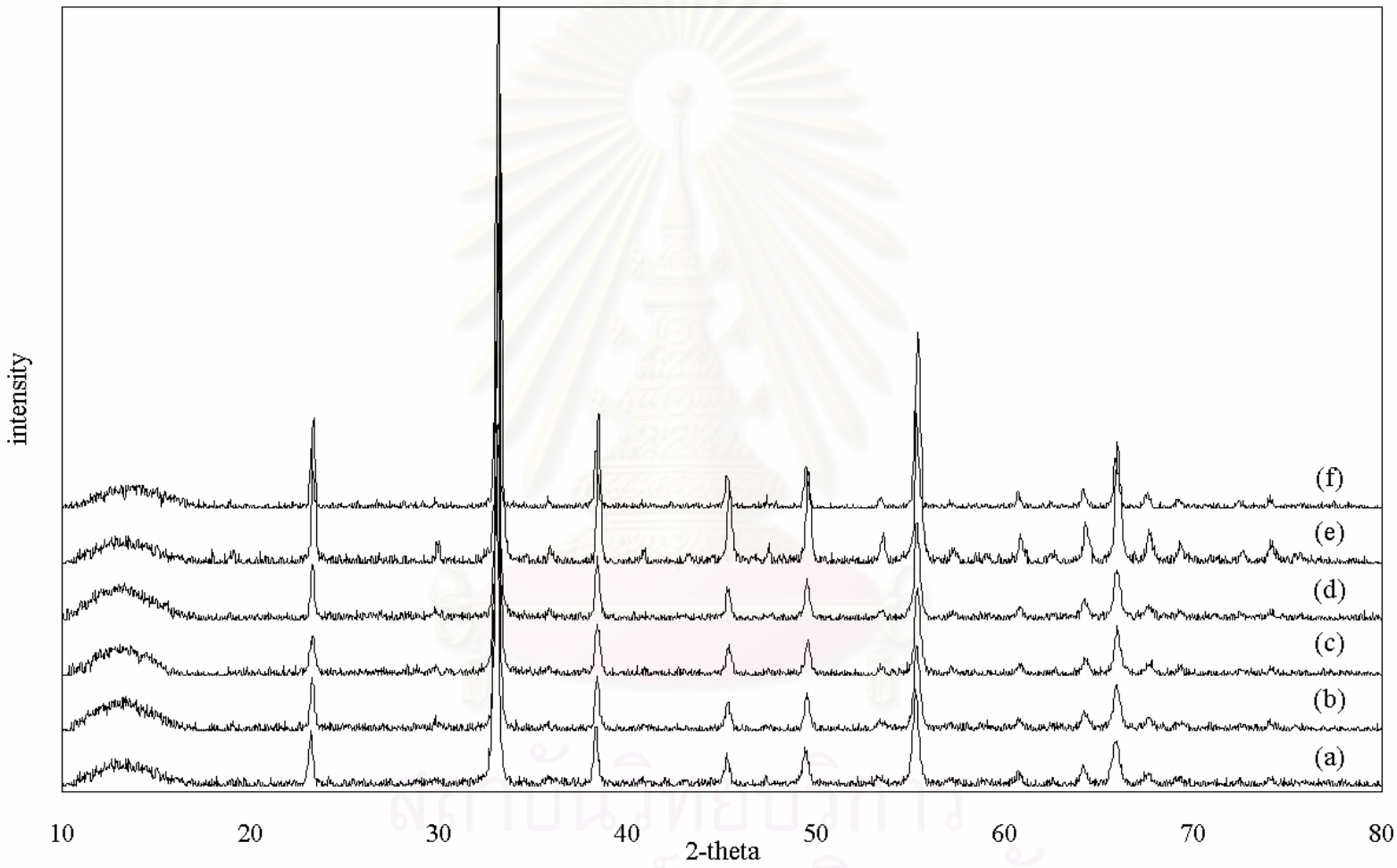

Figure 5.17 XRD patterns of manganese oxide synthesized at 300 °C after calcined at (a) 500°C (b) 600°C (c) 700°C (d) 800°C (e) 900°C and (f) 1000°C.

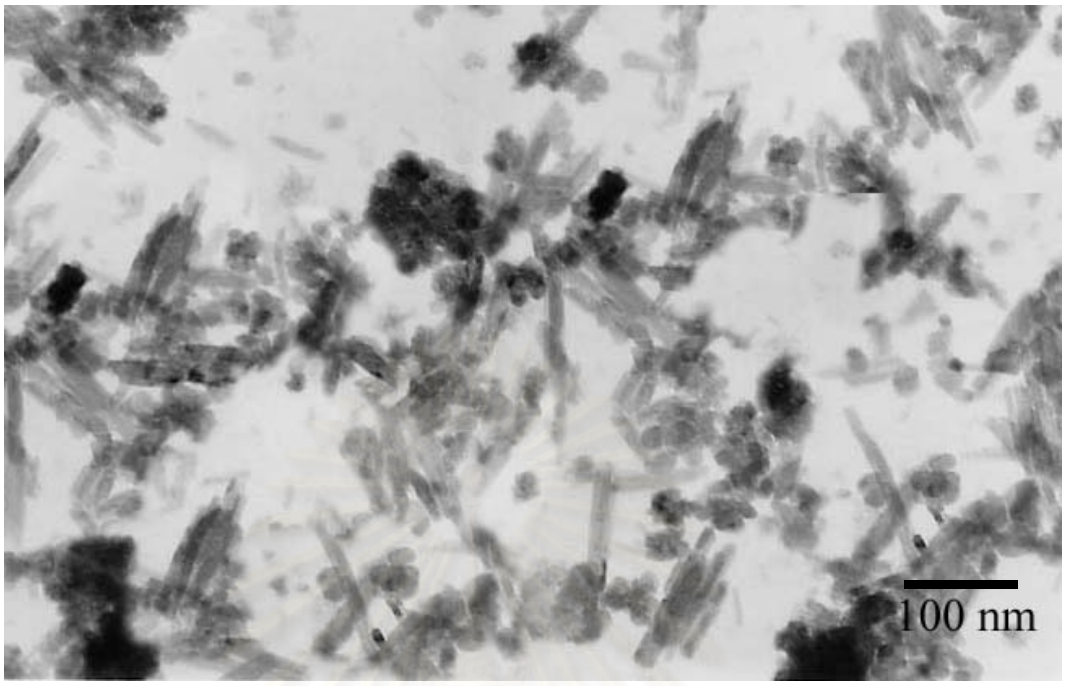

Figure 5.18 (a) TEM photograph of as-synthesized product synthesized at 250 °C.

Figure 5.18(b) TEM photograph of manganese oxide synthesized at 250°C after calcined at 500°C (x150,000)

Figure 5.18(c) TEM photograph of manganese oxide synthesized at 250°C after calcined at 900°C (x100,000)

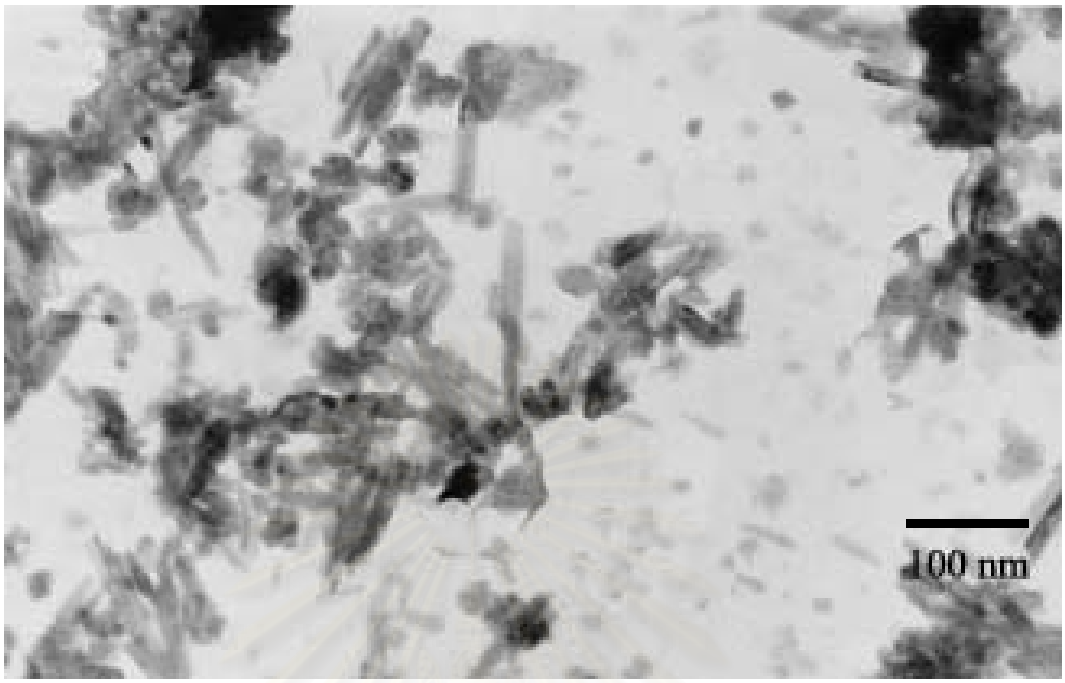

Figure 5.19 (a) TEM photograph of as-synthesized product synthesized at 300°C

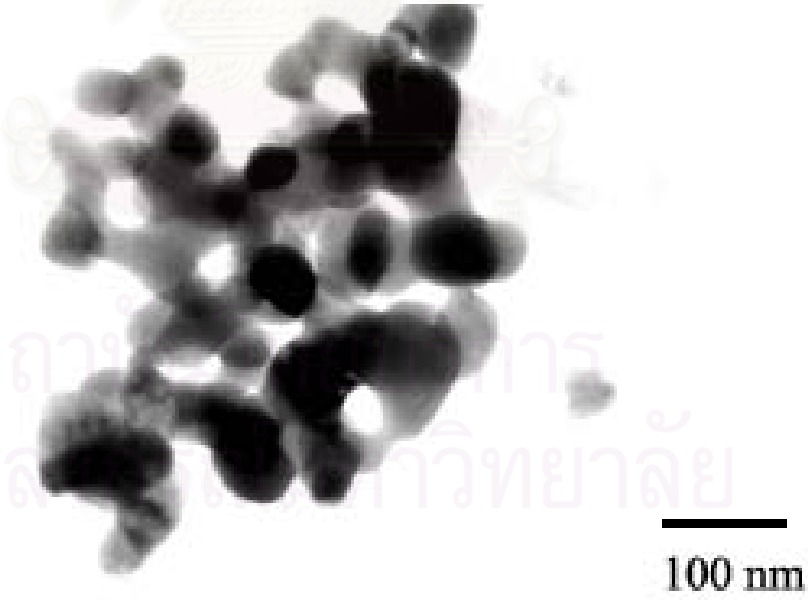

Figure 5.19(b) TEM photograph of manganese oxide synthesized at 300°C after calcined at 500°C (x150,000)

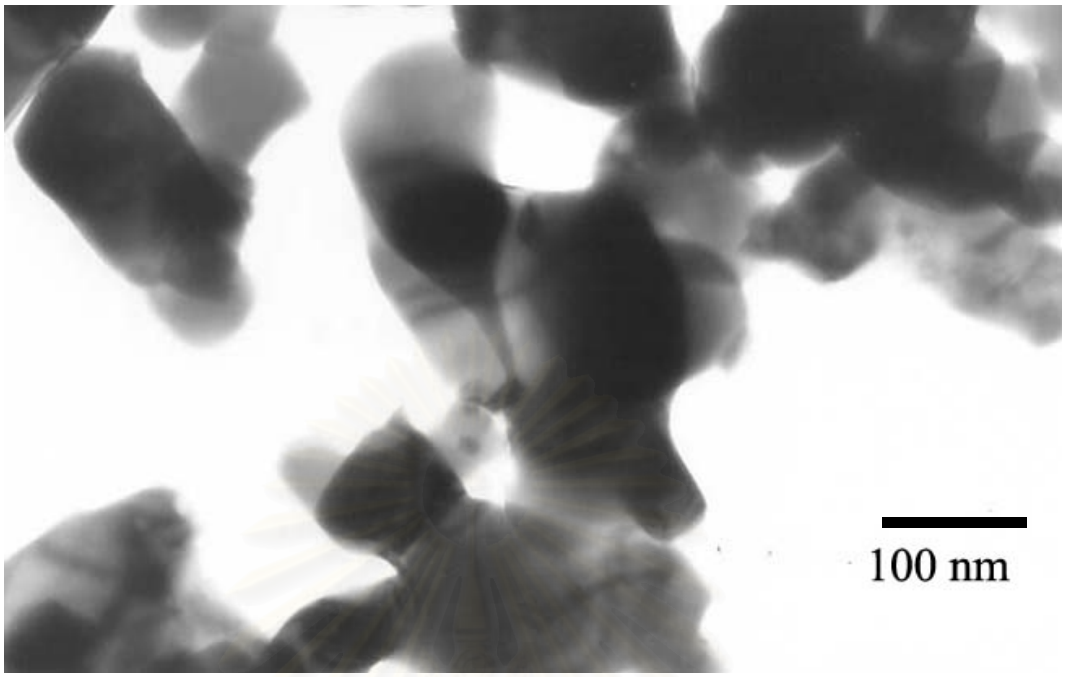

Figure 5.19(c) TEM photograph of manganese oxide synthesized at 300°C after calcined at 900°C (x100,000)

5.1.4 Formation of pure iron oxide (Fe_2O_3).

Nanocrystalline iron oxides are prepared by glycothermal reaction in 1,4-butanediol at difference temperature 250°C and 300°C and holding at that temperature for 2 h. The XRD patterns of obtained products were shown in Figure 5.20. Compare with the XRD patterns of product after calcination in Figure 5.21 and 5.22. There is phase transformation of as-synthesized product from γ-Fe_2O_3 to α-Fe_2O_3 since calcination temperature of 500°C.

As-synthesized iron oxide were calcined at various temperatures from 500 up to 900ºC. The XRD patterns and the BET surface areas of the products after calcination were investigated (Figure 5.21, 5.22). The crystallite size, which calculated by the XRD broadening was 26.5 nm for product synthesized at 250°C and 33.0 for product synthesized at 300°C. The particle size observed by the transmission electron micrographs (TEM) of the product is in good agreement with the crystallite size, indicating that each primary particle observed by TEM is a single crystal. BET surface area of iron oxide prepared at 250°C and 300°C were 25.1 and 22.7 m^2/g, respectively. After calcination at 900°C, BET surface area of iron oxide synthesized at 250°C is 0.4 m^2/g and 4.5 m^2/g for iron oxide synthesized at 300°C. Table 5.4 was shown the crystallite size and BET surface area of all product after calcined at various temperatures.

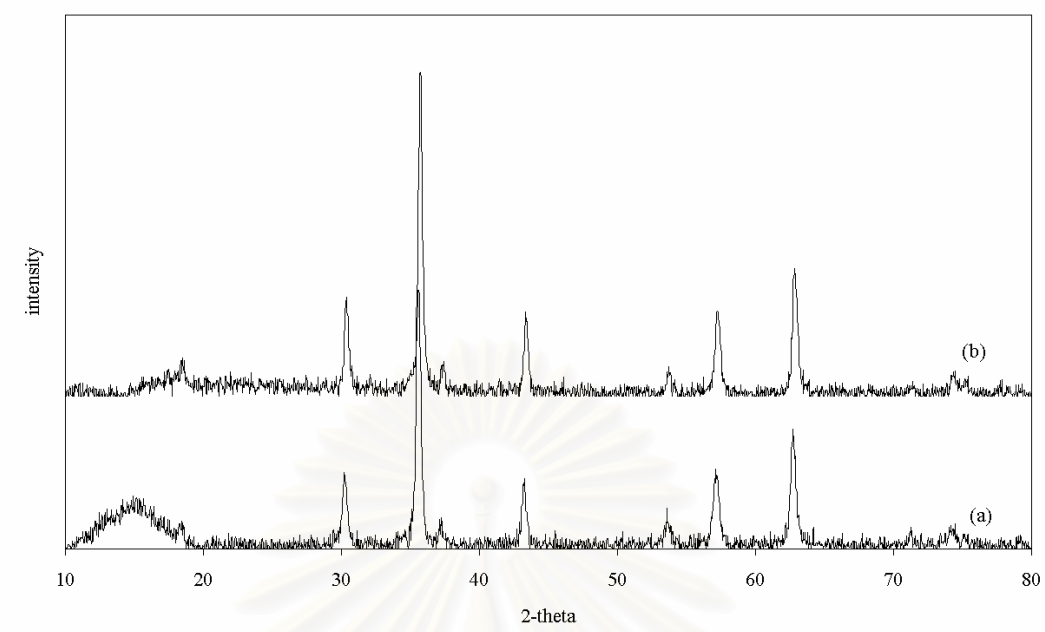

Figure 5.20 XRD patterns of iron oxide obtained from synthesized at (a) 250°C and (b) 300°C

Table 5.4 BET surface area and crystallite size of the as-synthesized and calcined products iron oxide synthesized at different reaction temperature.

Reaction temperature, °C	Calcination temperature, °C	Surface area (m^2/g)		d^c (nm)
		S_1[a]	S_2[b]	
250	As-synthesized	25.1	43.5	26.5(27.3)[d]
	500	9.0	27.6	41.7
	600	6.1	21.1	54.5
	700	4.3	16.6	69.2
	800	2.6	13.9	82.6
	900	1.0	10.2	112.3
300	As-synthesized	22.7	34.9	33.0(33.8)[d]
	500	10.5	27.6	41.8
	600	7.3	23.3	49.4
	700	6.8	21.7	57.3
	800	5.2	16.8	71.2
	900	4.5	9.6	89.8

[a] Surface area measured by BET method(Appendix B)

[b] Surface area calculated from crystallite size(Appendix B)

[c] Crystallite size from the line broadening using Scherrer equation.

[d] Particle size observed from TEM photograph.

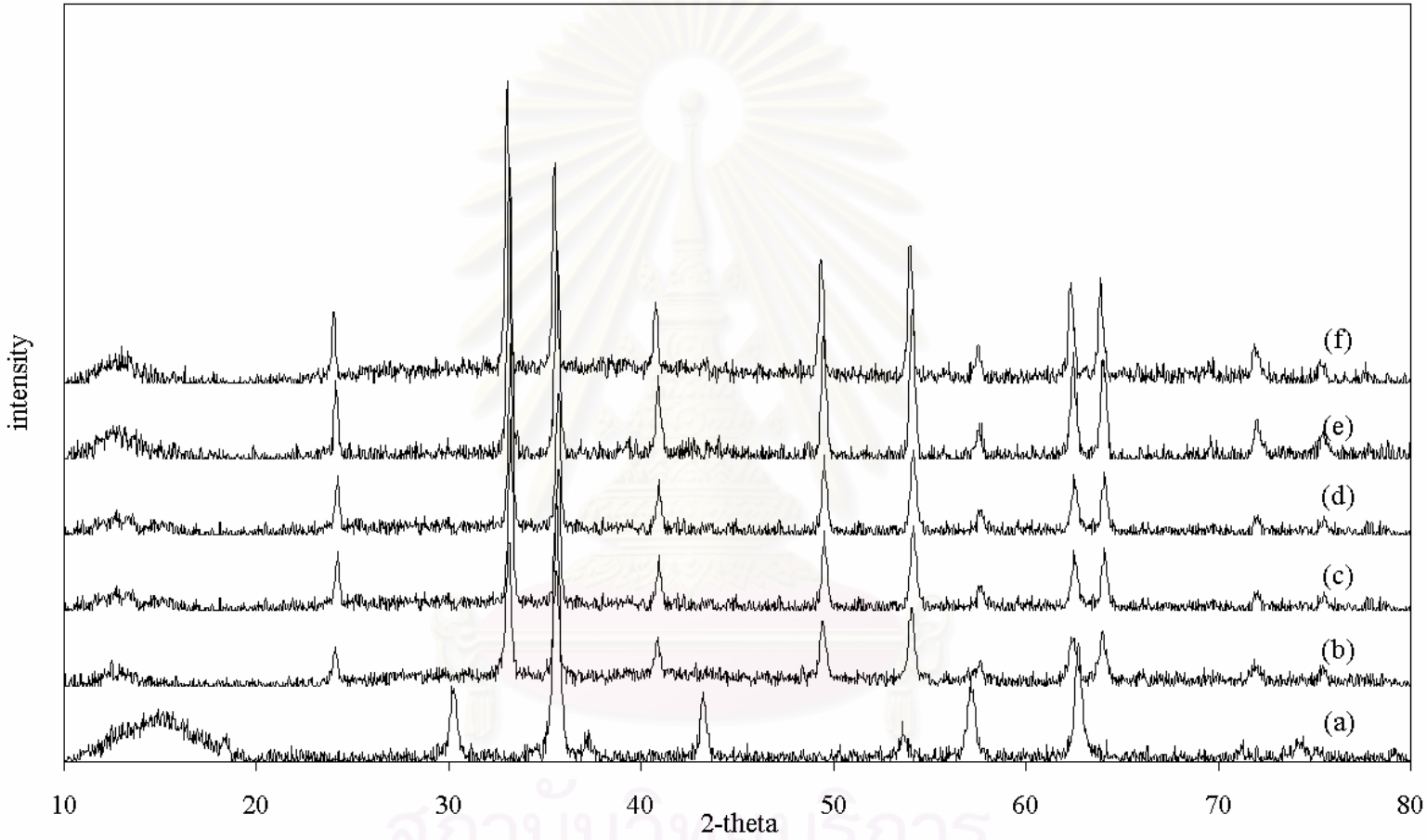

Figure 5.21 XRD patterns of iron oxide synthesized at 250°C (a) before and after calcined at (b) 500°C (c) 600°C (d) 700°C (e) 800°C and (f) 900°C.

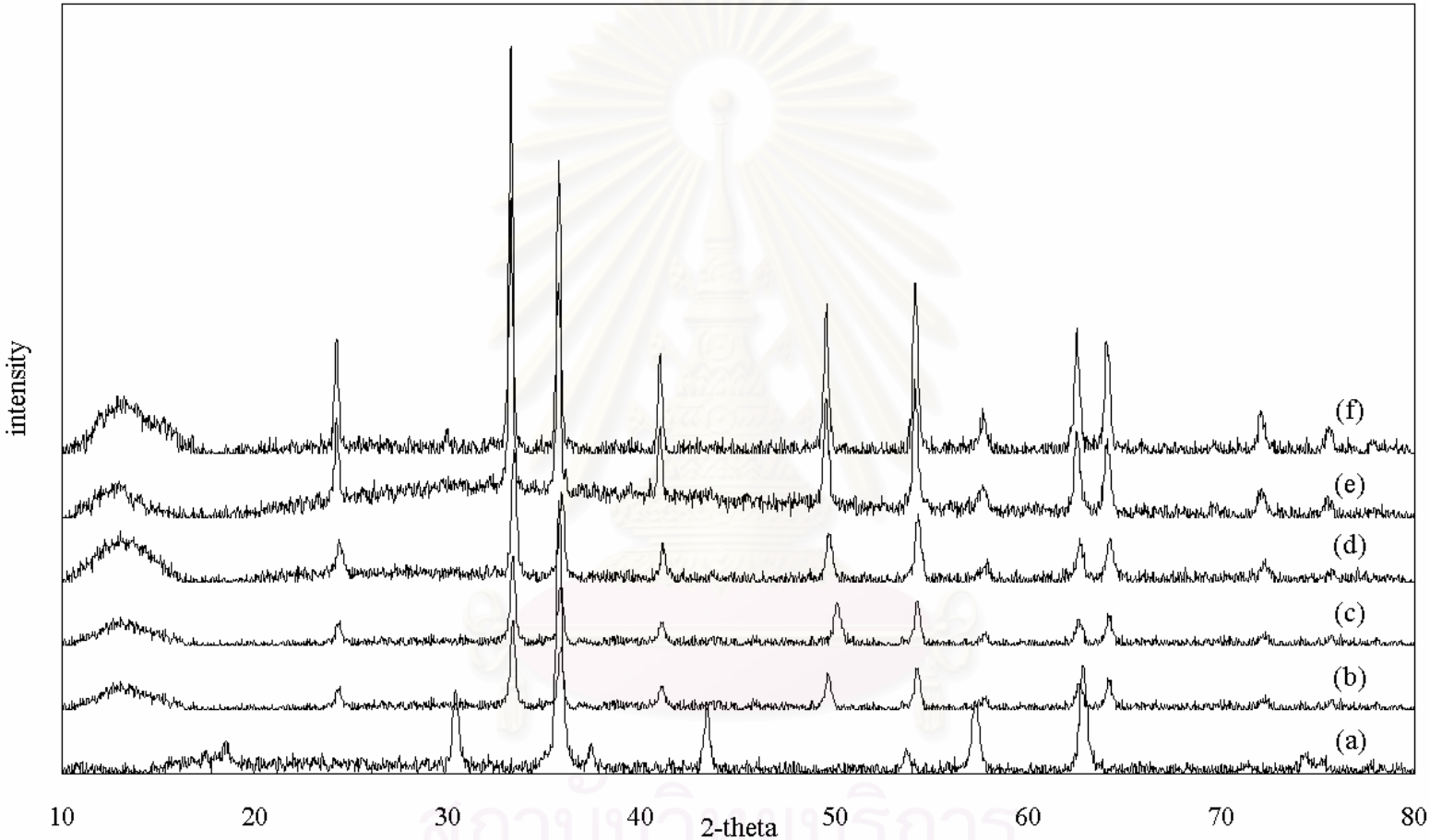

Figure 5.22 XRD patterns of iron oxide synthesized at 300 °C (a) before and after calcined at (b) 500°C (c) 600°C (d) 700°C (e) 800°C and (f) 900°C.

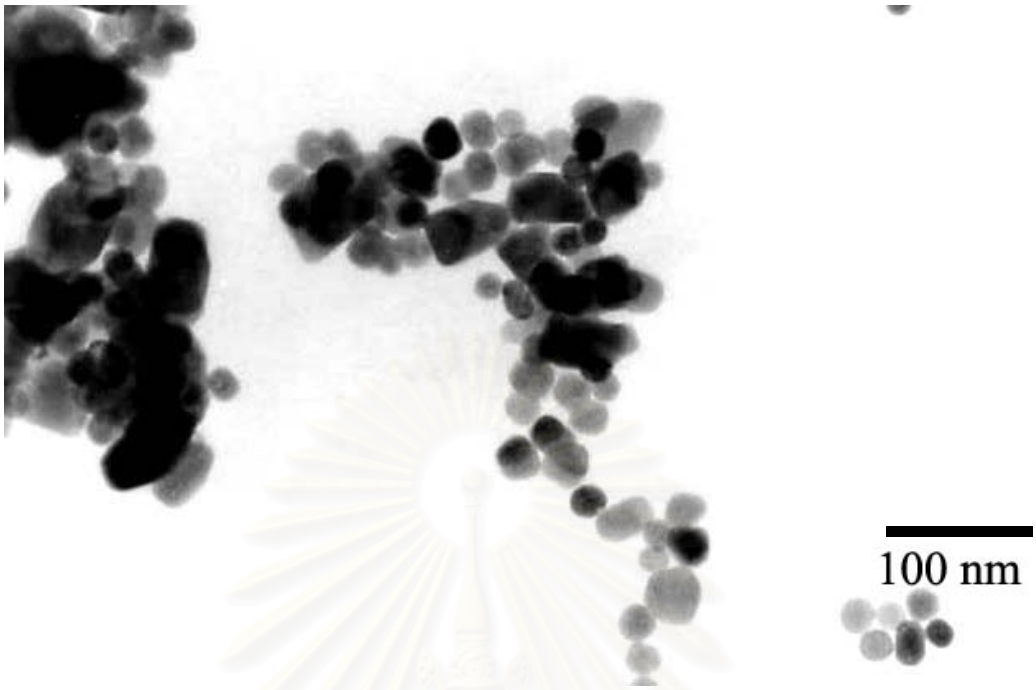

Figure 5.23(a) TEM photograph of as-synthesized iron oxide synthesized at 250 °C (x150,000).

Figure 5.23(b) TEM photograph of iron oxide synthesized at 250°C after calcined at 900°C (x100,000).

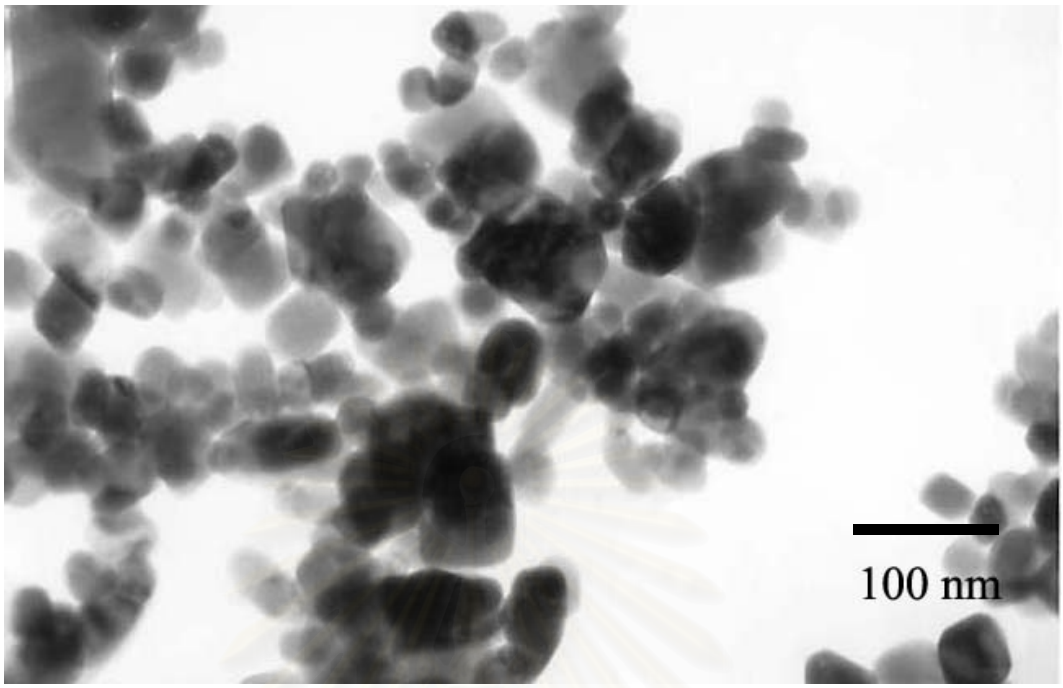

Figure 5.24(a) TEM photograph of as-synthesized iron oxide synthesized at 300°C (x150,000).

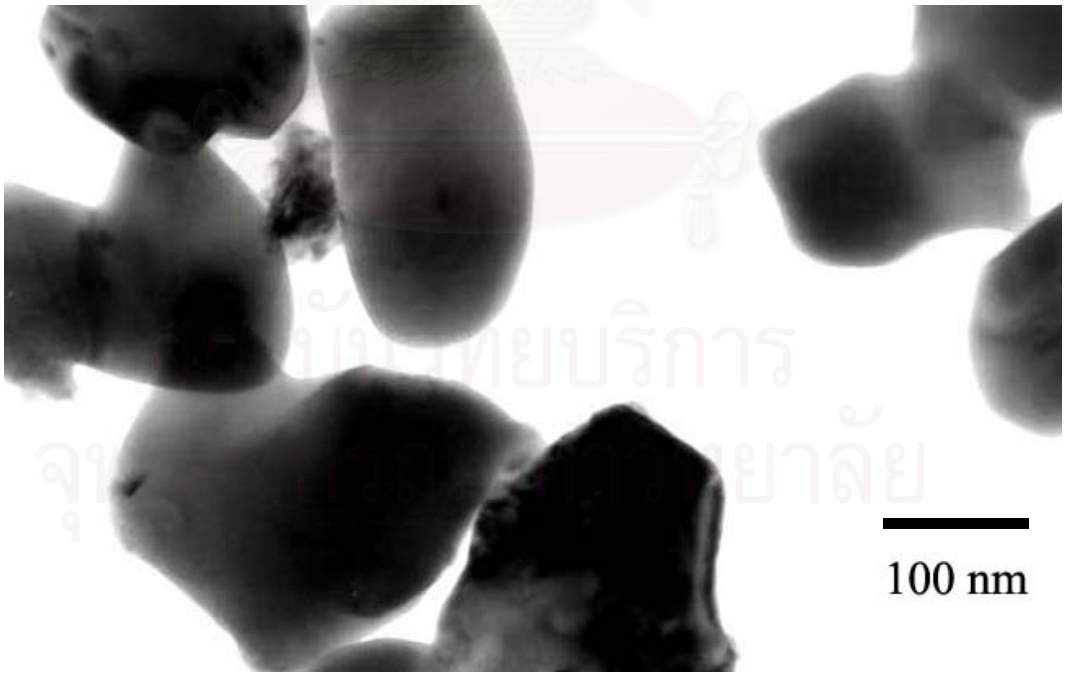

Figure 5.24(b) TEM photograph of iron oxide synthesized at 300°C after calcined at 900°C (x100,000).

5.1. 5 Formation of pure zinc oxide, (ZnO).

Zinc oxide were prepared by reaction in 1,4-butanediol at various temperature (200, 250 and 300°C). The XRD patterns of as-synthesized and product after calcination was shown in Figure 5.25 to Figure 5.27. Their XRD patterns were almost identical to that before calcination except the fact that the peaks were sharper. Unlikely all previous metal oxides, crystallite size of zinc oxide obtained from glycothermal reaction are very strong depend on reaction temperature. Crystallite size, which calculated by the XRD broadening, was 20.3, 70.1 and 139.3 for product synthesized at 200, 250 and 300°C, respectively. This crystallite size is in good agreement with the crystallite size observed by TEM, suggests that each particle is a single crystal. The BET surface area of zinc oxides synthesized at 200, 250 and 300°C were 13.2, 8.0 and 9.8 m^2/g, respectively.

Zinc oxide obtained from all temperature were calcined at temperature of 500° to 900°C. The BET surface area and XRD patterns of the calcined products were investigated. TEM photograph of as-synthesized products and product after calcination at 900°C was shown in Figure 5.28 to Figure 5.29. The particle size of zinc oxide obtained from lower reaction temperature are increase more rapidly. The BET surface area and crystallite size of all products after calcination were summarized in Table 5.5.

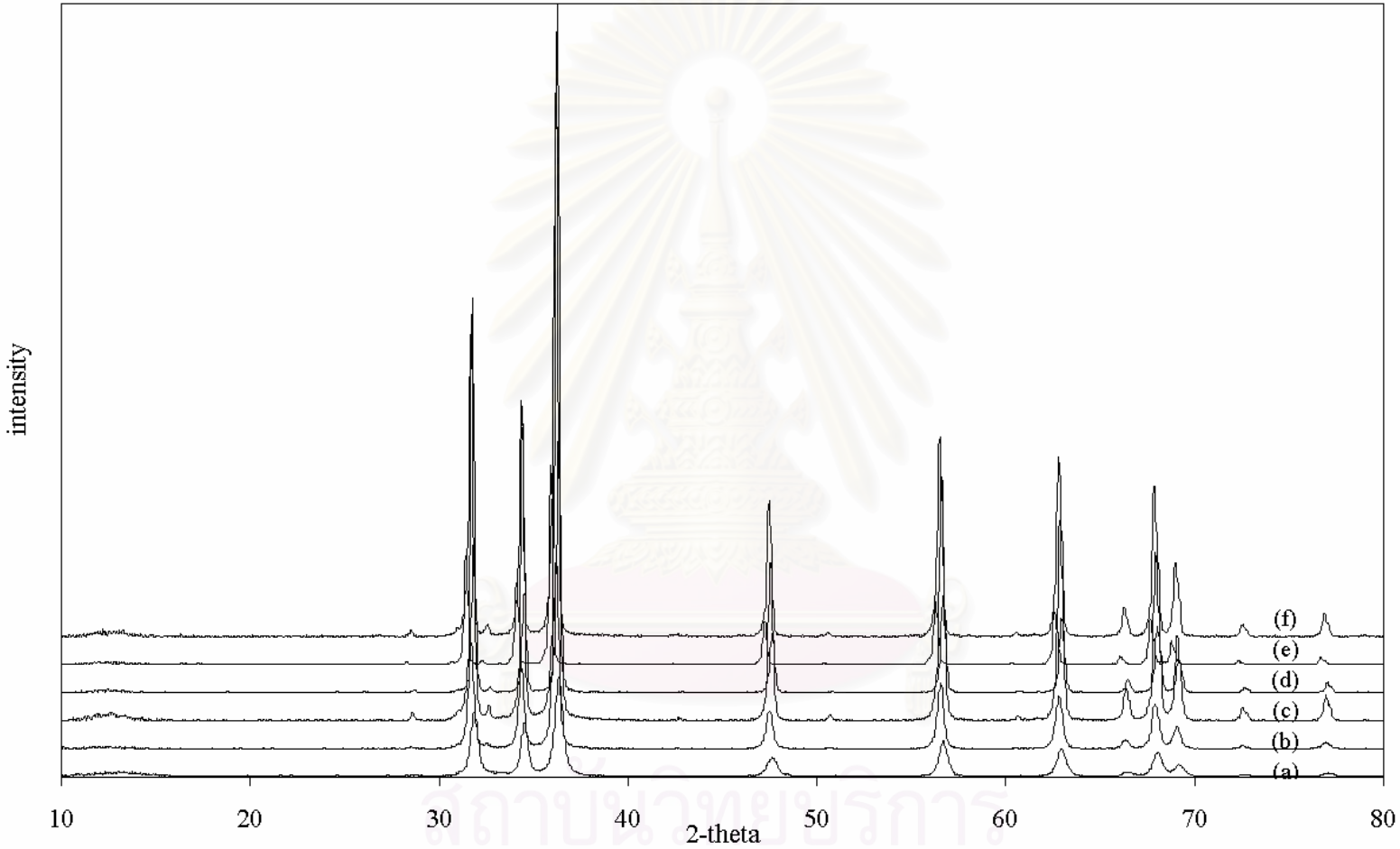

Figure 5.25 XRD patterns of zinc oxide synthesized at 200°C (a) before and after calcined at (b) 500°C (c) 600°C (d) 700°C (e) 800°C and (f) 900°C.

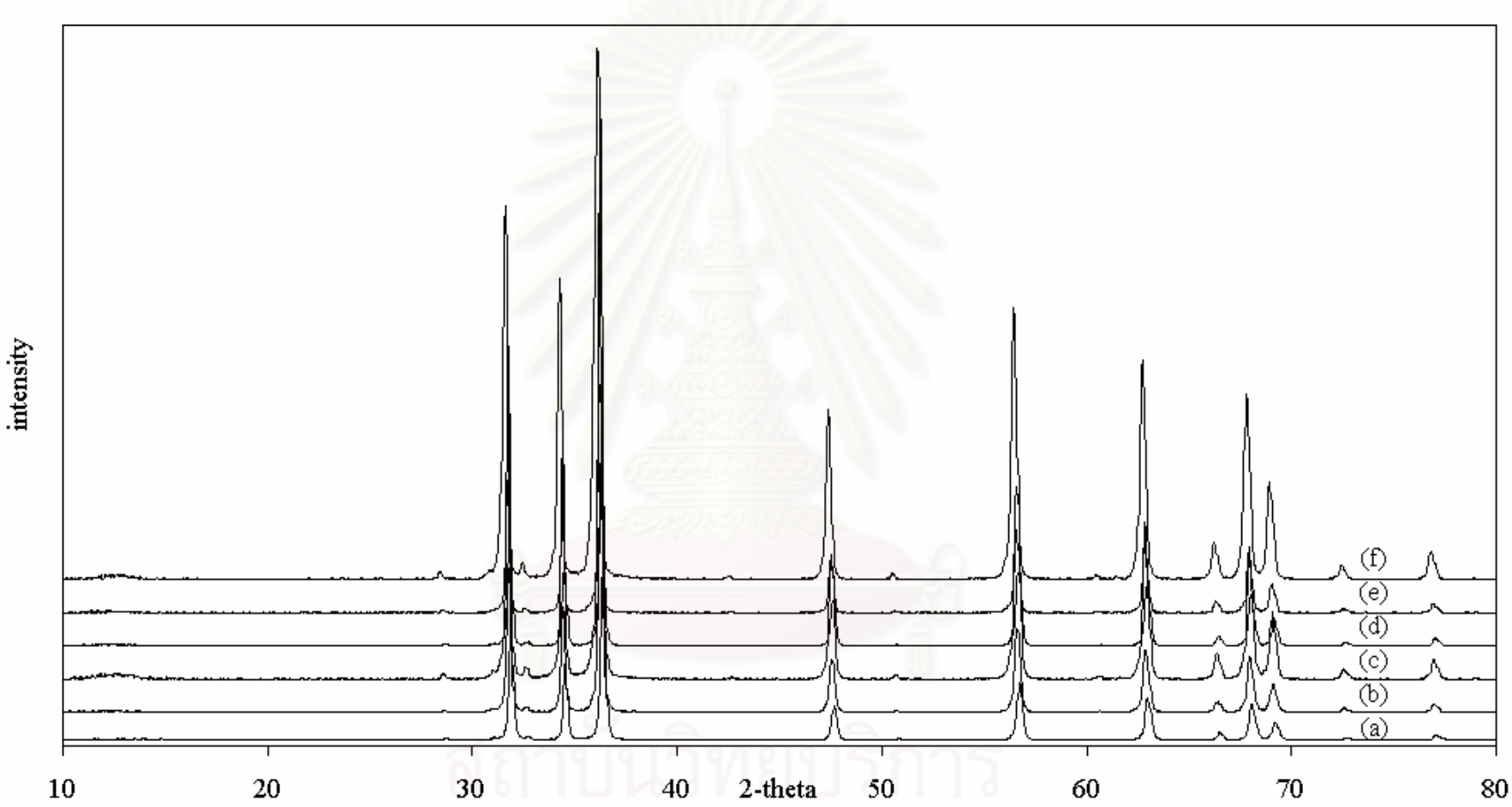

Figure 5.26 XRD patterns of zinc oxide synthesized at 250 °C (a) before and after calcined at (b) 500°C (c) 600°C (d) 700°C (e) 800°C and (f) 900°C.

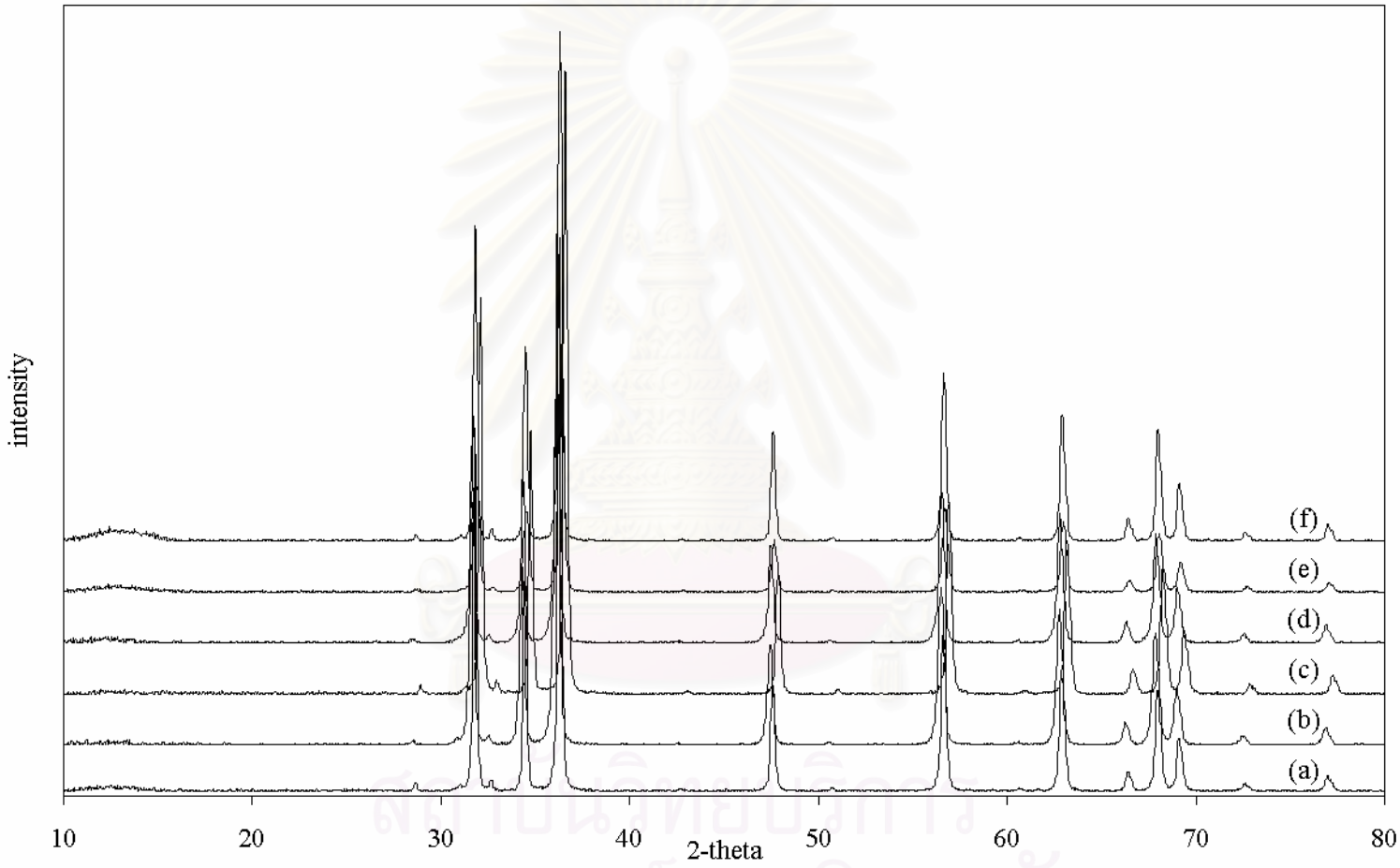

Figure 5.27 XRD patterns of zinc oxide synthesized at 300°C (a) before and after calcined at (b) 500°C (c) 600°C (d) 700°C (e) 800°C and (f) 900°C.

Table 5.5 BET surface area and crystallite size of the as-synthesized and calcined products zinc oxide synthesized at different reaction temperature.

Reaction temperature, °C	Calcination temperature, °C	Surface area (m^2/g)		d^c (nm)
		S_1[a]	S_2[b]	
200	As-synthesized	13.2	52.7	20.3(21.9)[d]
	500	1.9	30.5	44.0
	600	1.1	18.0	59.3
	700	1.0	13.5	78.9
	800	0.9	10.9	97.5
	900	0.6	8.9	120.3
250	As-synthesized	8.0	15.2	70.1(72.4)[d]
	500	3.2	13.9	77.1
	600	1.6	10.8	99.1
	700	1.5	10.0	106.6
	800	1.4	9.3	114.6
	900	1.3	8.1	121.6
300	As-synthesized	9.8	9.7	139.3(142.5)[d]
	500	6.5	7.1	148.9
	600	5.1	7.0	151.6
	700	4.0	7.0	152.1
	800	3.6	6.1	173.1
	900	2.8	6.0	178.2

[a] Surface area measured by BET method(Appendix B)

[b] Surface area calculated from crystallite size(Appendix B)

[c] Crystallite size from the line broadening using Scherrer equation.

[d] Particle size observed from TEM photograph.

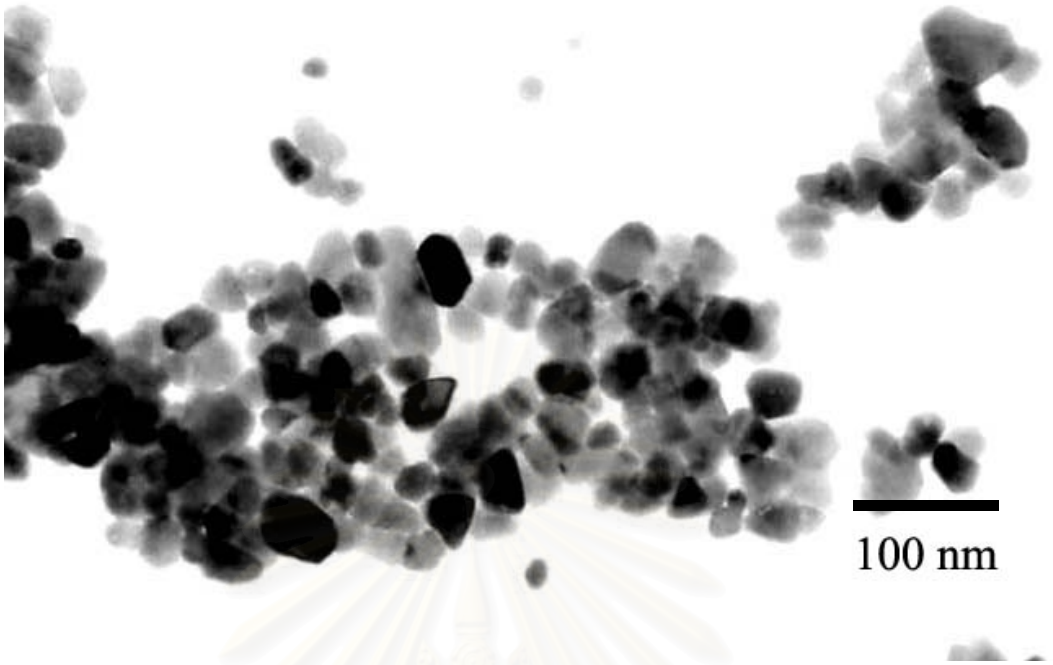

Figure 5.28(a) TEM photograph of as-synthesized zinc oxide synthesized at 200°C (x150,000).

Figure 5.28(b) TEM photograph of zinc oxide synthesized at 200°C after calcined at 900°C (x100,000).

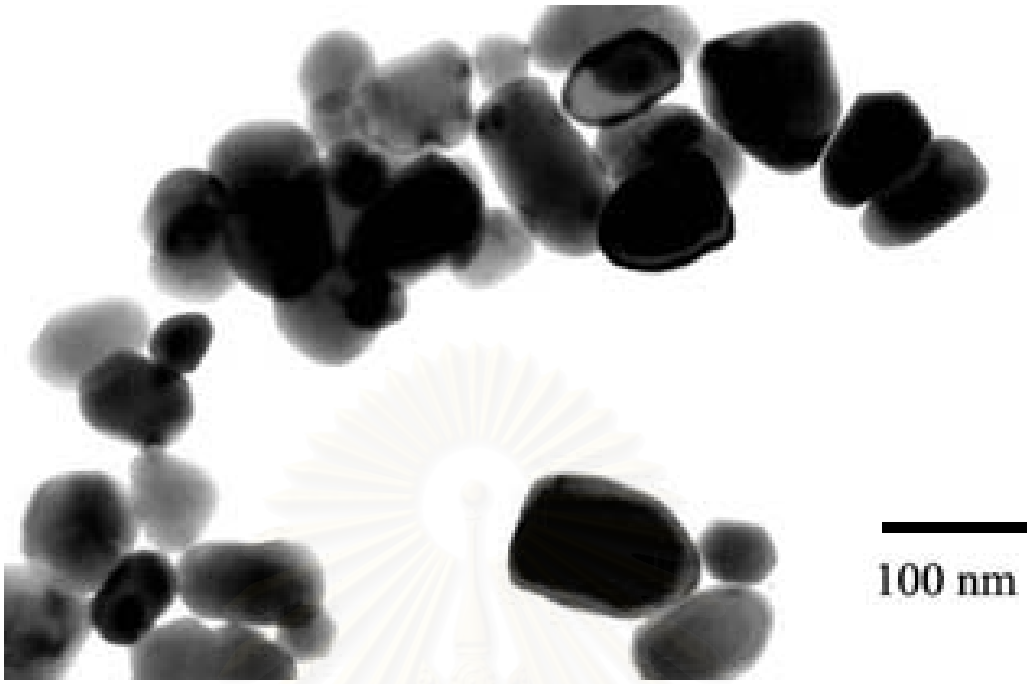

Figure 5.29(a) TEM photograph of as-synthesized zinc oxide synthesized at 250 °C (x150,000).

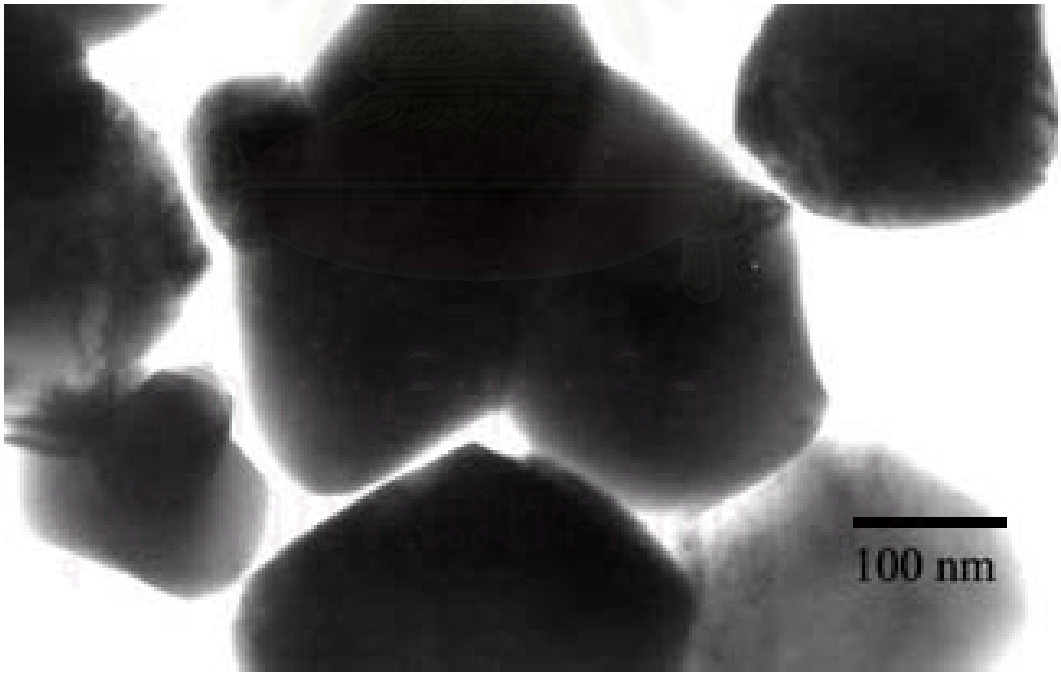

Figure 5.29(b) TEM photograph of zinc oxide synthesized at 250°C after calcined at 900°C (x100,000).

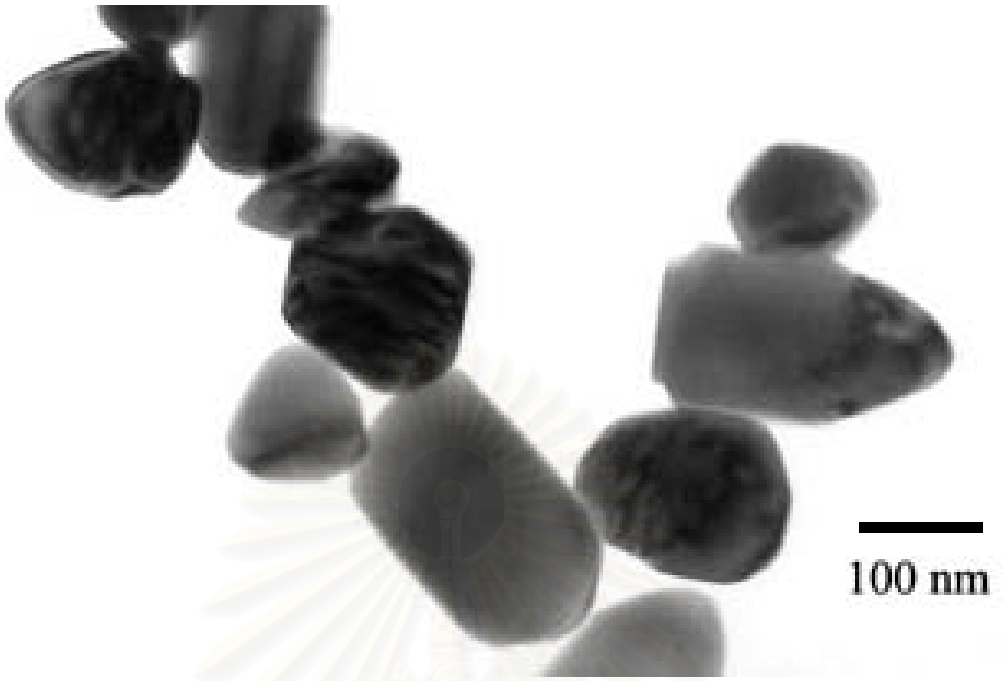

Figure 5.30(a) TEM photograph of as-synthesized zinc oxide synthesized at 300°C (x150,000).

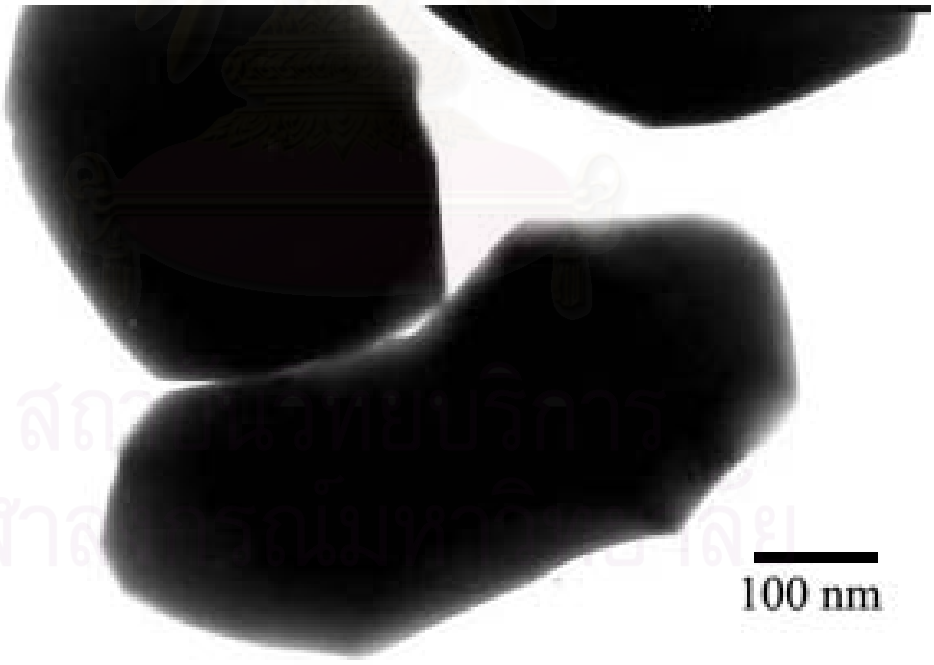

Figure 5.30(b) TEM photograph of zinc oxide synthesized at 300°C after calcined at 900°C (x100,000).

5.1. 6 Formation of pure nickel oxide (NiO).

Reaction of nickel acetylacetonate in 1,4-butanediol at 250°C and 300°C under autogeneous pressure yields product of different structure. An XRD pattern of the products obtained by all reactions was shown in Figure 5.31. The XRD patterns of as-synthesized product from reaction at 300°C show srtucture of nickel oxide, NiO. But XRD patterns of product from reaction at 250°C showed an unidentified phase. The crystallization of nickel oxide is analyze by TGA of product synthesized at 250°C. The TGA result was shown in Figure 5.32. The product was heating from room temperature to 800°C with the heating rate of 10°C min^{-1}. The weight curve is raising when the temperature increased. This can explained that the nickel metal retains in the product and adsorbs oxygen to form nickel oxide (NiO). The formation of nickel oxide was similar to that of manganese oxide.

By the XRD patterns of as-synthesized product, only product obtained from reaction at 300°C was calcined in temperature range of 500-900°C. From Figure 5.33, all product after calcined at various temperature were almost identical to that before calcination except the fact that the peaks were more sharp. The crystallite sized of as-synthesized product at 300°C is 24.0 nm with quite agreement with the crystallite size observed from TEM. TEM photograph of product after calcined at 900°C (Figure 5.34(b))

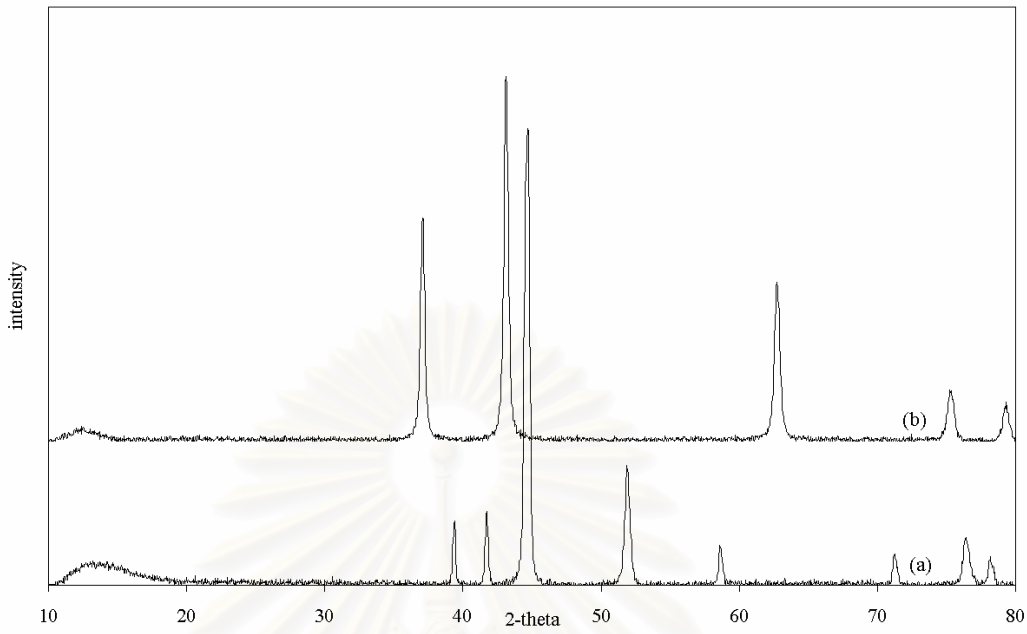

Figure 5.31 XRD patterns of as-synthesized product obtained from reaction of Ni acetylacetonate (a) at 250°C and (b) at 300°C.

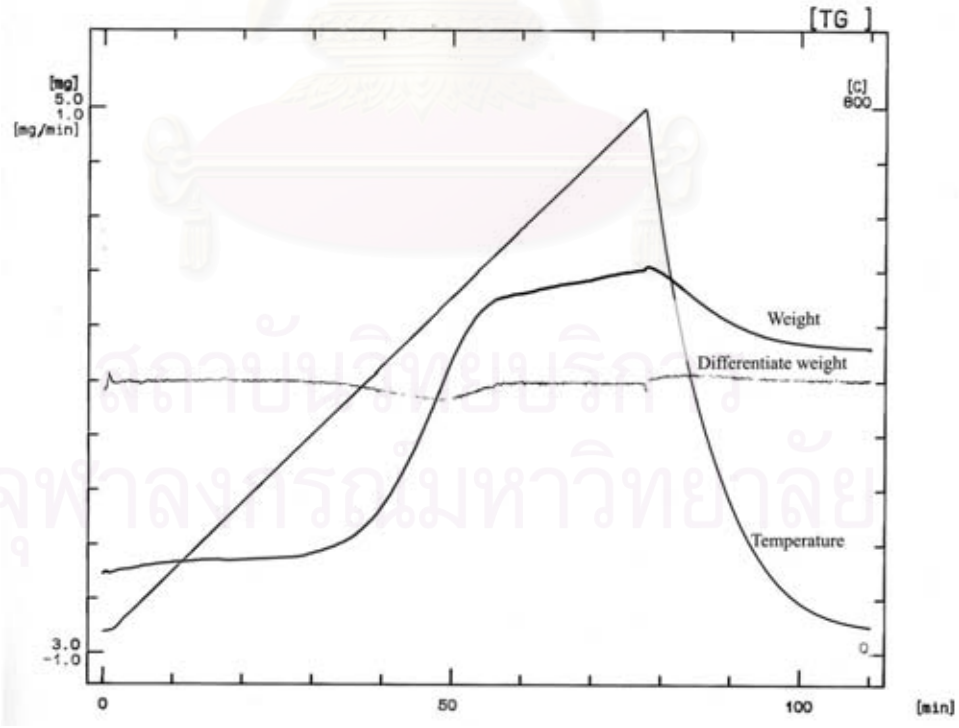

Figure 5.32 TGA thermogram of product obtained from reaction of Ni acetylacetonate at 250°C.

Table 5.6 BET surface area and crystallite size of the as-synthesized and calcined products nickel oxide synthesized at 300°C.

Reaction temperature, °C	Calcination temperature, °C	Surface area (m^2/g)		d^c (nm)
		S_1[a]	S_2[b]	
300	As-synthesized	5.5	37.2	24.0(26.4)[d]
	500	2.1	26.3	33.8
	600	1.4	16.4	53.2
	700	1.2	12.4	70.9
	800	1.1	7.0	125.4
	900	0.8	6.0	145.1

[a] Surface area measured by BET method(Appendix B)

[b] Surface area calculated from crystallite size(Appendix B)

[c] Crystallite size from the line broadening using Scherrer equation.

[d] Particle size observed from TEM photograph.

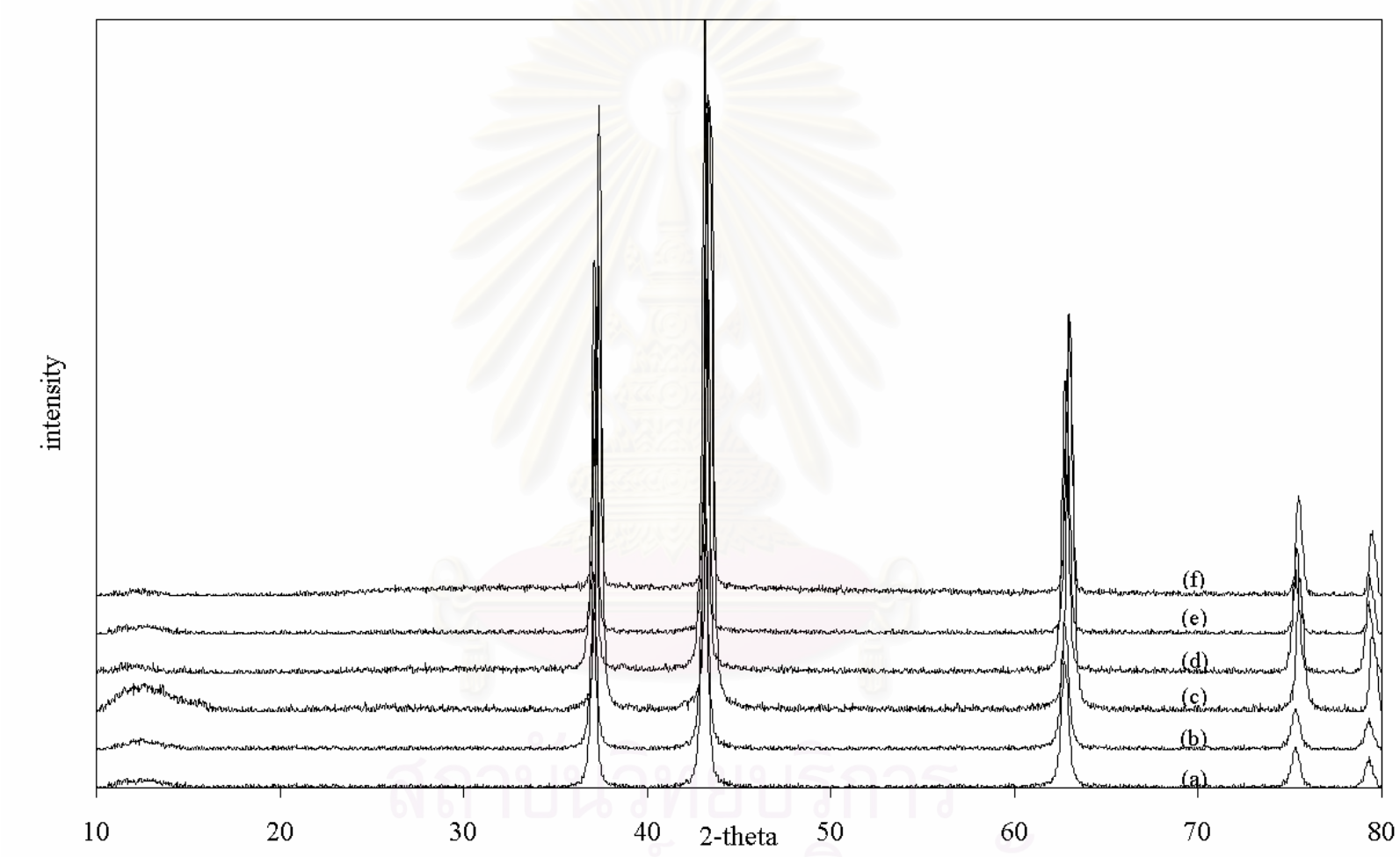

Figure 5.33 XRD patterns of nickel oxide synthesized at 300°C (a) before and after calcined at (b) 500°C (c) 600°C (d) 700°C (e) 800 °C and (f) 900°C.

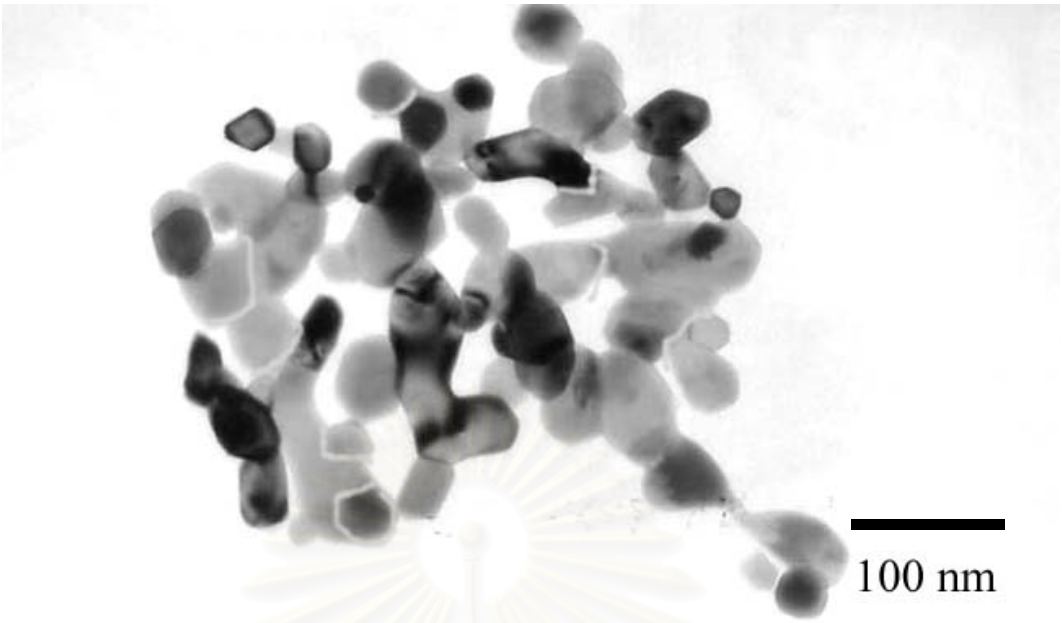

Figure 5.34(a) TEM photograph of as-synthesized nickel oxide synthesized at 300°C (x150,000)

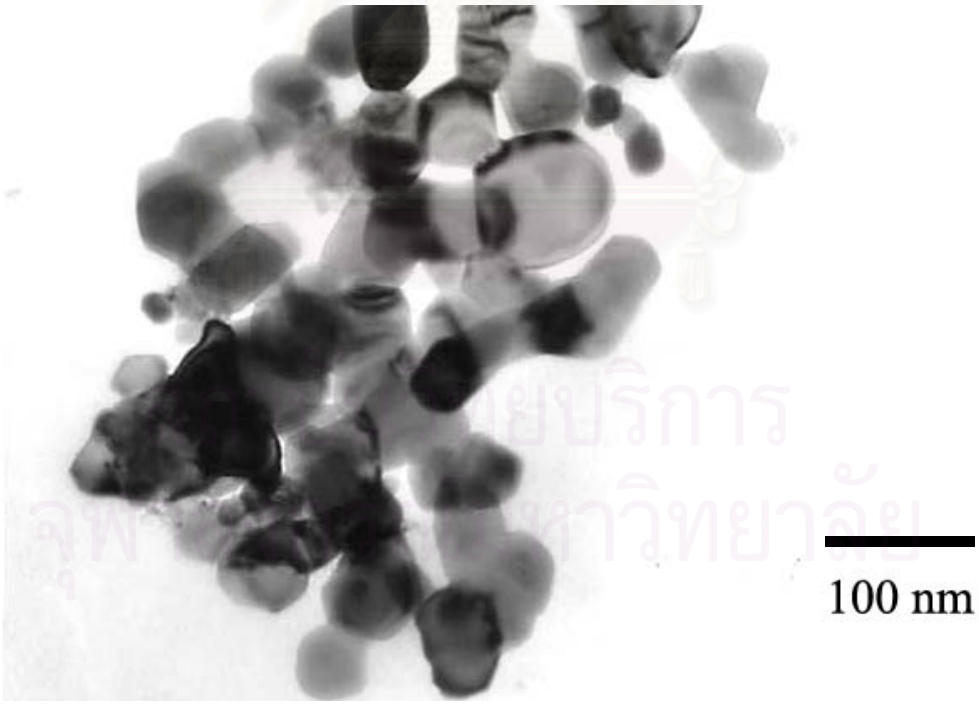

Figure 5.34(b) TEM photograph of as-synthesized nickel oxide synthesized at 300°C after calcined at 900°C (x100,000).

5.2 Determination of the thermal stability of the products

The properties and thermal stability of products can be controlled by the formation of the crystal (i.e. reaction condition, structure of starting material, type of organic). The mechanism of formation of titanium oxide crystal was studies by Theinkaew [30]. The reaction of titanium tert-butoxide in 1,4-butanediol at 300°C (Glycothermal reaction) yielded nanocrystalline titanium oxide. Under glycothermal conditions, titanium tert-butoxide was easily converted to glycoxide. Thermal decomposition of the glycoxide molecule proceeded by intra molecular participation of the remaining hydroxyl group of glycol moiety, yielding a ≡Ti-O^- anion. The nucleophilic attack of this titanate ion on another ion and crystallization of titanium oxide took place, finally yielding the anatase titanium oxide. The mechanism of titanium tert-butoxide in 1,4-butanediol can be depicted as follow:

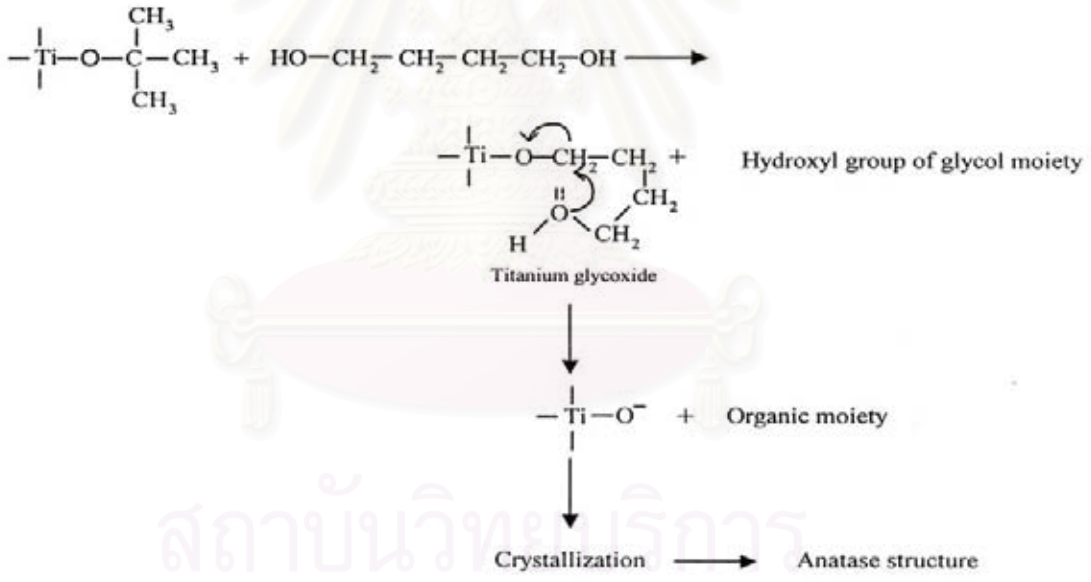

Figure 5.35 Mechanism of glycothermal reaction for the titanium oxide formation

For reaction of metal acetylacetonate (where M = Cr, Fe and Zn) in 1,4-butanediol , metal acetylacetonate can also form metal glycoxide. But the thermal decomposition of glycoxide may not complete. The product will crystallization after heated treatment at desired temperature. Reaction of iron acetylacetonate and zinc

acetylacetonate obtain of iron oxide and zinc oxide directly, respectively. The mechanism of metal acetylacetonate has shown in Figure 5.36

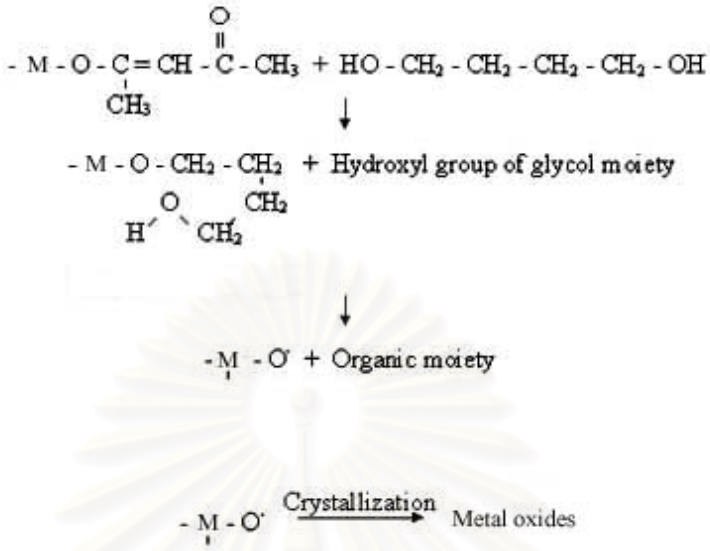

Figure 5.36 Mechanism of glycothermal reaction for the metal oxide formation (where M = Cr, Fe and Zn)

However, the formation mechanism of manganese oxide and nickel oxide is different from the former mechanism in Figure 5.36. This mechanism includes the solid state reaction. The propose mechanism is

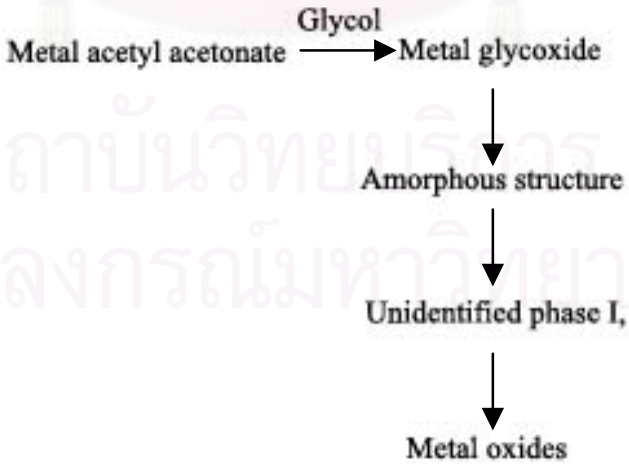

Figure 5.37 Propose mechanism of glycothermal reaction for metal oxide formation (where M = Ni, Mn)

To determine the thermal stability of metal oxide, in this work has defined

Thermal stability = specific surface area of product after calcination/ specific surface area of as-synthesized product

$$= BET/BET_0$$

From this relation, the product with higher thermal stability must have higher value of BET/BET_0. To discuss the effect of as-synthesized crystallite size (d_0) on thermal stability of transition metal oxide must compare the thermal stability of sample with different as-synthesized crystallite size.

For chromium oxide synthesized at different reaction temperature, data were plotted between log BET/BET_0 and log $T/\sqrt{d_0}$. The data was shown in Table 5.7.

In Figure 5.35 relation between thermal stability of chromium oxide with different as-synthesized crystallite size are almost linearly. When compare product at the same calcination temperature, product with smaller crystallite size will exhibited lower thermal stability.

Table 5.7 Thermal stability data for metal oxides synthesized at different temperature

Metal oxides	Product synthesized at 250°C		Product synthesized at 300°C	
	$T/\sqrt{d_0}$	BET/BET_0	$T/\sqrt{d_0}$	BET/BET_0
Cr_2O_3	192.053	0.745	154.507	0.944
	216.899	0.490	174.495	0.874
	241.744	0.296	194.483	0.622
	266.589	0.133	214.471	0.402
	291.434	0.088	234.459	0.192
TiO_2	285.957	0.686	204.661	0.893
	322.950	0.153	231.137	0.815
	359.943	0.086	257.614	0.603
	396.936	0.052	284.090	0.511
	433.929	0.034	310.566	0.320
Mn_2O_3	141.742	0.575	126.535	0.744
	157.979	0.400	141.029	0.592
	174.215	0.311	155.524	0.475
	190.451	0.218	170.018	0.370
	206.687	0.132	184.512	0.181
Fe_2O_3	150.161	0.360	134.562	0.461
	169.587	0.245	151.970	0.321
	189.012	0.173	169.378	0.298
	208.438	0.104	186.785	0.229
	227.864	0.040	204.193	0.200
ZnO	92.325	0.401	65.494	0.660
	104.269	0.203	73.967	0.518
	116.213	0.188	82.440	0.407
	128.157	0.177	73.967	0.362
	140.100	0.166	99.385	0.284

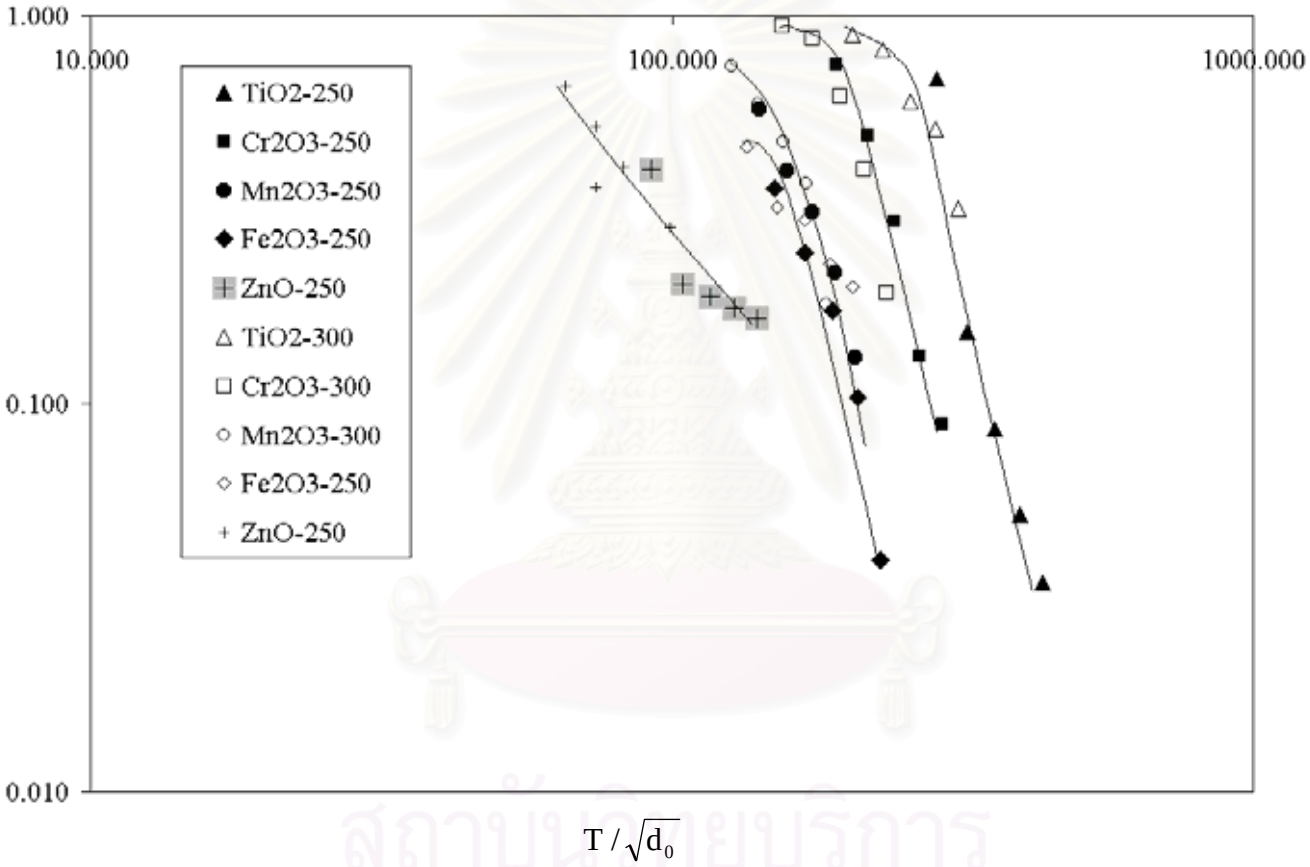

Figure 5.38 The relation between log BET/BET$_0$ and log T / $\sqrt{d_0}$ of metal oxides synthesized at different reaction temperature.

Another section is to compare the thermal stability between different metal oxides. The crystallite size data of the products were plotted as the relation between d/d_0 versus d_0. From this relation the thermal stability can be defined as,

Thermal stability = d/d_0

where d = crystallite size of product after calcined at 900°C

d_0 = crystallite size of product before calcined at 900°C

The crystallite size is subjected to change after calcination. The product with higher thermal stability would be the least change in crystallite size. All the d_0 used in the figure were the crystallite sizes of as-synthesized products and calcined products, at calcination temperature lower than 900ºC

Table 5.8 Crystallite size data of product before calcination (d_0) and calcined product at 900ºC (d).

Metal oxides	d_0	d
TiO_2	14.27	111.59
	14.99	74.06
	22.54	49.73
	34.93	52.3
	45.28	67.32
Cr_2O_3	16.09	88.30
	25.03	72.36
	30.48	68.45
	40.10	66.73
	48.50	79.04
Mn_2O_3	35.92	91.36
	42.13	83.13
	47.63	78.3
	59.6	87.33
Fe_2O_3	26.84	112.26
	34.08	118.7
	41.8	103.7
	54.5	99.4
	67.5	92.6
ZnO	20.2	120.3
	44.6	123.1
	70.1	121.6
	139.3	178.0
NiO	24.04	145.4
	33.82	152.5
	49.11	149.8
	53.2	140.7
	71.1	148.5

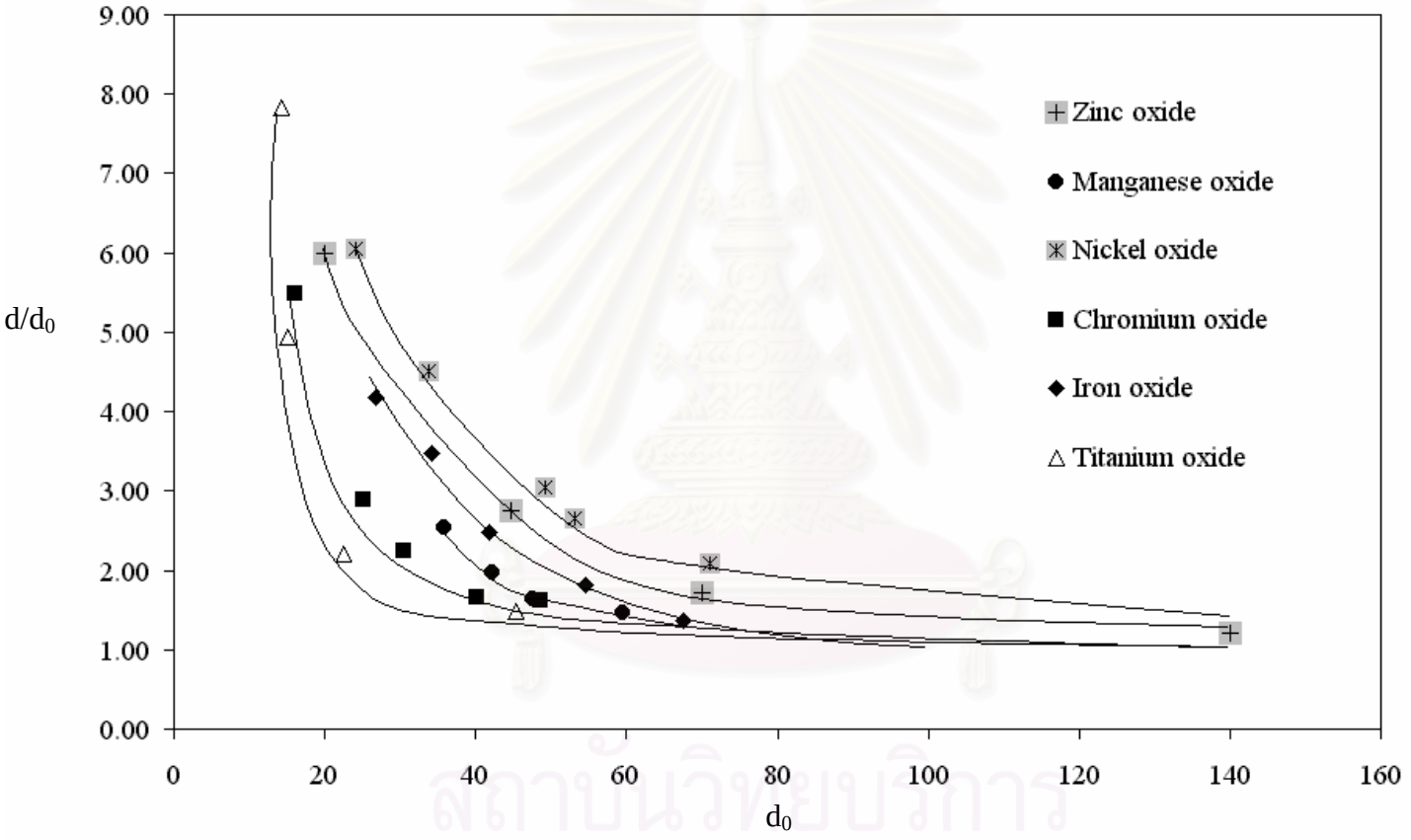

Figure 5.39 Relation between d/d_0 versus d_0 of different metal oxides

Comparison of thermal stability between different metal oxides will consider at the same crystallite. As shown in the figure 5.38 titanium oxide exhibited the highest thermal stability because at the same as-synthesized crystallite size it has lowest rate of the growth of crystallite size, compared to the other metal oxides. And nickel oxide exhbited the highest rate of crystal growth. So, nickel oxide is more sensitive to the increasing of crystallite size than the others. , in order to vary the crystallite size before calcination at 900ºC. The products, as-synthesized and calcined products, after calcined at 900ºC exhibited on the same line, revealed that they performed the same performance even after high calcination temperature. The thermal stability in order of rate of change in crystallite size of product after heat treatment is:

$TiO_2 > Cr_2O_3 > Mn_2O_3 > Fe_2O_3 > ZnO > NiO$

This result can explain by result of crystal structure. Titanium oxide has a structure of tetragonal [31]. For chromium oxide, manganese oxide and iron oxide which have the same structure of corundum. The factor that effect thermal stability of these metal oxides is the bond strength between metal ions and oxygen ions. Zinc oxide has a structure of hexagonal and cubic structure for nickel oxide.

Table 5.9 Strength of chemical bonds between metal ion and oxygen ion [32].

Molecule	Bond dissociation energy ($kJ\ mol^{-1}$)
Ti – O	672.4 ± 9.2
Cr – O	461.9 ± 9
Mn – O	402.9 ± 41.8
Fe –O	390.4 ±17.2
Ni – O	382.0 ± 16.7
Zn – O	159.4 ± 4

Because the crystal growing is related to the reconstruction of oxide surface [17]. A thermodynamically stable surface structure will not reconstruct on heating, provided the temperature is not too high, while a metastable surface would undergo

reconstruction. When a crystal of oxide is cleaved to generate the new surface, the ions in the cleavage plane are partitioned into solids in such a manner that charge neutrality is maintained in each solid. The factor which involved the reconstruction of oxide surface may including of crystal structure, bond strength between metal ion and oxygen ion, polarity of surface etc. All these factor can be integrated to the heat of formation of each transition metal oxide which represent the macroscopic property.

Table 5.10 Heat of formation of transition metal oxides [32].

Metal oxides	Heat of formation ($kJ\ mol^{-1}$)
TiO_2(Rutile phase)	-944
Cr_2O_3	-1140
Mn_2O_3	-959
Fe_2O_3	-824
NiO	-240
ZnO	-350

CHAPTER VI

CONCLUSIONS AND RECOMMENDATION

6.1 Conclusions

The conclusions of the present research are the following,

1) The reaction temperature of the crystallite formation can control physical properties and thermal stability of metal oxides.

2) Comparison of the thermal stability of transition metal oxide using rate of crystal growth are revealed the correlation,

$TiO_2 > Cr_2O_3 > Mn_2O_3 > Fe_2O_3 > ZnO > NiO$

6.2 Recommendation for the further studies

From the previous conclusions, the following recommendations for the further studies are proposed.

1) To study the mechanism of crystallization of nickel oxide and manganese oxide from glycothermal method.

2) To verify the effect of bond strength between metal ion and oxygen ion on thermal stability of metal oxides by temperature-programmed reduction.

REFERENCES

[1] P. Moriceau, B. Grzybowska , Y. Barbaux, G. Wrobel and G. Hecquet. Oxidative dehydrogenation of isobutane on Cr-Ce-O oxide: I. Effect of the preparation method and of the Cr content. Appl. Catal.A 168(1998): 269-277.

[2] S. DeRossi, G. Ferraris, S. Fremiotti, V. Indovina and A. Cimino. Isobutane dehydrogenation on chromia/zirconia catalysts. Appl. Catal.A 106(1993): 125-141.

[3] S. DeRossi, G. Ferraris, S. Fremiotti, E. Garrone, G. Ghiotti, Mc. Campa and V. Indovina. Propane dehydrogenation on chromia silica and chromia alumina catalysts. J. Catalysis 148(1994): 36-46.

[4] S. Udomsak, R. Anthony. Isobutane dehydrogenation oil chromia/silica-titania mixed oxide and chromia/gamma-alumina catalysts. Ind.Eng.Chem.Res. 35(1996): 47-53.

[5] F. Cavani, M. Koutyrev, F. Trifiro, A. Bartolini, D. Ghisletti, R. Iezzi, A. Santucci and G. DelPiero. Chemical and physical characterization of alumina-supported chromia-based catalysts and their activity in dehydrogenation of isobutane. J. Catalysis 158(1996): 236-250.

[6] B. Grzybowska, J. Sloczynski, R. Grabowski, K. Wcislo, J. Stoch and A. Kozlowska. Chromium oxide/Alumina catalysts in oxidative dehydrogenation of isobutane. J. Catalysis 178(1998): 687-700.

[7] L. R. Mentasty, O. F. Gorriz and L. E. Cadus. Chromium oxide supported on different Al_2O_3 supports: catalytic propane dehydrogenation. Ind. Eng. Chem. Res. 38(1999): 396-404.

[8] J. Engweiler, J. Nickl, A. baiker, K. Kohler, CW. Schlapfer and A. Vonzelewsky. Chromia supported on titania .2. Morphological properties and catalytic behavior in the selective reduction of nitric-oxide by ammonia. J. Catalysis 145(1994): 141-150.

[9] TA. Ramanarayanan, JD. Mumford, CM. Chun and R. Petkovic. Transport through chromia films. Solid State Ionics 136(2000): 89-90.

[10] M. Chatterjee, B. Siladitya and D. Ganguli. Chromia microspheres by the sol-gel techniqe. Mat.Lett. 25(1995): 261-263.

[11] H. Edward Curry-Hyde and A. Baiker. Catalytic reduction of nitric oxide over amorphous and crystalline chromia. Appl. Catal. A 90(1992): 183-197.

[12] T. Tsuzuki, and PG. McCormick. Synthesis of Cr_2O_3 nanoparticles by mechanochemical processing. Acta Materialia 48(2000): 2795-2801.

[13] J. Mougin, T. Le Bihan and G. Lucazeau. High pressure study of Cr_2O_3 obtained by high temperature oxidation by X-ray diffraction and Raman spectroscopy. J. Phy.Chem.Solids. 62(2001): 553-563.

[14] A. E. Gash, T. M. Tillotson, J. H. Satcher Jr., L. W. Hrubesh, and R. L. Simpson. New sol-gel synthetic route to transition and main-group metal oxide aerogels using inorganic salts precursors. J. Non-Cryst. Solids. 285(2001): 22-28.

[15] J. Kirchnerova, D. Klvana, and J. Chaouki. Preparation and characterization of alumina and chromia cryogel-based catalysts. Appl.Catal. A 196(2000): 191-198.

[16] N. Arul Dhas, Y. Koltypin and A. Gedanken. Sonochemical preparation and characterization of ultrafine chromium oxide and manganese oxide powders. Chem. Mater. 9(1997): 3159-3163.

[17] H. H. Kung, Transition Metal Oxides: Surface Chemistry and Catalysis, Elsevier Science Publishers (1991).

[18] Y. Oguri, R. E. Riman and H. K. Bowen. Processing of anatase prepared from hydrothermally treated alkoxy-derived hydrous titania. J. Mater. Sci. 23(1988): 2897-2904.

[19] M. Kondo, K. Shinozaki, R. Ooki and N. Mizutani. Crystallization behavior and microstructure of hydrothermal treated monodispersed titanium dioxide particles. J. Cerm. Soc. Japan 102(1994): 740-744.

[20] M. Inoue, Y. Kondo and T. Inui. An ethylene glycol derivative of boehmite. Inorg. Chem. 27(1988): 215-221.

[21] M. Inoue, and H. Tanino. Formation of microcrystalline α-alumina by glycothermal treatment of gibbsite. J. Am. Cerm. Soc. 72(1989): 352-353.

[22] M. Inoue, and H. Kominami. Thermal transformation of α-alumina formed by thermal decomposition of aluminum alkoxide in organic media. J. Am. Cerm. Soc. 75(1992): 2597-2598.

[23] M. Inoue, and H. Kominami. Novel synthetic method for the catalytic use of thermally stable zirconia: Thermal decomposition of zirconium alkoxide in organic media. Appl. Catal. A 97(1993): L25-L30.

[24] M. Inoue, H. Otsu, H. Kominami and T. Inui. Synthesis of submicron spherical crystals of gadolinium gallium garnets by the glycothermal method. J. Mater. Sci. Lett. 14(1995): 1303-1305.

[25] M. Inoue, H. Otsu and T. Inui. Glycothermal synthesis of rare earth aluminum garnets. J. Alloys Comp. 226(1995): 146-151.

[26] H. Kominami, J. Kato, and Y. Takada. Novel synthesis of microcrystalline titanium (IV) oxide having high thermal stability and ultra high photocatalytic activity: Thermal decomposition of titanium alkoxide in organic solvent. J. Catal. Lett. 46(1997): 235-240.

[27] H. Kominami, M. Kohno, and Y. Takada. Hydrolysis of titanium alkoxide in organic solvent at high temperature: A new synthetic method for nanosized, thermally stable titanium (IV) oxide. J. Ind. Chem. Res. 38(1999) 3925-3931.

[28] I. Findlay, T. J. Victor, SI Chemical Data, John Wiley & Sons Australia, Ltd., 1998.

[29] R. V. Kumar, Y. Diamant, and A. Gedanken. Sonochemical synthesis and characterization of nanometer-size transition metal oxides from metal acetates. Chem. Mater. 12(2000): 2301-2305.

[30] S. Theinkaew. Synthesis of large-surface area silica modified titanium (IV) oxide ultra fine particles. Master degree, Departmant of Chemical Engineering Faculty of Engineering Chulalongkorn University, 2000.

[31] D. L. Trimm, Design of Industrial Catalysts, Elsevier Scientific Publishing Company, 1980.

[32] Handbook of Chemistry and Physics, CRC Press, 81st edition 2000.

APPENDICES

APPENDIX A

CALCULATION OF CRYSTALLITE SIZE

X-ray diffraction is the important technique to characterization of crystalline materials and for the determination of crystal structures. The crystallite size are calculated from the x-ray diffraction broadening by using Scherrer formula:

$$d = \frac{K\lambda}{\beta \cos\theta} \qquad (A.1)$$

Where, d = Crystallite size, Å

K = Crystallite-shape factor = 0.89

λ = X-ray wavelength, for CuKα = 1.5406 Å

θ = Observed peak angle

β = X-ray diffraction broadening, rad

The X-ray diffraction broadening is the pure breadth of a powder reflection free of all broadening due to the experimental equipment, by using Warren's correction for instrumental broadening.

$$\beta^2 = \beta_P^2 - \beta_R^2 \qquad (A.2)$$

$$\beta = \sqrt{\beta_P^2 - \beta_R^2}$$

Where, β_P = The measured peak width in radians at half peak height

β_R = The corresponding width of a peak of standard material

Which is to say that the squared breadth of the pure diffraction profile equals to the squared of observed peak subtracted by the squared of the instrumental broadening profile. Standard α-alumina is used to observe the instrumental broadening.

Example A.1: The crystallite size of chromium oxide synthesized at 300 °C

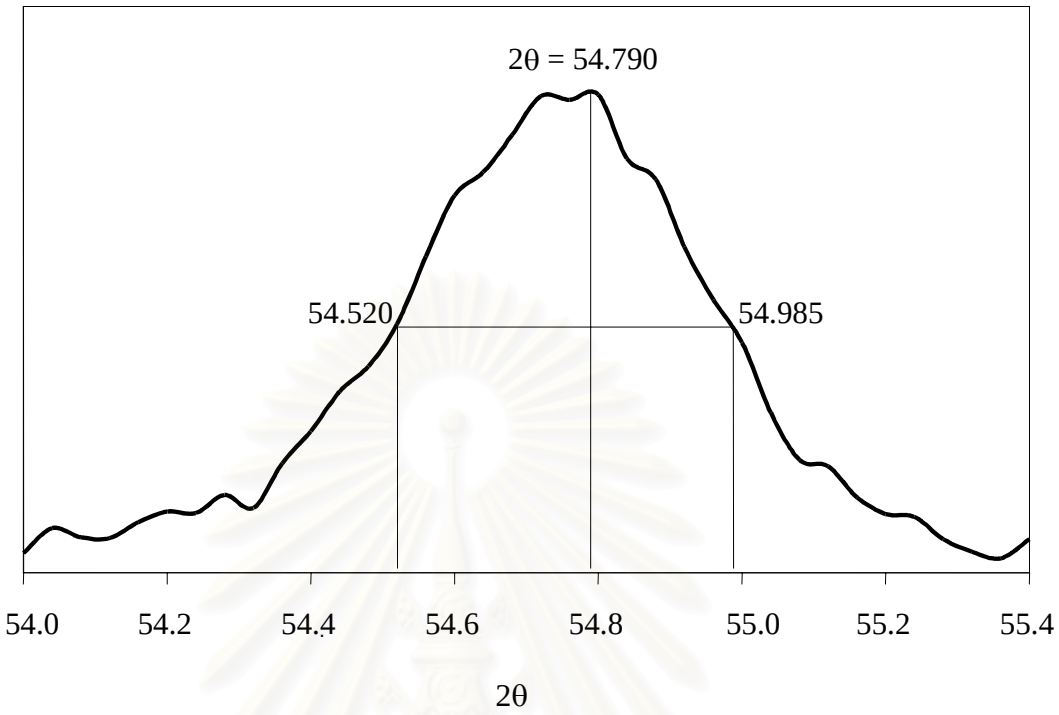

Figure A.1 The observation peak of chromium oxide to calculate the crystallite size

The observed peak broadening = 54.985º - 54.520º

= 0.465º

= 8.116×10^{-3} rad

The instrumental broadening = 5.23×10^{-3} rad

The pure diffraction profile = $\sqrt{\beta_P^2 - \beta_R^2}$ rad

= $\sqrt{\left(8.116 \times 10^{-3}\right)^2 - \left(5.230 \times 10^{-2}\right)^2}$ rad

β = 6.205×10^{-3} rad

2θ = 54.790º

θ = 27.38º

λ = 1.5406 Å

The crystallite size = $\frac{0.89 \times 1.5406}{0.006205 \times \cos 27.38}$ Å

= 250.31 Å

d = 25.031 nm

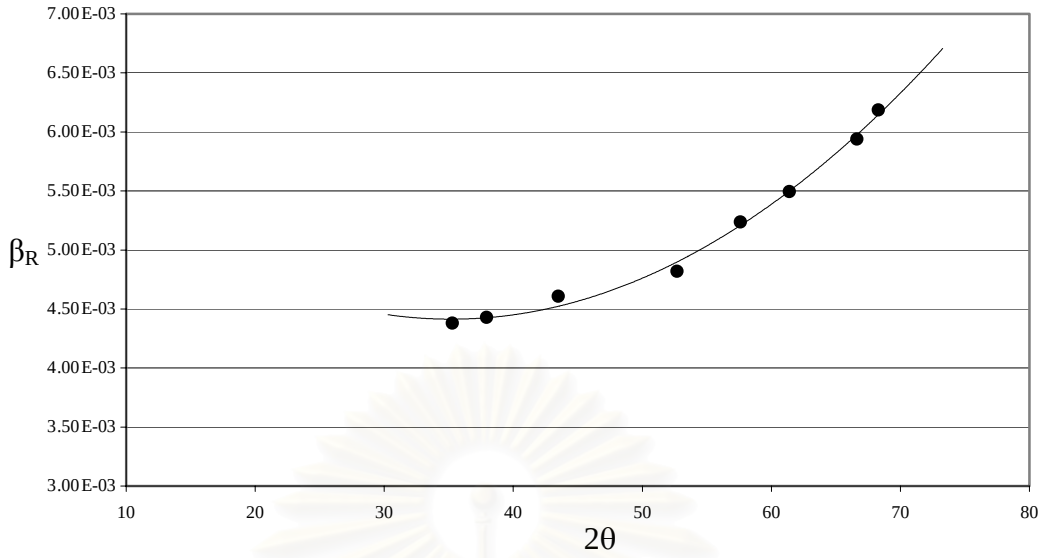

Figure A.2 The graph indicating the value of the line broadening attribute to the experimental equipment from the α-alumina standard

APPENDIX B

CALCULATION OF SPECIFIC SURFACE AREA

From Brunauer-Emmett-Teller (BET) equation

$$\frac{p}{n(1-p)} = \frac{1}{n_m C} + \frac{(C-1)p}{n_m C} \qquad \text{(B.1)}$$

Where, p = Relative partial pressure of adsorbed gas, P/P_0

P_0 = Saturated vapor pressure of adsorbed gas in the condensed state at the experimental temperature, atm

P = Equilibrium vapor pressure of adsorbed gas, atm

n = Gas adsorbed at pressure P, ml. at the NTP/g of sample

n_m = Gas adsorbed at monolayer, ml. at the NTP/g of sample

C = Exp $[(H_C - H_l)/RT]$

H_C = Heat of condensation of adsorbed gas on all other layers

H_l = Heat of adsorption into the first layer

Assume $C \rightarrow \infty$, then

$$\frac{p}{n(1-p)} = \frac{p}{n_m}$$

$$n_m = n(1 - p) \qquad \text{(B.2)}$$

The surface area, S, of the catalyst is given by

$$S = S_b \times n_m \qquad \text{(B.3)}$$

From the gas law

$$\frac{P_b V}{T_b} = \frac{P_t V}{T_t} \qquad \text{(B.4)}$$

Where, P_b = Pressure at 0°C

P_t = Pressure at t°C

T_b = Temperature at 0°C = 273.15 K

T_t = Temperature at t°C = 273.15 + t K

V = Constant volume

Then, $P_b = (273.15/ T_t) \times P_t = 1$ atm

Partial pressure

$$P = \frac{[\text{Flow of } (He + N_2) - \text{Flow of } He]}{\text{Flow of } (He + N_2)} \quad (B.5)$$

$$= 0.3 \text{ atm}$$

For nitrogen gas, the saturated vapor pressure equals to

$$P_0 = 1.1 \text{ atm}$$

then, $p = P/P_0 = 0.3/1.1 = 0.2727$

To measure the volume of nitrogen adsorbed, n

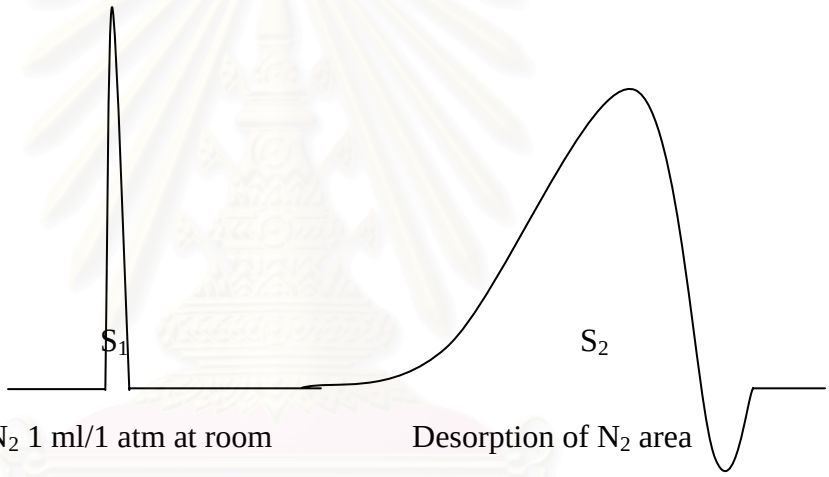

N_2 1 ml/1 atm at room temperature area

Desorption of N_2 area

$$n = \frac{S_2}{S_1} \times \frac{1}{W} \times \frac{273.15}{T} \text{ ml. /g of catalyst} \quad (B.6)$$

Where, S_1 = N_2 1 ml/1 atm at room temperature area

S_2 = Desorption of N_2 area

W = Sample weight, g

T = Room temperature, K

Therefore,

$$n_m = \frac{S_2}{S_1} \times \frac{1}{W} \times \frac{273.15}{T} \times (1 - p)$$

$$n_m = \frac{S_2}{S_1} \times \frac{1}{W} \times \frac{273.15}{T} \times 0.7272 \quad (B2.1)$$

Whereas, the surface area of nitrogen gas from literature equal to

S_b = 4.373 m^2/ml of nitrogen gas

Then,

$$S = \frac{S_2}{S_1} \times \frac{1}{W} \times \frac{273.15}{T} \times 0.7272 \times 4.343$$

$$S = \frac{S_2}{S_1} \times \frac{1}{W} \times \frac{273.15}{T} \times 3.1582 \ m^2/g \qquad \text{(B.7)}$$

Another method for surface area calculation is using the crystallite size from XRD line broadening and density of each metal oxide.

$$\text{Surface area} = \frac{6}{\rho d}$$

Where ρ = density of metal oxide

d = crystallite size calculated from scherrer equation

Table B.1 Density of transition metal oxide [28].

Metal oxides	Density ($g\ cm^{-3}$)
TiO_2	4.2
Cr_2O_3	5.2
Mn_2O_3	4.5
Fe_2O_3	5.2
NiO	6.7
ZnO	5.6

Example B.1 Specific surface area calculation for chromium oxide synthesized at 250°C after calcined at 350°C.

Crystallite size = 16.1 nm

Density of chromium oxide = 5.2 g cm^{-3}

$$\text{Surface area} = \frac{6}{5.2x\,10^{6}\,x\,16.1x\,10^{-9}}$$

$$= 60.22\ m^2/g$$

APPENDIX C

CALCULATION OF PARTICLE SIZE FROM TEM PHOTOGRAPH

Particle sizes measured from TEM photograph of the as-synthesized products and calcined products of the metal oxides were calculated as follows,

Example C1: The measurement of as-synthesized particle size of chromium oxide synthesized at 250°C

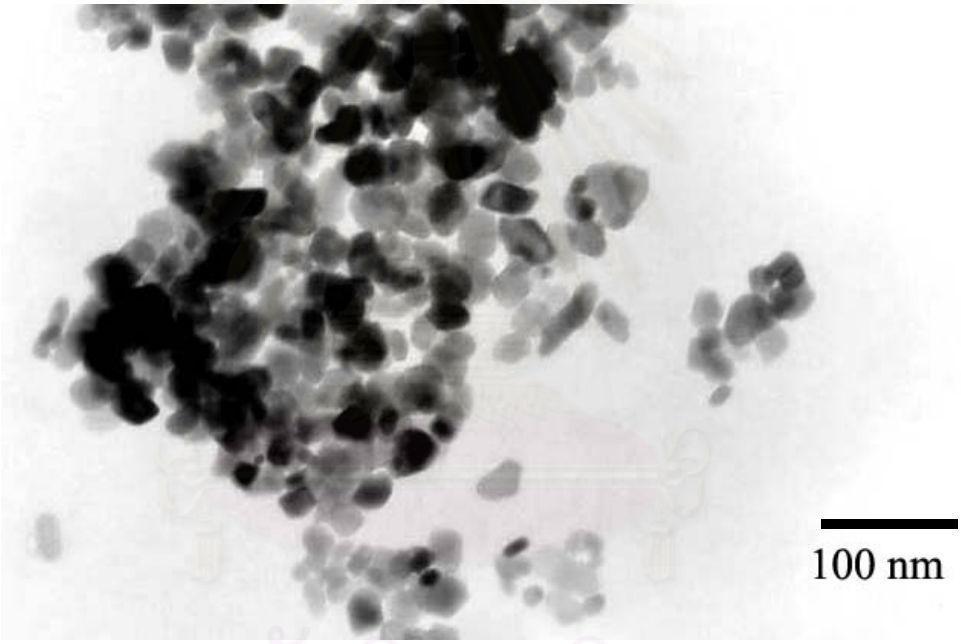

Figure C1 TEM photograph of as-synthesized chromium oxide

At X150000 magnification, the scale is

150 mm = 1 μm

= 1000 nm

From TEM photograph, it was found that the crystallite size of the particles closed to each other and that was 2.5 mm. Therefore, the crystallite size observed by TEM is

Table C.1 The particle size of chromium oxide synthesized at 250°C observed from TEM photograph

Size(mm)	1.6	2.2	2.3	2.5	2.7	2.8	3.0
Number	2	1	3	17	10	4	3

The total measured particle is 40 particles. And the average size is 2.5 mm.

$$\text{Particle size} = \frac{1000\ nm}{150\ mm} \times 2.5\ mm$$

Particle size = 17.1 nm

The particle size distribution of chromium oxide which observed from TEM photograph as shown below.

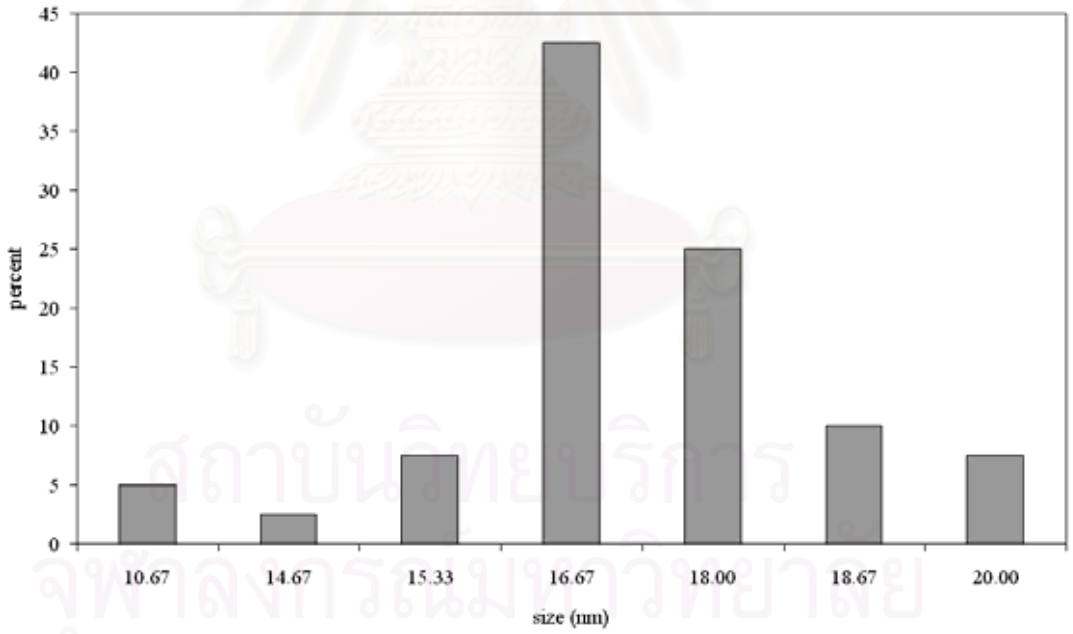

Figure C.2 The particle size distribution of chromium oxide synthesized at 250°C.

Example C2: The measurement of as-synthesized particle size of chromium oxide synthesized at 300°C

Table C.2 The particle size of chromium oxide synthesized at 300°C observed from TEM photograph

Size(mm)	2.9	3.1	3.3	3.5	3.6	3.7	4.0	4.2
Number	1	1	2	2	11	10	3	3

The total measured particle is 30 particles. And the average size is 3.61 mm.

At X150000 magnification, the scale is

150 mm = 1 μm

= 1000 nm

Particle size $= \frac{1000\ nm}{150\ mm} \times 2.5\ mm$

Particle size = 24.1 nm

The particle size distribution of chromium oxide which observed from TEM photograph as shown below.

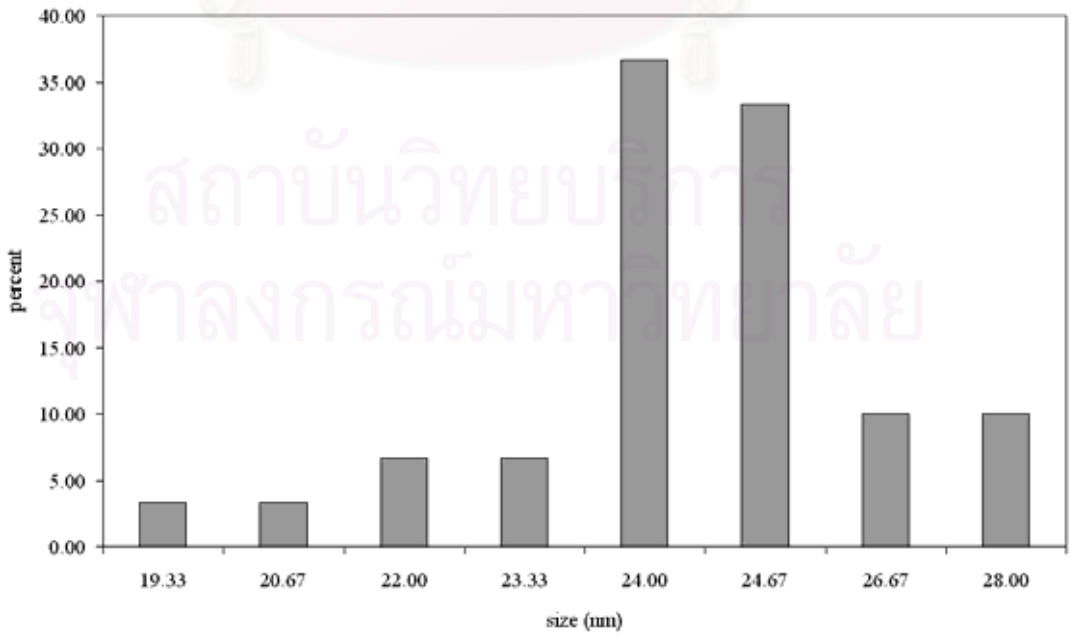

Figure C.3 The particle size distribution of chromium oxide synthesized at 300°C.

Example C3: The measurement of as-synthesized particle size of titanium oxide synthesized at 300°C

Table C.3 The particle size of titanium oxide synthesized at 300°C observed from TEM photograph

Size(mm)	1	1.5	2.0	2.5	3.0
Number	3	4	8	11	4

The total measured particle is 30 particles. And the average size is 2.15 mm.

At X150000 magnification, the scale is

150 mm = 1 μm

= 1000 nm

Particle size $= \frac{1000\ nm}{150\ mm} \times 2.5\ mm$

Particle size = 14.3 nm

The particle size distribution of titanium oxide, which observed from TEM photograph as shown below.

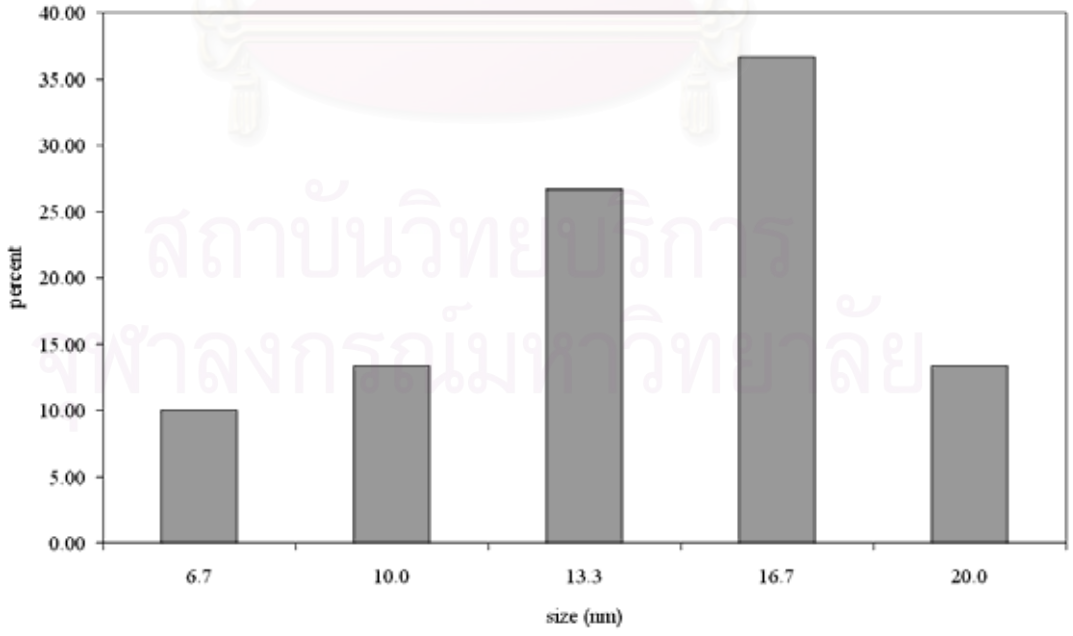

Figure C.4 The particle size distribution of titanium oxide synthesized at 300°C.

Example C4: The measurement of as-synthesized particle size of manganese oxide synthesized at 300°C

Table C.4 The particle size of manganese oxide synthesized at 300°C observed from TEM photograph

Size(mm)	3.5	4.0	4.5	5.5	6.0	6.5	7.0
Number	1	1	2	2	5	2	2

The total measured particle is 15 particles. And the average size is 5.63 mm.

At X150000 magnification, the scale is

150 mm = 1 μm

= 1000 nm

Particle size $= \frac{1000\ nm}{150\ mm} \times 2.5\ mm$

Particle size = 38.5 nm

The particle size distribution of manganese oxide, which observed from TEM photograph as shown below.

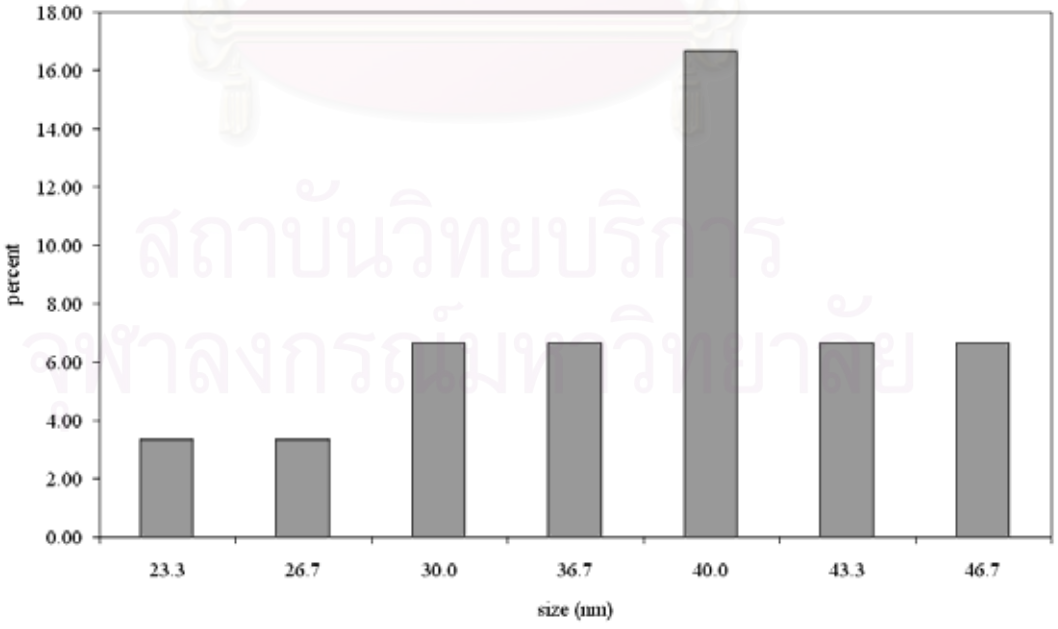

Figure C.5 The particle size distribution of manganese oxide synthesized at 300°C.

Example C5: The measurement of as-synthesized particle size of iron oxide synthesized at 300°C

Table C.5 The particle size of iron oxide synthesized at 300°C observed from TEM photograph

Size(mm)	3.9	4.3	4.5	5.1	6.5	7	8
Number	2	3	5	7	2	2	1

The total measured particle is 21 particles. And the average size is 5.1 mm.

At X150000 magnification, the scale is

150 mm = 1 μm

= 1000 nm

Particle size $= \frac{1000\ nm}{150\ mm} \times 2.5\ mm$

Particle size = 34.0 nm

The particle size distribution of iron oxide, which observed from TEM photograph as shown below.

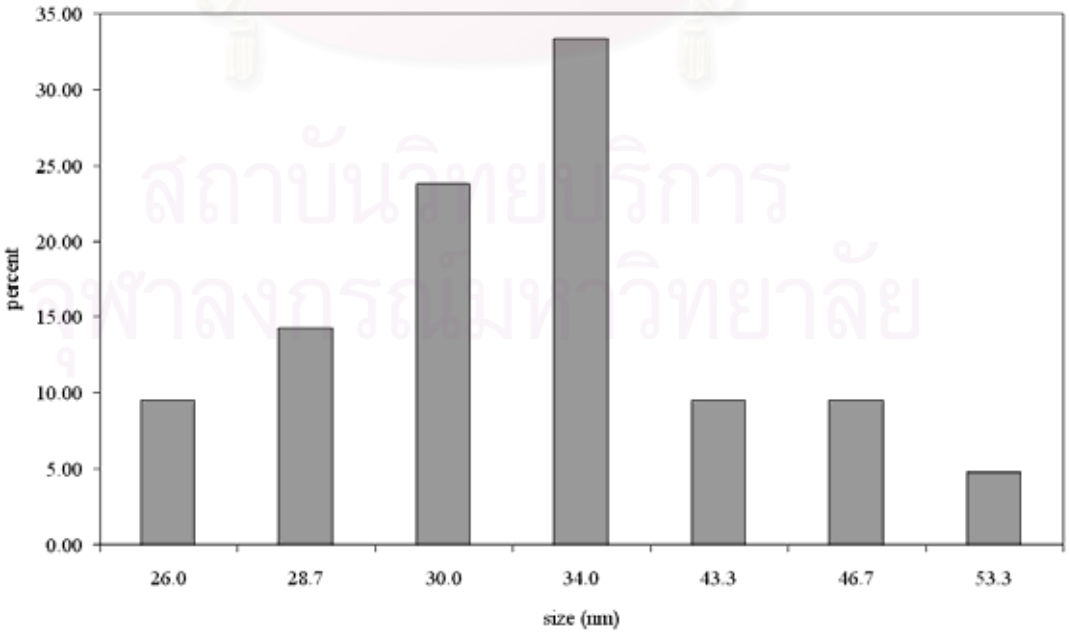

Figure C.6 The particle size distribution of iron oxide synthesized at 300°C.

Example C6: The measurement of as-synthesized particle size of zinc oxide synthesized at 200°C

Table C.6 The particle size of zinc oxide synthesized at 200°C observed from TEM photograph

Size(mm)	2	2.2	2.5	3	3.5	3.7	4
Number	1	2	4	12	9	5	2

The total measured particle is 35 particles. And the average size is 3.1 mm.

At X150000 magnification, the scale is

150 mm = 1 μm

= 1000 nm

Particle size $= \frac{1000\ nm}{150\ mm} \times 2.5\ mm$

Particle size = 21.2 nm

The particle size distribution of zinc oxide, which observed from TEM photograph as shown below.

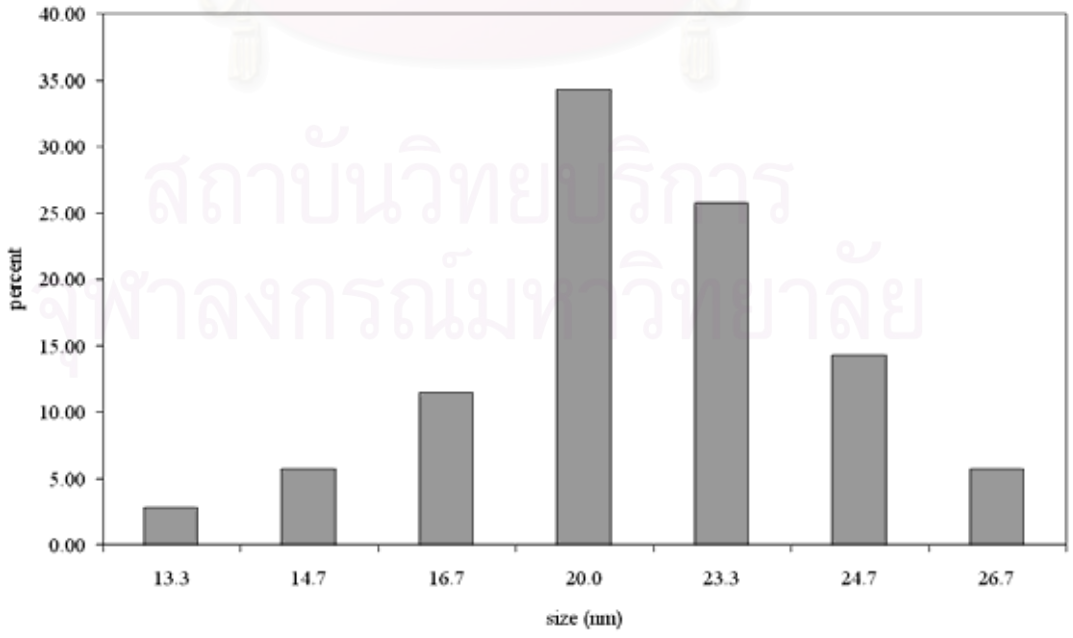

Figure C.7 The particle size distribution of zinc oxide synthesized at 200°C.

VITA

Miss Jirathana Phungphadung was born on December, 1977 in Bangkok, Thailand. She received the Bachelor Degree from Faculty of Science, Chulalongkorn University in 2000. She continued her Master's Study at Chulalongkorn University in June, 2000.